SELF-ASSEMBLY OF SQUARAINE DYES

by

MAHER A. QADDOURA
B.S. University of Damascus, 1991
M.S. University of Central Florida, 2003

A dissertation submitted in partial fulfillment of the requirements

for the degree of Doctor of Philosophy
in the Department of Chemistry
in the College of Sciences
at the University of Central Florida
Orlando, Florida

Spring Term
2011

Major Professor: Kevin D. Belfield

ABSTRACT

Squaraine dyes have been a subject of extensive investigations lately due to their wide applications in important technological fields such as bioimaging probes, bioconjucation, second generation photosensitizers for photodynamic therapy, second harmonic generating organic dyes, two-photon absorbing materials with large cross section values, and, finally, photoconducting materials in photovoltaic cells. While a large number of patents and papers has been produced regarding their applications limited work has been done concerning their thermotropic behavior, including their liquid crystalline properties, or correlation of the crystalline structure to both the solid state aggregation and their photophysical properties.

In the first chapter of this dissertation, a series of squaraine dyes, based on 2, 4-bis [4-(*N,N*-di-n-alkylamino)-2-hydroxyphenyl]squaraine including ethyl, propyl, butyl, pentyl, hexyl, and heptyl derivatives, were synthesized by condensation of the corresponding 4-(*N,N*-di-n-alkylamino)-2-hydroxyphenol with squaric acid. The thermal behavior of the series was recorded using both thermogravemetic analysis (TGA) and differential scanning calorimetry (DSC) while their crystalline structures were elucidated via single crystal X-ray diffraction. The length of the alkyl chain proved to have a significant effect on both the thermotropic behavior and the crystalline structure of the squaraine series. Two derivatives, butyl and heptyl, revealed the presence of liquid crystalline mesophases, smectic and nematic, respectively, that were confirmed and characterized via polarized light microscopy (PLM) and X-ray diffraction.

In the second chapter, J- and H- aggregates were investigated in thin films by UV-vis spectroscopy; several of the derivatives formed H- and/or J-aggregates upon thin film formation via spin coating before and after thermal annealing, as indicated by UV-vis spectroscopy. The molecular structure, crystal structure, aggregation, and thermal behavior provide insight into the supramolecular assembly of this important class of materials. Photophysical measurements revealed large molar absorptivity, reasonably high fluorescence quantum yields, and significant fluorescence anisotropy, making these derivatives suitable candidates for a number of electro-optic and photonics applications.

The third chapter was devoted to investigate liquid crystal-directed supramolecular assembly of a squaraine dye. Thus, The squaraine (SQ) dye, 2, 4-bis [4-(*N,N*-di-n-hexylamino)-2-hydroxyphenyl]squaraine was used to prepare a series of SQ dye/cholesteryl pelargonate mixtures with varying dye concentrations (1%, 3%, 7.5%, 10.8%, 15%, and 20% w/w). Their phase transitions were investigated using differential scanning calorimetry, polarized light microscopy and X-ray diffraction. The squaraine dye itself exhibits no liquid crystalline behavior. The concentration of the dye in the cholesteric compound proved to have a significant effect on the dye aggregation behavior and phase transitions in cholesteryl pelargonate manifested by the appearance of new mesophases and formation of J- and H- aggregates. The texture morphology, X-ray diffraction analyses, and UV-vis absorbance spectra provide compelling evidence of the viability of the self-assembly of squaraines in the liquid crystalline mesophase. In the last chapter we will discuss possible modifications that can improve the aggregation systems.

I dedicate this dissertation to my family.

ACKNOWLEDGMENTS

I would like thank and express my gratitude to my advisor Dr. Kevin D. Belfield for his great support, trust, motivation, and advice during this journey. I wish to thank all the current and former members of Dr. Belfield's research group, with whom I've shared valuable experience. I also would like to thank our collaborators, Dr Paul A. Heiney from Department of Physics and Astronomy, University of Pennsylvania and Dr Tatiana V. Timofeeva from Department of Chemistry, New Mexico Highlands University. Finally, many thanks to the friendly chemistry department staff and faculty.

TABLE OF CONTENT

LIST OF FIGURES

LIST OF TABLES

LIST OF SCHEMES

LIST OF ACRONYMS AND ABREVIATIONS

^{13}C	Carbon 13 isotope
^{1}H	Hydrogen 1 isotope
2PA	Two-photon absorption
A-π-A	Acceptor-π-acceptor
ACN	Acetonitrile
$CDCl_3$	Deuterated chloroform
d	Doublet
D-π-A	Donor-π-acceptor
dd	Doublet of doublets
DSC	Differential scanning calorimetry
EtOH	Ethanol
g	Gram
GM	Goppert-Mayer unit for the 2PA cross section ($1x10^{-50}$ cm^4 s $photon^{-1}molecule^{-1}$)

h	Hour
Hz	Hertz
J	Coupling constant
KHz	Kilohertz (10^3 Hertz)
L	Liter
m	Multiplet
M	Molar
m.p.	Melting point
mg	Milligram (10^{-3} grams)
MHz	Megahertz (10^6 Hertz)
min	Minute
mL	Milliliter (10^{-3} Liters)
mmol	Millimoles (10^{-3} moles)
MS	Mass spectrum
ms	Millisecond (10^{-3} seconds)
N*	Chiral nematic

NIR	Near Infrared
nm	Nanometer (10^{-9} meters)
NMR	Nuclear magnetic resonance
PLM	Polarized light microscopy
ppm	Parts per million
r. t.	Room temperature
s	Seconds
Sm	Smectic
S_1	First excited state, singlet
S_n	A Higher excited state
S_o	Ground state, singlet
THF	Tetrahydrofurane
TLC	Thin layer chromatography
UV	Ultraviolet
W	Watts
ε	Molar absorptivity coefficient

λ_{max}	Wavelength of maximum absorption
KJ	Kilojoules (10^{-6} Joules)
mM	millimolar (10^{-6} Molar)
μL	microliter (10^{-6} Liters)
Φ	Fluorescence quantum yield
XRD	X-ray diffraction

CHAPTER 1. **SYNTHESIS, CHRACTERIZATION AND THERMOTROPIC BEHAVIOR OF SERIES OF SQUARAINE DYES**

1.1 **Abstract**

A series of squaraine dyes, based on 2, 4-bis [4-(*N,N*-di-n-alkylamino)-2-hydroxyphenyl]squaraine, including ethyl, propyl, butyl, pentyl, hexyl, and heptyl derivatives, were synthesized by condensation of the corresponding 4-(*N,N*-di-n-alkylamino)-2-hydroxyphenol with squaric acid. The thermal behavior of the series was recorded using both thermogravemetic analysis (TGA) and differential scanning calorimetry (DSC) while their crystalline structures were elucidated via single crystal X-ray diffraction. The length of the alkyl chain proved to have a significant effect on both the thermotropic behavior and the crystalline structure of the squaraine series. Two derivatives, butyl and heptyl, revealed the presence of liquid crystalline mesophases, smectic and nematic, respectively, that were confirmed and characterized via polarized light microscopy (PLM) and X-ray diffraction.

1.2 **Introduction**

Squaraine dyes have been a subject of extensive investigations due to their applications in a number of important fields such as bioimaging probes, bioconjugation, second generation photosensitizers for photodynamic therapy, second harmonic generating organic dyes, two-photon absorbing materials with large cross section values, and light harvesting and photoconductor materials in photovoltaic cells.[1] While a large number of patents and papers have appeared regarding their applications,[2-10] limited work has been reported concerning their

thermotropic behavior, including their liquid crystalline properties and correlation of the crystalline structure to both solid state aggregation and photophysical properties.[11]

The squaraine dyes that are the subject of this research have a donor-acceptor-donor chromophore, characterized by sharp and intense absorption bands in the long wavelength visible accompanied by red to near-IR fluorescence in liquid solution. They can be synthesized by condensation of aromatic electron-rich compounds, such as *N*,*N*-dialkylaniline, phenols, benzothiazoles, and pyrroles, with squaric acid.[12] One of the fundamental electron-rich structures that has been reported is based on *N, N*-dialkylaniline derivatives, paving the way to construct a myriad of squaraine dyes.[13-15] One of these derivatives emanates from *3*-(N, N-di-n-alkylamino)phenol, and has been employed to produce relatively stable squaraine dyes for different purposes such as aggregation[16,17] or sublimation.[18]

Although several compounds based on 3-(dialkylamino)phenol were investigated for their fluorescence and aggregation properties in solutions, such as methyl, ethyl, propyl, and butyl derivatives of 2, 4-bis [4-(*N,N*-di-n-alkylamino)-2-hydroxyphenyl]squaraine,[19,20] very limited work was devoted to both their self-assembly in the solid state and even less to their thermotropic liquid crystalline behavior. In this work, the series is expanded to include three new compounds in the series, i.e., pentyl, hexyl, and heptyl derivatives, along with a comprehensive investigation of their thermal behavior and self-assembly of the entire series, including liquid crystalline properties. The photophysical properties of the entire series (ethyl to heptyl) were also investigated.

1.3 **Results and Discussion**

1.3.1 *Synthesis of Series of Squaraine Dyes*

A series of six squariane dyes, varying in the length of their peripheral alkyl groups, was investigated for their thermal properties, phase transitions, crystalline structure, aggregation, and photophysical properties. The synthetic procedure for their preparation involved amination with the corresponding 1º alkyl bromide with 3-aminophenol, followed by a subsequent condensation reaction between the 3-(di-n-alkylamino) phenol derivative with squaric acid in a mixture of butanol and toluene[15,21] as shown in Scheme 1-1. The detailed steps[22] of the condensation reaction is illustrated in scheme 1-2.

Scheme 1-1. The general synthetic procedure to synthesize the series of 2,4-bis [4-(N,N-di-n-alkylamino)-2-hydroxyphenyl] squaraines; n= 2: (SQC2OH); n = 3: (SQC3OH); n = 4: (SQC4OH); n = 5: (SQC5OH); n = 6: (SQC6OH); n = 7: (SQC7OH).

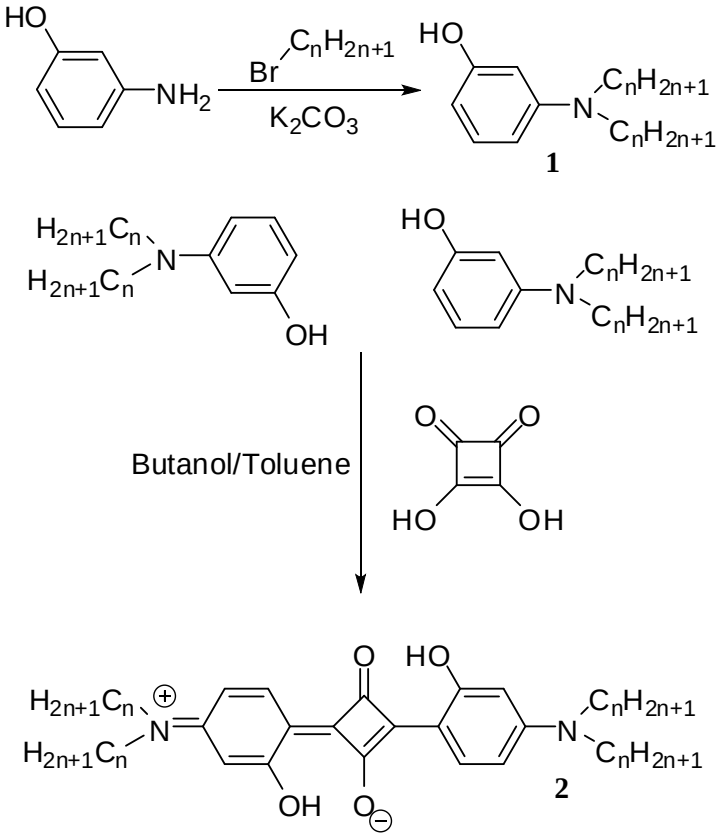

Scheme 1-2. The detailed steps of squaraine formation.

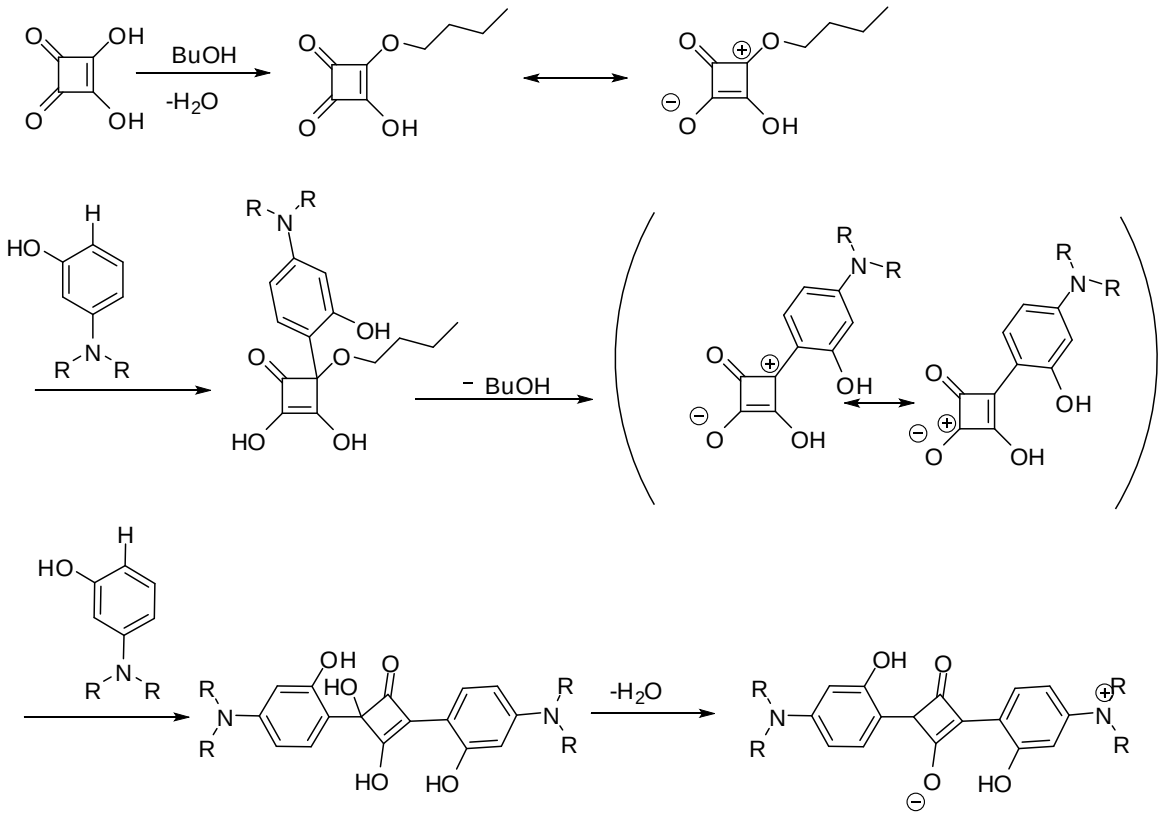

1.3.2 *Crystal Structures*

Crystalline structures of both **SQC2OH** and **SQC4OH** were reported previously.[23,24] However, for consistency, we repeated the crystalline structure of **SQC4OH** and obtained the heretofore first report of the crystalline structures of **SQC3OH**, **SQC5OH**, **SQC6OH**, and **SQC7OH**. Crystal structures of the squaraine derivatives were obtained via single crystal X-ray diffraction analysis (Figure 1-1); all hydrogen atoms were refined within the Riding model. Fourier electron density synthesis revealed the presence of disorder in compounds **SQC4OH**, **SQC5OH**, and **SQC6OH**. The crystal structure of **SQC2OH** was not repeated as we were

unable to obtain suitable single crystals. In the molecule **SQC4OH** the hydroxyl groups are disordered by two symmetrical positions with occupancy 0.5. Six distance restraints were used to fit the ideal conformation for the disordered alkyl chain in molecule **SQC5OH**. The C-C distances were fixed at 1.54Å (4) (C6-C7', C7'-C8', C8'-C9' and C9'-C10); the C…C distances were fixed at 2.48 Å (2) (C6…C8', C7'…C9'). In the crystals of **SQC6OH**, three of the four alkyl chains are disordered over two positions with occupancies 0.1, 0.5 and 0.4. In all molecules, the central fragments that include a four-membered ring and two phenyl rings are planar and the alkyl chains deviate from the plain of the central core in a different manner. The planarity of the central core is sustained by the presence of the conjugation and the hydrogen bonding between the hydroxyl groups and the carbonyl atoms. The central core in the series can be presented by two canonical structures reflecting a symmetrical electron distribution in the central fragment (Table 1-1 and Scheme 1-3). The squaraine structure also demonstrates a quinoid character of both phenyl substituents that have donor and acceptor groups in *para* positions. Additional impact on the planarity of the central core is generated by strong hydrogen bonding between the hydroxy and the carbonyl groups in which geometry parameters are very close in all molecules studied except molecule **SQC6OH** where deviations were caused by the crystal structure disorder.

Despite of the similarity of the central molecular fragments and their high symmetry, the shapes of all molecules differ significantly due to different orientations and conformations of the flexible alkyl substituents. Only three of five molecules, **SQC4OH**, **SQC5OH**, and **SQC7OH**, demonstrated a centrosymmetric crystalline structure. The short alkyl chains of **SQC3OH** and **SQC4OH** are located on both sides of central core and they have different orientation and

conformation. In the molecule **SQC5OH**, significant deviations of disordered alkyl chains in "up" and "down" directions relative to the core were observed. In **SQC6OH**, two alkyl chains are extended in the plane of the main core and the other two are oriented nearly perpendicular on both sides of central planar fragment. The molecules in the **SQC7OH** crystalline structure occupy a centrosymmetric position with the alkyl chains located in planes nearly parallel to central core "above" and "below" this plane.

It is known that in some cases solid crystalline liquid crystalline (LC) precursors can demonstrate a 3D structure similar to 1D or 2D structures of liquid crystalline phases. The packing in the crystal might also demonstrate the type of molecular associates that can be formed by certain materials in solution. We carried out a careful analysis of the molecular packing in crystals for the entire series (Figure 1-1); no similarity in the crystal packing as well as no formation of π-π stacking arrangements was found for the series. In the crystals **SQC3OH**, **SQC4OH**, and **SQC5OH** the molecular core packing can be loosely presented as a herring-bone arrangement. In the crystals **SQC6OH** and **SQC7OH** the molecular cores are oriented in one direction and surrounded by alkyl substituents, so this arrangement might be considered as a LC precursor, a prediction confirmed from texture observations using polarized light microscopy. From the crystalline structure of both **SQC3OH** and **SQC4OH** molecules, one can see that they both form ribbons with the position of the cores in one plane that might be considered as associates (Figure 1-2). Similar aggregates can be formed for both **SQC5OH** and **SQC7OH** in solution but not in crystals where close packing most likely prevents it. Crystal data, details of data collection and structure refinement for squaraine compounds can be found in Table 1-2 and Table 1-3.

Scheme 1-3. Bonds length in the series of squaraine dyes

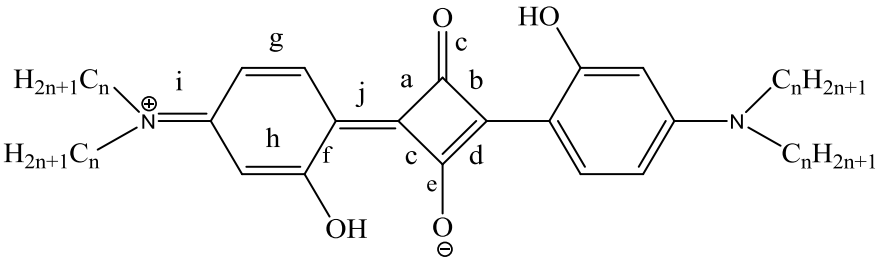

Table 1-1.Selected bond lengths for squaraine compounds.

	a	b	c	d	e	f	g	h	i	j
SQC3OH	1.46(3)	1.46(3)	1.46(3)	1.46(3)	1.25(3)	1.25(2)	1.36 (3)	1.38(3)	1.36(3)	1.40(3)
SQC4OH	1.46	1.46	1.47	1.46	1.25	1.25	1.37	1.38	1.36	1.40
SQC5OH	1.46(2)	1.46(2)		1.46(2)	1.24 (16)		1.38(16)	1.362(2)	1.35	1.34(2)
SQC6OH	1.45(6)	1.45(6)	1.46(6)	1.45(6)	1.25 (5)	1.24 (5)	1.36(6)	1.38(6)	1.36(5)	1.34(6)
SQC7OH	1.46(2)	1.47(19)		1.46(2)	1.24 (16)		1.38(19)	1.37(2)	1.36 (18)	1.40(19)

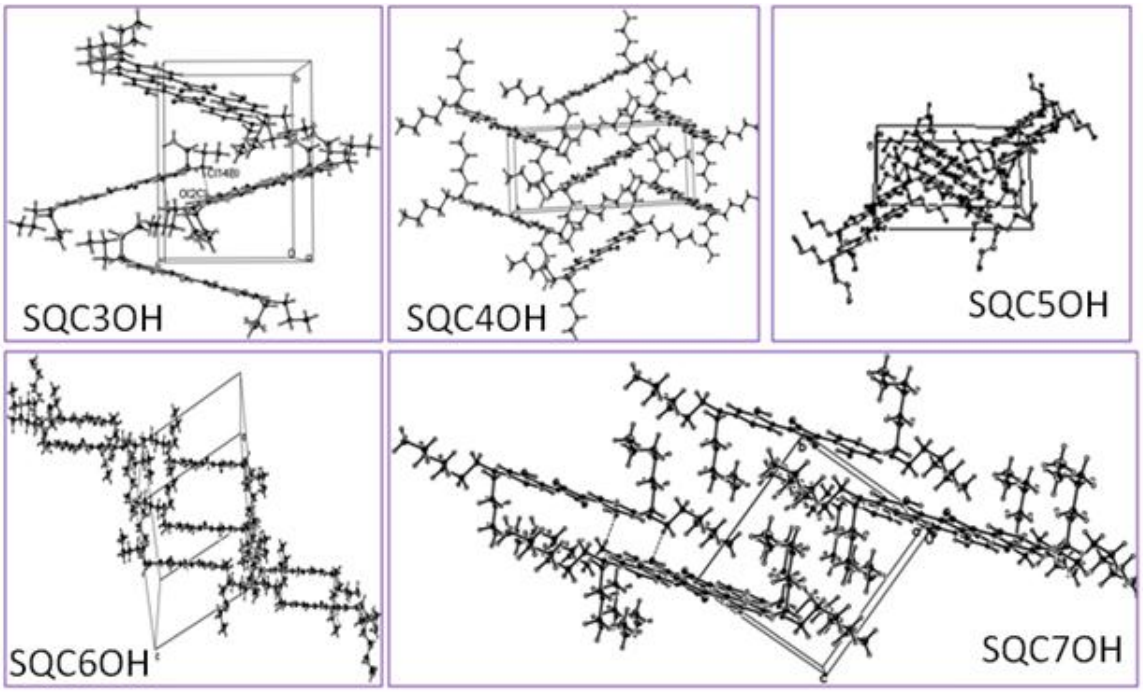

Figure 1-1. The crystalline packing structures for the series of squaraine dyes; all revealed monoclinic crystal systems except SQC7OH which exhibit triclinic crystal system.

Table 1-2. Crystal data, details of data collection and structure refinement for squaraine compounds.

Compound	SQC3OH	SQC4OH	SQC5OH	SQC6OH	SQC7OH
Formula	C28 H36 N2 O4	C32 H44 N2 O4	C36 H52 N2 O4	C40 H60 N2 O4	C44 H68 N2 O4
FW	464.59	520.69	576.80	632.90	689.00
T, K	100	100	100(2)	100(2)	100(2)
Crystal size, mm	0.40 x 0.20 x 0.10	0.10 x0.08 x0.05	0.40 x 0.20 x 0.10	0.40 x 0.20 x 0.10	0.40 x 0.20 x 0.10
Crystal system	Monoclinic	Monoclinic	Monoclinic	Monoclinic	Triclinic
Space group	P21	P21/n	P21/n	P21/c	P-1
a, Å	7.5803(9)	9.1321(4)	8.8756(7)	15.869(3)	7.5427(9)
b, Å	15.2938(18)	19.6935(9)	8.5380(7)	11.865(2)	10.7138(12)
c, Å	10.5753(12)	9.1949(4)	21.9793(18)	20.090(4)	12.3231(14)
α, deg.	90	90	90	90	86.549(2)
β, deg.	94.940(2)	119.75(7)	95.341(2)	101.942(4)	84.498(2)
γ, deg.	90	90	90	90	85.512(2)
V, Å3	1221.5(2)	1435.55(11)	1658.4(2)	3700.8(13)	986.8(2)
Z(Z')	2(1)	2(1)	2(1)	4(1)	1(1)
dc, g · cm-3	1.263	1.205	1.155	1.136	1.159
F(000)	500	564.00	628	1384	378
2θmax	58	54	58	52	58

Table 1-3. Crystal data, details of data collection and structure refinement for squaraine compounds.

Compound	SQC3OH	SQC4OH	SQC5OH	SQC6OH	SQC7OH
Tmin; Tmax	0.9671; 0.9916	0.9922; 0.9961	0.9709; 0.9926	0.9718; 0.9928	0.9715; 0.9928
no. of rflns collected	19781	19747	26233	46735	16252
(Rint)					
No. of unique rflns	6488	3132	4406	7286	5261
Completeness (%)	99.9	100	100	99.9	100
data/restraints/param	6488/1/316	3132/0/344	4406 / 2 / 180	7286 / 0 / 407	5261 / 0 / 233
R1; wR2 (I > 2σ(I))	0.0483;0.1043	0.0360;0.0936	0.0568;0.1362	0.0942; 0.2193	0.0483; 0.1199
R1; wR2 (all data)	0.0808;0.1186	0.0371; 0.0946	0.0788;0.1527	0.2400; 0.2853	0.0829; 0.1374
GOF on F2	0.990	1.033	1.006	1.198	1.039
ρmax,ρmin, eÅ-3	0.327; -0.216	0.293;-0.195	0.486;-0.460	0.567; -0.404	0.362; -0.219
μ(MoKα), mm-1	0.084	0.079	0.074	0.072	0.073

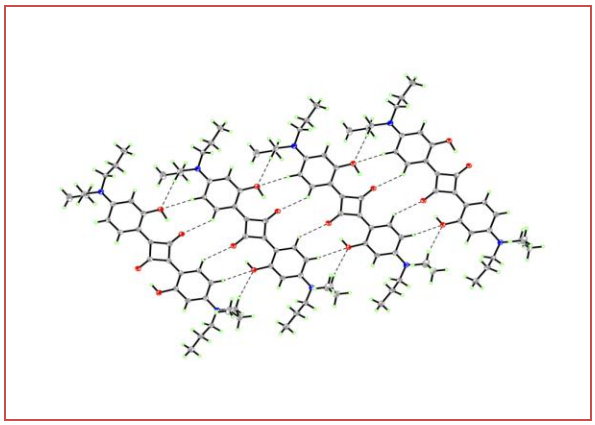

Figure 1-2. The formation of the molecular associates for SQC3OH.

1.3.3 *Thermotropic Behavior*

The length of the peripheral alkyl group for each compound appeared to exert a profound effect on their thermal stability. It was observed that the shorter the alkyl group, the higher the decomposition temperature (Table 1-4, Figure 1-4), an observation that can be explained by the strong intermolecular interaction, including both hydrogen bonding and van der Waals for electron rich regions for the lower peripheral alky chain structure. However, by increasing the length of the hydrophobic alkyl chains, the intermolecular forces become weaker, and, as a result, lower both the melting and the decomposition temperatures.

The thermotropic behavior was investigated for each of the squaraine dyes using differential scanning calorimetry (DSC, Figure 1-3). The n-propyl (Figure 1-3B), n-pentyl (Figure 1-3D), and n-hexyl (Figure 3E) derivatives revealed sharp melting transition temperatures in addition to weak crystalline transitions for n-pentyl (Figure 1-3D) and n-hexyl (Figure 1-3E) derivatives, as observed by polarized light microscopy, while the n-butyl (Figure 1-3C) and n-heptyl (Figure 1-3F) analogs exhibited liquid crystalline phase transitions. Only the ethyl derivative did not show any melting process but rather only decomposition (Figure 1-3A).

Although, the cooling cycles did not show recrystallization for the series of squaraine compounds except for **SQC3OH** (Figure 1-3B), the polarized light microscopy (PLM) analysis confirmed the recrystallization process (Figures 1-5, 1-6, and 1-9). The behavior may be due to sample preparation and container. Whilst the DSC pan offered a smooth and clean surface that hindered the alkyl squaraines to pack and recrystallized owing to the smaller surface area and smaller London attractions of the branched alkyl chains , the surface of the glass slides used in polarized light microscopy likely caused the induction of both the nucleation and the crystal growth process due to surface scoring or defects.

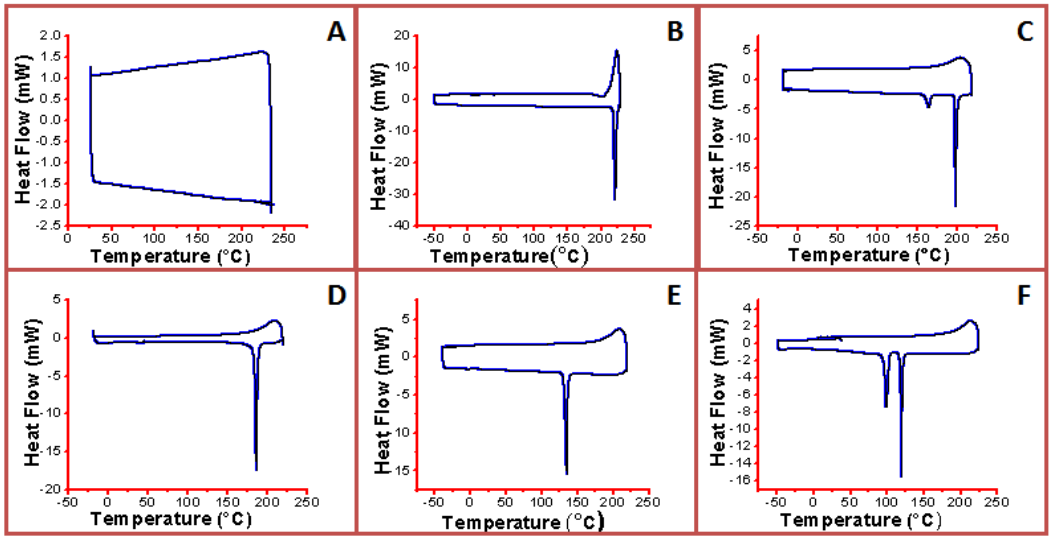

Figure 1-3. The thermotropic behavior for the series of squaraine dyes. A) The DSC thermogram for **SQC2OH**, no melting point was detected, it decomposed at 240 °C. B) The DSC thermogram for **SQC3OH**, it exhibited a melting point at 221 °C followed by recrystallization at 220 °C. C) DSC thermogram for **SQC4OH** revealed a phase transition at 164 °C and a melting temperature at 196 °C. D) DSC thermogram for **SQC5OH** showed a melting point at 185 °C. E) The DSC thermogram for **SQC6OH** exhibited a melting point at 135 °C. F) DSC thermogram for **SQC7OH** revealed a phase transition at 99 °C and a melting temperature at 119 °C. No recrystallization was observed during the cooling process for C, D, E, and F due to the alkyl structure of the squaraine dye and the smooth and clean surface of the DSC sample pan.

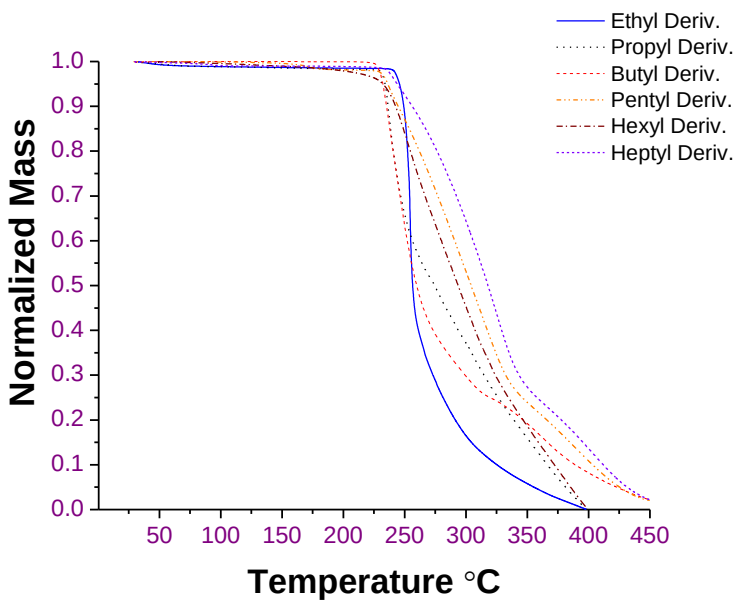

Figure 1-4. The decomposition temperatures for the series of squaraine dyes bearing different alkyl lengths.

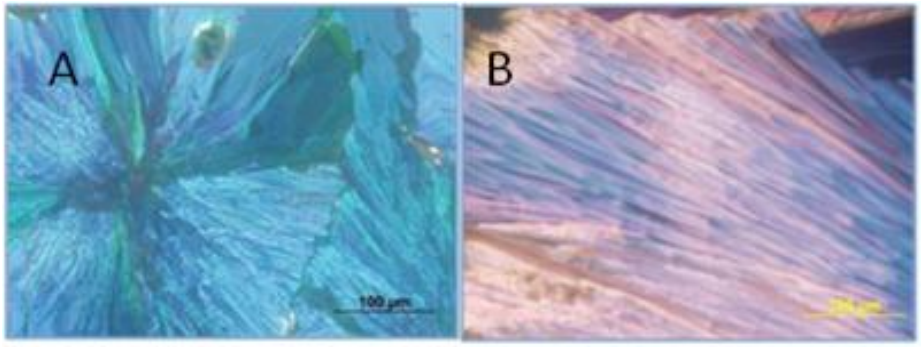

Figure 1-5. The recrystallization texture of pentyl and hexyl derivatives of squaraine dyes as can be seen under polarized light microscopy; the colored texture is a result of the birefringence. A) The crystalline texture of SQC5OH. B) The crystalline texture of SQC6OH.

Table 1-4. Summary of the thermotropic behavior of squaraines

	Decomposition ^{0}C	Phase Transition-1. ^{0}C	Enthalpy KJmol-1	Phase Transition-2 (melting point) ^{0}C	Enthalpy KJmol-1
SQC2OH	240	n/a	n/a	n/a	n/a
SQC3OH	227	n/a	n/a	221	53.4
SQC4OH	224	164	9.08	196	37.6
SQC5OH	226	n/a	n/a	185	50.4
SQC6OH	228	n/a	n/a	135	33.4
SQC7OH	232	99	24.5	119	24.8

SQC3OH also revealed a sharp melting point followed by recrystallization upon cooling; any further heating above 221 °C resulted in abrupt decomposition (Figure 1-3B). It was discovered that **SQC4OH** and **SQC7OH** have the capability to exhibit liquid crystalline mesophases; the mesophase occurrence is dependent on the intrinsic properties of the dye such as the crystalline structure, the conformation and arrangement of the molecule, and the intermolecular interactions. Typically, the generation of a liquid crystalline mesophase implies the loss of long-range crystalline order. A smectic phase is characterized by short-range, liquid-like positional order within well-defined sheets or layers, while in a nematic phase the molecules have long-range orientational order of the long axis director but only short-range positional order. Upon further heating all order is lost, forming the isotropic liquid.[25,26]

SQC4OH displayed two phase transitions upon heating, as can be seen in Figure 1-3C. Although, crystallization upon cooling was not observed by DSC, the phase transition was clearly observed by polarized light microscopy upon cooling (Figure 1-6C). The transition temperatures and the enthalpy of transitions, determined by DSC, are shown in Table 1. At 164

°C, 9.08 kJmol^{-1} of energy was released attributed to the disruption of the translational order of the crystal lattice, likely ascribed to the crystalline-smectic-like mesophase. However, at 196 °C, a significantly larger enthalpy value was of 37.6 kJmol^{-1} was recorded due to major disruption in the molecular packing order to both the positional and orientational order, forming anisotropic liquid.

The mesophase for **SQC4OH** was observed and identified by the texture morphology observed by polarized light microscopy (PLM) upon cooling of the molten crystals. The principle of the phase identification depends on observing the microscopic textures by PLM, characterized by the defects, the elastic deformation, and the birefringence between two glass slides. The interaction of the polarized light with the topology of the defects and the deformation elasticity, in combination with the birefringence, results in characteristic texture morphology for each liquid crystalline phase. [27,28] When external forces are applied, e.g., shear stress on the slides, during sample preparation, the difference in the bulk elasticity and the fluidity (elastic constants) for each phase results in a distinguished texture morphology.[29] Figure 1-6A, presents the growth of the mesophase from the melt upon cooling. The fan shaped nuclei are characterized by extinction crosses that appear dark when the optical axis is parallel to either the polarizer or the analyzer. In Figures 1-6B and 1-6C the nuclei begin to grow and coalesce to form the new mesophase. Finally, the transition from the mesophase to the crystalline texture is illustrated in Figure 1-6D; while Figures 1-6E and 1-6F show the crystalline texture at different thickness and birefringence.

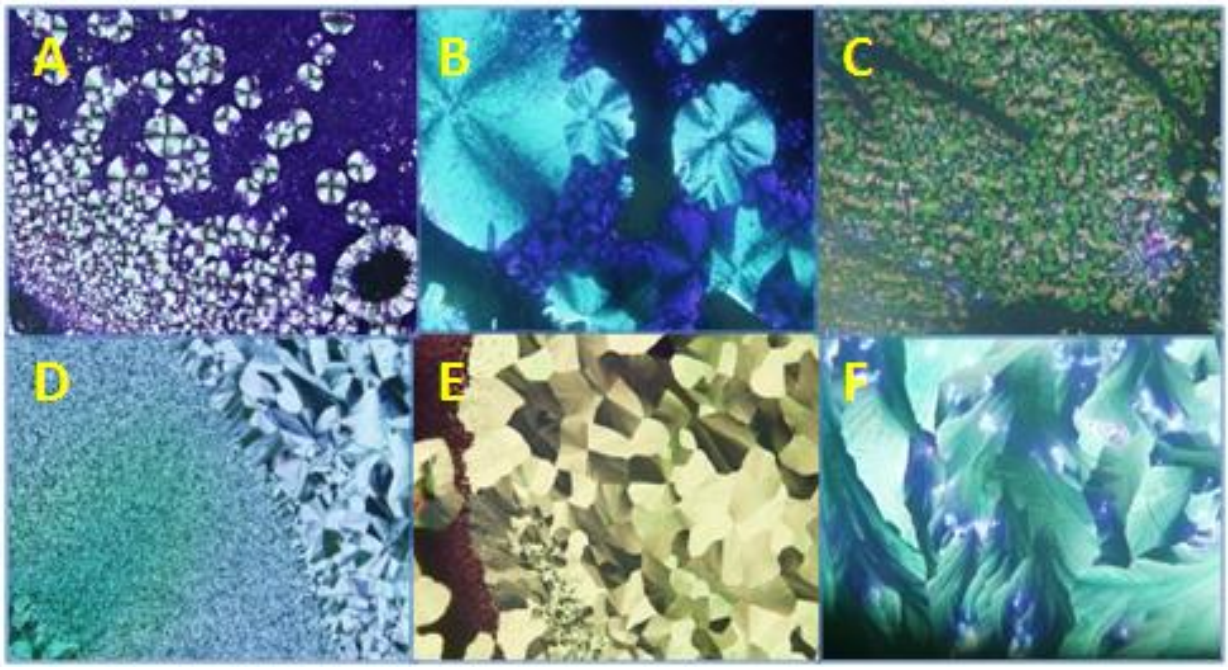

Figure 1-6. Phase transitions for SQC4OH. A) The growth of the mesophase from the melt upon cooling at 196 °C; the fan shaped nuclei are characterized by extinction crosses which appear dark when the optical axis is parallel to either the polarizer or the analyzer. These extinction crosses rotate along the direction of the rotating polarizer, indicating that the liquid crystal is optically positive. B) and C) The nuclei begin to grow and coalesce to form the new mesophase. D) The transition from the mesophase to the crystalline morphology at 164 °C. E) and F) The crystalline texture morphology at both different thickness and birefringence.

Differential scanning calorimetry analysis for **SQC5OH** showed only sharp melting point at 185 °C as can be seen in Figure 1-3D. However, PLM revealed the presence of a phase transition assumed to be a crystalline phase; the crystalline-to-crystalline transition can be observed in Figure 7A.

The packing of the crystalline structure of **SQC5OH**, determined by single crystal X-ray crystallography (Figure 1-1), may provide reasonable rationale to account for the crystalline-to-crystalline transition. This type of constrained packing impedes the molecule from undergoing considerably favorable translational and rotational effect towards forming a liquid crystalline

phase. However, it is only capable of undergoing a crystalline-to-crystalline transition as this requires minimum translational and rotational energy. The same argument pertains to **SQC6OH**. Similarly **SQC6OH** not only demonstrate a sharp melting point, as can be seen in the DSC thermogram (Figure 1-3E), but also a weak phase transition when observed by PLM. The unknown phase transition is assumed to be crystalline-to-crystalline transition see Figure 1-7B.

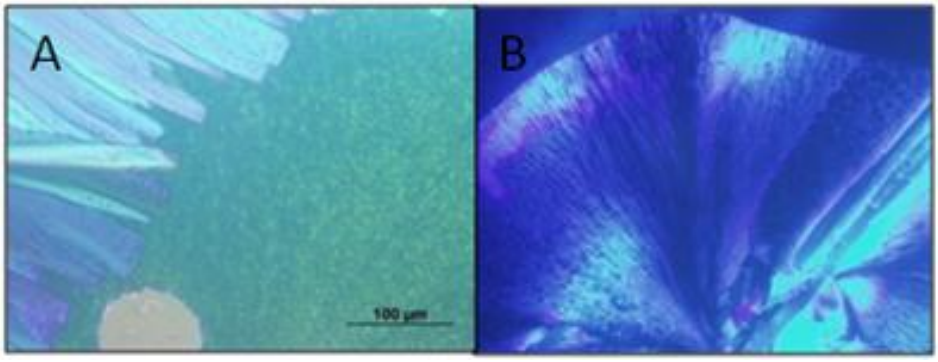

Figure 1-7. A) Crystalline-to-crystalline phase transition at 140 °C for **SQC5OH**; the difference in both morphologies' color is attributed to deformations and birefringence (the difference between extraordinary ray and ordinary ray of the polarized light when entering the sample). B) Crystalline-to-crystalline transition for **SQC6OH** at 110 °C; each phase has a slightly different type of topological defect and deformation. The interaction of the polarized light with the deformation and defect for each phase results in different path differences and birefringence.

The DSC thermogram for **SQC7OH** (Figure 1-3F) clearly demonstrates the presence of a phase transition upon heating. Although, the crystallization process was not observed upon cooling by DSC, this phase transition was clearly observed by the PLM upon cooling. The transition temperatures and the enthalpy of transitions determined by DSC are shown in Table 1-4; at 99 °C, 24.5 $kJmol^{-1}$ of energy was released due to the disruption of the translational order of the crystal lattice, which might be ascribed to the crystalline-mesophase transition. However, at 119 °C, the energy released was 24.8 $kJmol^{-1}$ attributable to a major disruption in the molecular

packing of both the positional and orientational order to become an isotropic liquid. Powder X-ray diffraction was utilized to identify and confirm the phase transitions, a crystalline phase was observed at room temperature (see Figure 1-8A) while above 99 °C a phase with a nematic-like broad peak at 0.374 $Å^{-1}$ was observed that is consistent with the DSC data (Figure 1-8). At 129 °C the signal disappeared completely, most likely due to a transition to the isotropic phase.

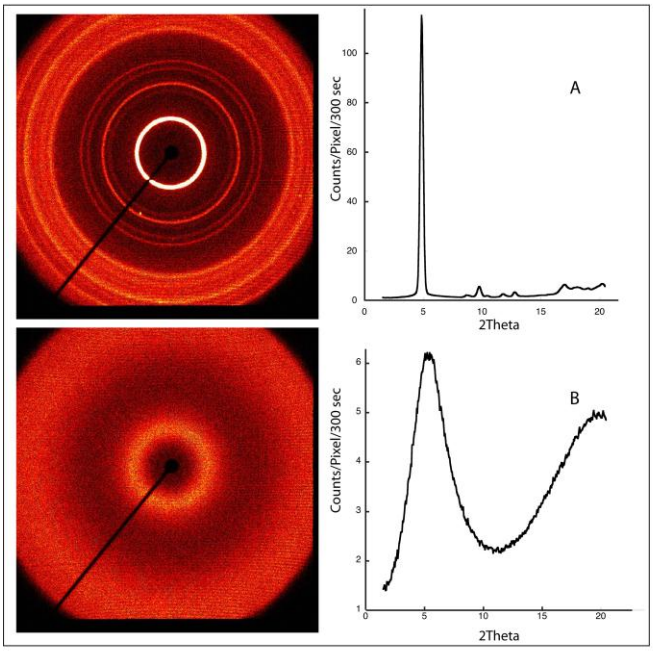

Figure 1-8. Powder X-ray diffraction patterns for SQC7OH. Left: false color images of measured intensity; Right: radial plots of circularly averaged intensity. A) Crystalline structure at 99 °C, showing Bragg peaks. B) Nematic phase at 103 °C, showing diffuse-liquidlike peak at 5° (the peak at wider angle is primarily due to the glass capillary).

The texture observations for **SQC7OH** were conducted using PLM upon cooling. Figure 1-9A shows the appearance of droplets out of the isotropic phase, while Figures 1-9B and 1-9C indicates the nucleation and the crystal growth process. The new phase morphology starts to fashion in Figure 8C and carried through to its final shape in Figure 1-9D, which is unusual for a

nematic liquid crystal. Finally, Figures 8E and 8F represent the transformation of the mesophase to the crystalline phase. The extinction crosses in Figure 1-9D are explained by the interaction of the polarized light with the optical axis of the squaraine molecule. The extinction crosses only appear when the optical axis of the molecule forms 90° or 0° with either the polarizer or the analyzer of the polarized light microscope, while the maximum brightness is observed when the optical axis of the molecule forms 45° with either the polarizer or the analyzer

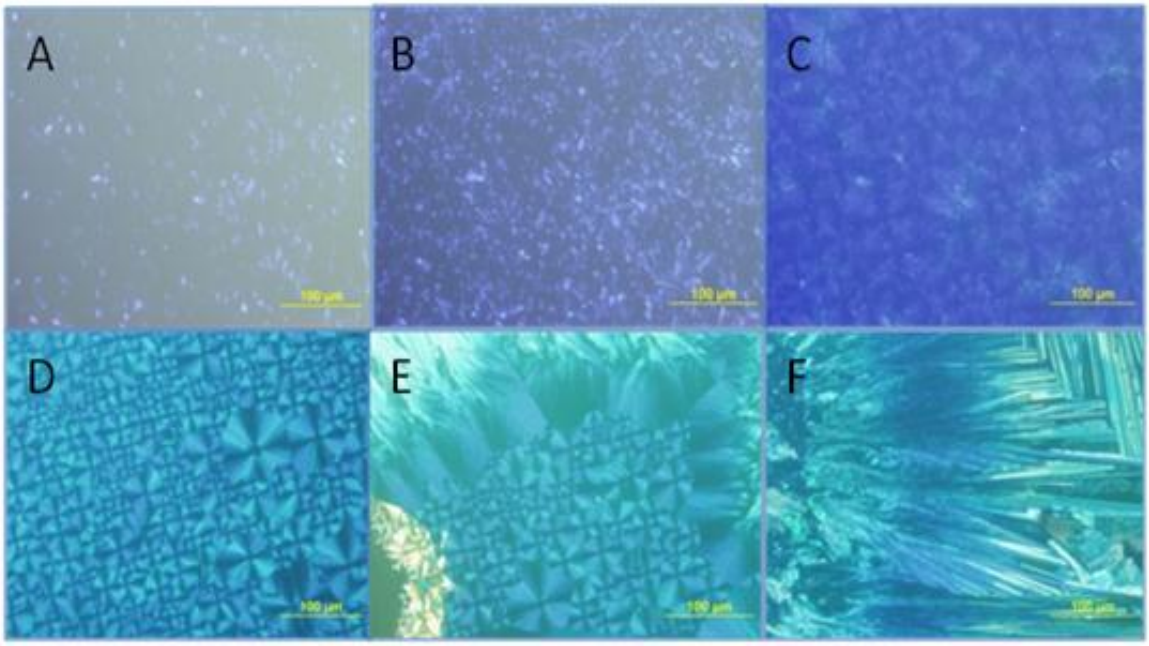

Figure 1-9. For SQC7OH, A) The droplets appear from the isotropic phase. B) Nucleation and the crystal growth process. C) and D) Growth of the mesophase, the extinction crosses are explained by the interaction of the polarized light with the optical axis of the squaraine molecule; the extinction crosses only appear when the optical axis of the molecule forms 90° or 0° with either the polarizer or the analyzer of the polarized light microscopy. E) Transformation of the mesophase to the crystalline phase. F) Crystalline phase. morphology.

Surprisingly, although the X-ray diffraction studies revealed the existence of a nematic phase, polarized light microscopy, as evidenced in Figure 1-9D, revealed an unusually rigid smectic-like mesophase texture. The explanation of this difference can be found in the sample preparation technique. While, the X-ray analysis required using capillary tubes allowing the nematic fluid phase to flow freely in the tube without forming defects or triggering any aggregation behavior, the PLM analysis required positioning the crystals between two glass slides along with rubbing the sample. This type of preparation results in forming defects and deformations in the crystals in addition to triggering an aggregation process when exerting external pressure due to both intermolecular charge-transfer interactions between the electron-donor and –acceptor group of squaraine structure[30,31] and to C-O dipole–dipole interactions[32]. This type of external pressure effect has been exploited in the literature to trigger the aggregation of the squaraine dyes in Langmuir-Blodgett films.[33,34] Consequently, both the defects and the aggregation manifest themselves in inducing the new texture. Moreover, the absorption spectra of the squaraine dye in the mesophase state shows a broad absorption band extending from 532 to 730 nm covering both H- and J-aggregate ranges; providing further support for aggregation (Figure 1-10). Furthermore, by investigating the texture morphology of the mesophase under polarized light microscopy while the squaraine dye was undergoing a phase change in the same capillary tube used for the powder X-ray analysis, a Schleiren nematic-like texture was observed, consistent with the X-ray studies (Figure 1-11A). Finally, polarized light microscopy images for the natural texture of the mesophase between two glass slides, without applying pressure and shear stress, also revealed a fluid morphology and marble texture, characteristic of the natural texture of the nematic mesophase (Figure 1-11B).

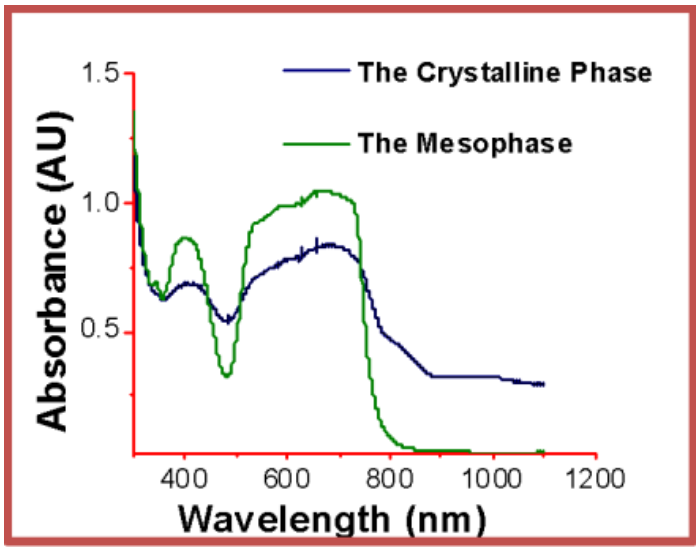

Figure 1-10. Absorption spectra for neat SQC7OH. A) The crystalline phase exhibited scattering phenomena as can be seen from the tail trend. B) The mesophase absorption spectrum, extending to both the H- and J-aggregate range.

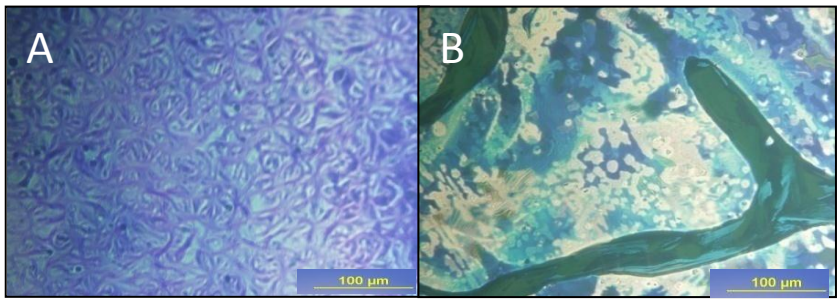

Figure 1-11. A) The texture for the mesophase as observed by polarized light microscopy upon heating SQC7OH in the powder X-ray capillary tube. B) The texture of the mesophase without treatment and without applying shear stress between the two slides; the texture flows freely as observed by PLM, forming wall and line defects of the marble texture, a characteristic feature of the natural nematic mesophase.

1.4 **Experimental Section**

1.4.1 *Materials and Methods*

1-Bromopropane (99%), 1-bromohexane (99+ %), 1-bromhepatne (99%), 3-(di-n-ethyamino)phenol (99%), 3-(di-n-butylamino)phenol (99%), aminophenol (99%), and 3, 4-dihydroxy-3-cyclobutane-1,2-dione (99%) were purchased from Acros Organics and Aldrich, 1-bromopentane was obtained from Eastman Organic Chemicals, and sodium carbonate (99.5%) was purchased from Spectrum. 3-(Di-n-propylamino)phenol, 3-(di-n-pentylamino)phenol, 3-(di-n-hexylamino)phenol, and 3-(di-n-heptylamino)phenol were prepared according to literature procedures.[35] **SQC2OH**, **SQC3OH**, and **SQC4OH** were prepared by methods previously reported.[36,37]

Thermogravimetric analysis (TGA) was performed using a TGA Q5000 thermogravimetric analyzer (TA Instruments) at a heating rate of 10 °C/min. The thermotropic behaviors of all compounds were determined by a combination of differential scanning calorimetry (DSC) and polarized optical microscopy. A TA Instruments Q1000 differential scanning calorimeter (DSC) was used to determine the thermal transitions during heating and cooling cycles; all heating and cooling rates were 10 °C/min.; thermal transitions were read from reproducible second scans. An Olympus BX51 polarized optical microscope (magnification ×40) equipped with both a DP70 microscope digital camera and an Instec HCS302 heating/cooling stage was used to detect and image the phase transitions by observing thin samples between a clean glass slide and a cover slip. Single crystals of the series of squaraine dyes were grown by slow evaporation from $CHCl_3$ for single crystal X-ray diffraction, carried out with a Bruker SMART APEX II diffractometer with CCD area detector (graphite monochromated Mo Kα

radiation, $\lambda = 0.71073$ Å) and ω-scans with a 0.5^{o} step in ω at 100K. The semi-empirical method SADABS was applied for absorption correction for all compounds and the structures were solved by direct methods and refined by the full-matrix least-squares technique against F2 with the anisotropic temperature parameters for all non-hydrogen atoms. All hydrogen atoms were calculated from geometrical point of view except for the hydroxyl protons in **SQC3OH** that were located from the fourier electron density synthesis. Data reduction and further calculations were performed using Bruker SAINT+ and SHELXTL NT program packages. Temperature-dependent X-ray diffraction measurements of powder samples employed a Bruker-Nonius FR591 fine-focus generator with a Cu target (λ=1.542 Å), Osmic confocal optics, and a Bruker HiStar wire detector. Measurements were carried out at a fixed sample-detector distance of 11 cm. The scattered intensity was recorded for scattering vectors in the range $0.2\ Å^{-1} \leq q\ (=4\pi \sin(\theta)/\lambda) \leq 1.7\ Å^{-1}$. Measurements were made between room temperature and the clearing point upon both heating and cooling. The heating and cooling rates were both 10 ºC/min, and data were collected for 5 minutes at each temperature. Primary data analysis was performed using Datasqueeze [http://www.datasqueezesoftware.com]. Thin films were prepared by spin coating a 2% solution of the dye in $CHCl_3$ at 2000 rpm. Absorbance measurements were performed using Agilant 8453 UV-vis spectrophotometer; the steady state emission studies and excitation anisotropy were performed using a PTI QuantaMaster spectrofluorimeter in 10 mm spectrofluorometric quartz cuvettes with $C \sim 10^{-6}$ M and Rhodamine 6G as reference. The fluorescence spectra were corrected for the spectral responsivity of the PTI emission monochromator and PMT. GC-MS analyses were conducted in the Chemistry Department mass spectrometry facilities at the

University of Florida. ^{1}H and ^{13}C NMR analyses were performed in $CDCl_3$ (referenced to TMS at δ 0.0 ppm) on a Varian NMR spectrometers (500 or 300 MHz for ^{1}H and 75 MHz for ^{13}C).

1.4.2 *Synthetic Procedures and Characterization*

2, 4-Bis [4-(*N, N*-diethylamino)-2-hydroxyphenyl]squaraine (SQC2OH).

3-(Diethylamino)phenol (2.0 g, 12.12 mmol) was mixed with 3, 4-dihydroxy-3-cyclobutane-1, 2-dione (0.69 g, 6.05 mmol) in a 1:1 mixture of butanol and toluene by volume 10:10 ml. After 8 h of reflux, the reaction mixture was cooled down to room temperature, resulting in a precipitate. The solvent was removed on a rotary evaporator *in vacuo* and the product was recrystallized from $CHCl_3$ to yield 1.1 g of 2, 4-bis [4-(*N,N*-di-n-ethylamino)-2-hydroxyphenyl] squaraine. ^{1}H NMR 300 MHz (δ ppm TMS, $CDCl_3$): 1.29 (m, 12H, CH_3), 3.48 (q, 8H, CH_2), 6.1 (d, J = 3 Hz, 2H), 6.3 (dd, J = 3 Hz) 7.86 (d, J = 3 Hz, 2H), 8.03 (d, J = 9 Hz, 2H); ^{13}C NMR (δ ppm TMS, $CDCl_3$): δ 12.39, 40.18, 100.3, 106.3, 110.0, 135.9, 156.7, 164.7, 171.5, 181.3.

2, 4-Bis [4-(*N, N*-di-n-propylamino)-2-hydroxyphenyl] squaraine (SQC3OH).

Preparation of the precursor, 3-(di-n-propylamino)phenol. 3-Aminophenol (5 g, 46 mmol) was dissolved in 20 mL of acetonitrile in two neck bottom flask, equipped with condenser, followed by 1-bromopropane (11.2 g, 91 mmol). The mixture was left reflux for 48 h in the presence of sodium carbonate (5 g, 47 mmol) as catalyst. The reaction was cooled to room temperature after completion and the catalyst was filtered using gravity filtration. The solvent was evaporated using a rotary evaporator, and the oily product was purified over the silica as the stationary phase and 1:2 ratio of mixture of ethyl acetate: hexanes as the mobile phase; resulting

in orange viscous oil. Yield 45% . ^{1}H NMR 500 MHz: 0.96 (t, 6H, CH_3), 1.58 (m, 4H, CH_2), 3.18 (t, CH_2N), 6.09 (m, 4H, Ar–*H*), 6.97 (m, 1H, Ar–*H*). ^{13}C NMR (δ ppm TMS, $CDCl_3$): 12.1, 21.3, 57.0, 98.2, 107.1, 109.2, 131.9, 152.2, 160.8.

Preparation of SQC3OH, 3-(Di-n-propylamino)phenol (1.7 g, 8.8 mmol) was added to 3, 4-dihydroxy-3-cyclobutane-1, 2-dione (0.5 g, 4.4 mmol) in 20 mL of 1:1 butanol and toluene. After 8 h of reflux, the reaction mixture was cooled to room temperature, obtaining the product as a precipitate. The solvent was removed on a rotary evaporator *in vacuo* and the product was recrystallized from $CHCl_3$ to yield 0.9 g (77%) of 2, 4-bis [4-(*N, N*-di-n-propylamino)-2-hydroxyphenyl] squaraine as green crystals. M.P =221°C. ^{1}H NMR 300 MHz (δ ppm TMS, $CDCl_3$) : 0.98 (m, 12H, CH_3), 1.68 (m, 8H, CH_2), 3.33 (q, 8H, CH_2), 6.12 (d, J = 3 Hz, 2H), 6.33 (dd, J = 3 Hz), 7.89 (d, J = 3 Hz, 2H), 8.04 (d, J = 9 Hz, 2H). ^{13}C NMR (δ ppm TMS, $CDCl_3$): δ 12.24, 21.5, 52.0, 98.51, 109.8, 114.4, 132.9, 156.4, 164.8, 173.0, 184.2.

2, 4-Bis [4-(*N, N*-di-n-butylamino)-2-hydroxyphenyl] squaraine (SQC4OH).

3-(Di-n-butylamino)phenol (0.5 g, 2.26 mmol) was added to 3, 4-dihydroxy-3-cyclobutane-1, 2-dione (0.129 g, 1.13 mmol) in 20 mL of 1:1 butanol and toluene. After 6 h of reflux, the reaction mixture was cooled to room temperature, obtaining the product as a precipitate. The solvent was removed on a rotary evaporator *in vacuo* and the product was recrystallized from $CHCl_3$ to yield 0.4 g (80%) of 2, 4-bis [4-(*N, N*-di-n-butylamino)-2-hydroxyphenyl] squaraine as green crystals. M.P = 196 °C. ^{1}H NMR 300 MHz (δ ppm TMS, $CDCl_3$) : 0.98 (m, 12H, CH_3), 1.16 (m, 8H, CH_2), 1.68 (m, 8H, CH_2), 3.33 (q, 8H, CH_2), 6.11 (d, J = 3 Hz, 2H), 6.31 (dd, J = 3 Hz) 7.88 (d, J

= 3 Hz, 2H), 8.03 (d, *J* = 9 Hz, 2H). ^{13}C NMR (δ ppm TMS, $CDCl_3$) : δ 12.64, 21.8, 25.8, 51.2, 98.31, 109.0,113.4, 132.6, 156.2, 164.3, 172.7, 180.2.

2, 4-Bis [4-(*N, N*-(di-n-pentylamino)-2-hydroxyphenyl] squaraine (SQC5OH).

Preparation of the precursor, 3-(di-n-pentylamino)phenol. 3-Aminophenol (5 g, 46 mmol) was dissolved in 20 mL of acetonitrile in a two-neck bottom flask, equipped with a condenser, followed by addition of 1-bromoheptane (11.0 g, 73 mmol). The mixture was refluxed for 48 h in the presence of sodium carbonate (5 g, 47 mmol) as catalyst. The reaction was cooled to room temperature and the catalyst was filtered using gravity filtration. The solvent was evaporated using rotary evaporator and the oily product was purified over silica as stationary phase using 1:2 ratio of mixture of ethyl acetate: hexanes as the mobile phase, resulting in orange viscous oil Yield 48%. ^{1}H NMR 500 MHz (δ ppm TMS, $CDCl_3$): 1.00 (m, 6H, CH_3), 1.30 (m, 4H, CH_2), 1.60 (m, 4H, CH_2), 3.23 (m, 4H, CH_2), 6.09-6.22 (m, 4H, Ar–*H*), 7.03 (m, 1H, Ar–*H*). ^{13}C NMR (δ ppm TMS, $CDCl_3$) 14.2, 22.1, 28.1, 29.3, 53.1, 98.8, 107.2, 109.3, 131.7, 152.1, 160.6.

Preparing SQC5OH, 3-(Di-n-pentylamino)phenol (2.66 g, 11.2 mmol) was added to 3, 4-dihydroxy-3-cyclobutane-1, 2-dione (0.7 g, 6.1 mmol) in 20 mL of 1:1 butanol and toluene. After 7 h of reflux, the reaction mixture was cooled to room temperature, obtaining the product as a precipitate. The solvent was removed on a rotary evaporator *in vacuo* and the product was recrystallized in $CHCl_3$ to yield 1.02 g (60%) of 2, 4-bis [4-(*N, N*-di-n-pentylamino)-2-hydroxyphenyl] squaraine as bright yellowish to greenish crystals. M.P= 185°C. ^{1}H NMR 300 MHz (δ ppm TMS, $CDCl_3$): 0.94 (m, 12H,CH_3), 1.18 (m,8H,CH_2), 1.34 (m, 8H, CH_2), 1.62 (m, 8H, CH_2), 3.36 (m, 8H, CH_2), 6.1 (d, *J* = 3 Hz, 2H), 6.3 (dd, *J* = 3 Hz), 7.87 (d, *J* = 3 Hz, 2H),

8.01 (d, *J* = 9 Hz, 2H). ^{13}C NMR (δ ppm TMS, $CDCl_3$) : 13.85, 22.03, 26.91, 28.84, 51.57, 98.24, 107.37, 109.31, 132.5, 155.49, 163.8, 172, 183. LCMS: Theoretical M^+ = 576.3922, found M/z = 576.3895.

2, 4-Bis [4-(*N, N*-di-n-hexylamino)-2-hydroxyphenyl] squaraine (SQC6OH).

Preparation of the precursor, 3-(di-n-hexylamino)phenol. 3-Aminophenol (2.5 g, 23.0 mmol) was dissolved in 20 mL of acetonitrile in a two-neck bottom flask, equipped with a condenser, followed by addition of 1-bromoheptane (7.6 g, 46 mmol). The mixture refluxed for 48 h in the presence of sodium carbonate (5 g, 47 mmol) as catalyst. The reaction was cooled to room temperature and the catalyst was filtered using gravity filtration. The solvent was evaporated using rotary evaporator and the oily product was purified over silica as stationary phase using a 1: 2 ratio of mixture of ethyl acetate: hexanes as the mobile phase, resulting in orange viscous oil Yield: 50%. ^{1}H NMR 300 MHz (δ ppm TMS, $CDCl_3$): 0.89 (m, 6H, CH_3), 1.30 (m, 4H, CH_2), 1.47 (m, 4H, CH_2), 1.62 (m, 4H, CH_2), 3.20 (m, 4H, CH_2), 6.09-6.20 (m, 4H, Ar–*H*), 7.03 (m, 1H, Ar–*H*). ^{13}C NMR (δ ppm TMS, $CDCl_3$): 14.0, 22.5, 26.8, 29.6, 31.4, 52.0, 98.4, 106.9, 108.5, 131.9, 151.2 159.0.

Preparation of SQC6OH, 3-(Di-n-hexylamino)phenol (1.3 g, 4.7 mmol) was added to 3, 4-dihydroxy-3-cyclobutane-1, 2-dione (0.44 g, 3.86 mmol) in 20 mL of 1:1 butanol and toluene. After 6 h of reflux, the reaction mixture was cooled to room temperature, obtaining the product as a precipitate. The solvent was removed on a rotary evaporator *in vacuo* and the product was recrystallized in $CHCl_3$ to yield 1.2 g (81%) of 2, 4-bis [4-(*N,N*-dihexylamino)-2-hydroxyphenyl] squaraine as shinny green crystals. M.P= 135°C. ^{1}H NMR 300 MHz (δ ppm TMS, $CDCl_3$): 0.93

(m, 12H, CH_3), 1.32 (m, 24H, CH_2), 1.63 (m, 8H, CH_2), 3.36 (q, 8H, CH_2), 6.10 (d, J = 3 Hz, 2H), 6.32 (dd, J = 3 Hz), 7.88 (d, J = 3 Hz, 2H), 8.00 (d, J = 9 Hz, 2H). ^{13}C NMR (δ ppm TMS, $CDCl_3$): 13.6, 22.3, 26.4, 31.5, 51.04, 98.5, 107.4, 109.8, 132.3, 156.0, 163.8, 164.5, 171.2, 173.1, 182.6. LC MS: Theoretical M^+ = 632.4548, found M/z = 632.4537.

2, 4-Bis [4-(*N, N*-di-n-heptylamino)-2-hydroxyphenyl] squaraine (SQC7OH)

Preparation of the precursor, 3-(di-n-heptylamino)phenol. 3-Aminophenol (2.0 g, 22.9 mmol) was dissolved in 20 mL of actonitrile in a two-neck bottom flask, equipped with a condenser, followed by addition of 1-bromoheptane (5.7 g, 45.8 mmol). The mixture was refluxed for 48 h in the presence of sodium carbonate (5 g, 47 mmol) as catalyst. The reaction was cooled to room temperature, and the catalyst was filtered using gravity filtration. The solvent was evaporated using rotary evaporator, and the oily product was purified over silica as stationary phase using 1:2 ratio of mixture of ethyl acetate:hexanes as the mobile phase; resulting in red viscous oil Yield: 55%. ^{1}H NMR 300 MHz (δ ppm TMS, $CDCl_3$): 0.89 (m, 6H, CH_3), 1.24 (m, 12H, CH_2), 1.27 (m, 8H, CH_2), 2.12 (m, 4H, CH_2) 3.19 (m, 4H, CH_2) 6.08-6.20 (m, 4H, Ar–H), 7.03 (m, 1H, Ar–H). ^{13}C NMR (δ ppm TMS, $CDCl_3$): 14.3, 22.2, 26.2, 28.1, 29.1, 31.2, 52.1, 98.6, 107.2, 108.4, 131.5, 160.1.

Preparation of SQC7OH, 3-(Di-n-heptylamino)phenol (2.08 g, 7.56 mmol) was added to 3, 4-dihydroxy-3-cyclobutane-1, 2-dione (0.39 g, 3.4 mmol) in 20 mL of 1:1 butanol and toluene. After 6 h of reflux, the reaction mixture was cooled to room temperature, obtaining the product as a precipitate. The solvent was removed on a rotary evaporator *in vacuo* and the product wad recrystallized from $CHCl_3$ to yield 1.4 g (60%) of 2, 4-bis [4-(*N,N*-diheptylamino)-2-

hydroxyphenyl] squaraine as bright yellowish to greenish crystals. M.P= 119°C. ^{1}H NMR 300 MHz (δ ppm TMS, $CDCl_3$): 0.90 (m, 12H, CH_3), 1.32 (m, 32H, CH_2), 1.60 (m, 8H, CH_2), 3.37 (q, 8H, CH_2), 6.11 (d, *J* = 3 Hz, 2H), 6.31 (dd, *J* = 3 Hz), 7.88 (d, *J* = 3 Hz, 2H), 8.03 (d, *J* = 9 Hz, 2H). ^{13}C NMR (δ ppm TMS, $CDCl_3$) : 14.29, 22.3, 26.4, 27.8, 29.3, 31.5, 51.6, 98.7, 107.4, 109.6, 131.8, 156.0, 163.5, 164.0, 171.7, 173.1, 182.6. LCMS: Theoretical M^+ = 688.5174, found M/z = 688.5189.

1.5 **Conclusions**

The alkyl chain in the series of squaraine compounds exerts a profound effect on the properties of these dyes. For each carbon atom added to each chain, a new behavior is revealed that is manifested in different crystalline structures and thermotropic phase transitions

Derivatives with four (**SQC4OH**) and seven (**SQC7OH**) carbon alkyl chains triggered the formation of two liquid crystalline mesophases (nematic and smectic) as determined by DSC, PLM, and X-ray studies. The LC assembly was most likely influenced by the unique C-O dipole-dipole interactions between these squaraine molecules, resulting in a new class of liquid crystals based on the squaraine molecular structure.

CHAPTER 2. **SELF-ASSEMBLY IN THE MICROCRYSTALLINE STATE AND PHOTOPHYSICAL PROPERTIES**

2.1 **Abstract**

Several of the squaraine derivatives formed H- and/or J-aggregates upon thin film formation via spin coating before and after thermal annealing, as indicated by UV-vis spectroscopy. The molecular structure, crystal structure, aggregation, and thermal behavior provide insight into the supramolecular assembly of this important class of materials. Photophysical measurements revealed large molar absorptivity, reasonably high fluorescence quantum yields, and significant fluorescence anisotropy, making these derivatives suitable candidates for a number of electro-optic and photonics applications.

2.2 **Aggregation in the Solid State**

Aggregation of squaraines in the microcrystalline state has been reported for squaraine structures bearing the N-pyrrolidine group for xerographic applications.[38,39] Spin casting of a symmetrical squaraine, 2,4-bis[4-(N,N-di-isobutylamino)-2,6-dihydroxyphenyl]squaraine, was investigated for enhancing the power conversion efficiency for photovoltaic cells.[40] Formation of a Langmuir-Blodgett film was utilized to study the aggregation of monolayers of select squaraines on the surface.[41-45] However, limited studies have been reported to systematically investigate the effect of molecular structure on the aggregation properties in solid state films.[24,46-48] Hence, we investigated the aggregation behavior of a series of squaraine compounds in the solid state (thin films) using a spin coating method on quartz substrates to probe the effect of the

peripheral alky chain on their aggregation behavior before and after thermal annealing, and correlate their aggregation properties with their crystalline structure. Exciton theory was used as a model to explain the shifts of the absorption band before and after the thermal annealing process.

Based on the molecular exciton theory, the angle observed between the long axis of the squaraine molecule and the straight line passing through the center of the molecular aggregates is called the slip angle and is considered essential in determining the type of aggregates, i.e., a large slip angle results in a parallel plane-to-plane stacking and formation of a sandwich-type arrangement (H-aggregate, blue shift) whereas a smaller slip angle results in end-to-end stacking and formation of a head-to-tail arrangement (J- aggregate, red shift).[49-51]

One can see from Figure 2-1 that, upon spin coating of **SQC3OH**, both large slip angles and smaller ones result in multiple H-aggregates at 503 nm and 566 nm and J-aggregates at 732 nm and 787 nm, compared with the monomer absorbance in $CHCl_3$ solution at 647 nm. After thermal annealing the vibrational and the rotational energies and collisions result in new state of equilibrium and new state of molecular arrangement manifested in a wider slip angle and formation of primarily of H- aggregates.

In Figure 2-2, a large slip angle appears dominant upon spin coating **SQC4OH**, resulting in prevailing H- aggregation at 546 nm. However, after thermal annealing, the slip angle became smaller, resulting in an H-aggregate shifted to a slightly longer wavelength (607 nm) triggering the formation of J-aggregates (767 nm).

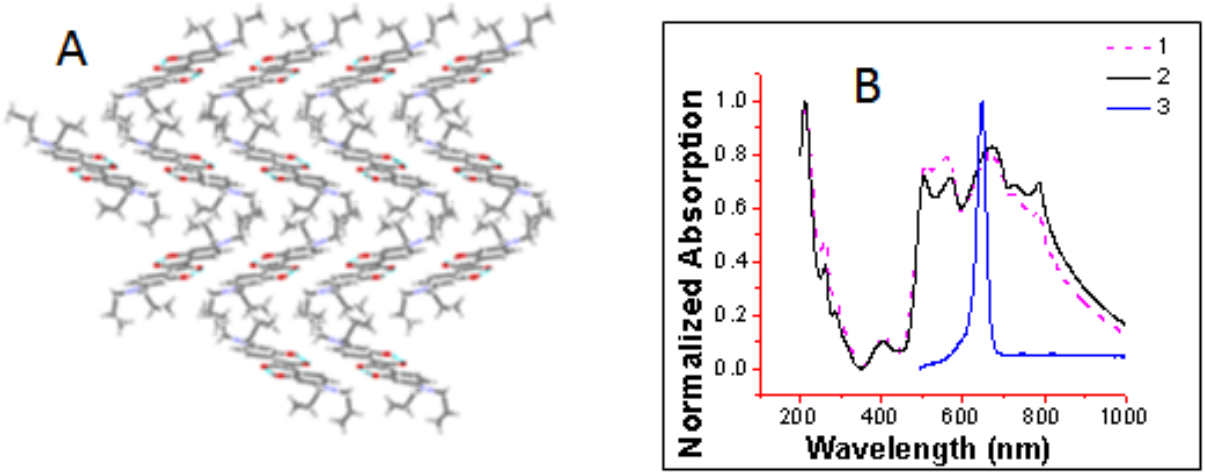

Figure 2-1. A) The crystalline packing of **SQC3OH** using single crystal X-ray diffraction data produced by Mercury 2.3. B) Comparison of the absorption spectra 1) after spin coating and thermal annealing, 2) after spin coating, and 3) in $CHCl_3$ solution, λ_{max} = 647 nm.

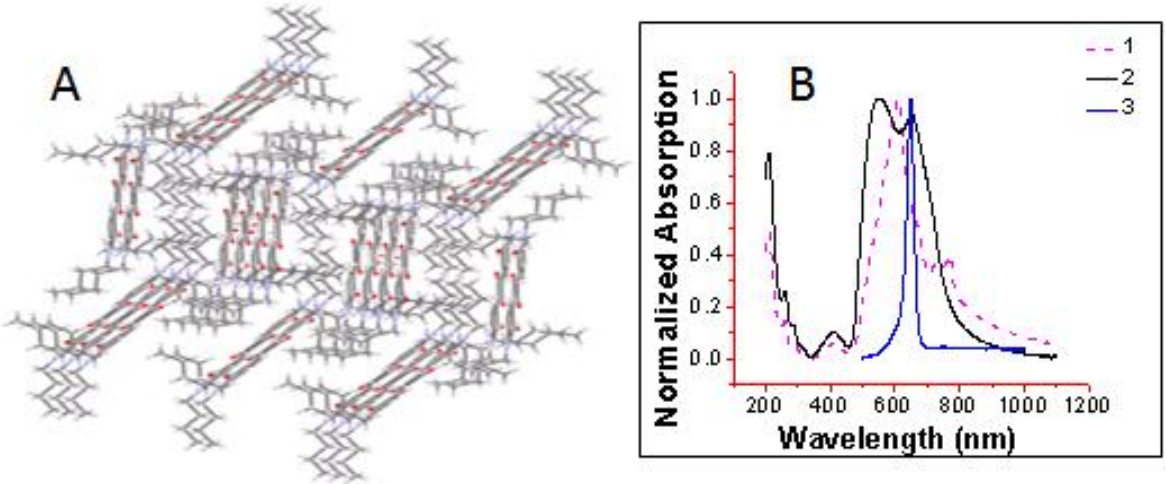

Figure 2-2. A) The crystalline packing of **SQC4OH** using single crystal X-ray diffraction data produced by Mercury 2.3. B) Comparison of the absorption spectra 1) after spin coating and thermal annealing, 2) after spin coating, and 3) in $CHCl_3$ solution, λ_{max} = 648 nm.

Similarly, **SQC5OH** underwent formation of H-aggregates upon spin coating (absorption at 537 nm) while the annealing process exerted little influence on the slip angle, resulting in shifting the H-aggregate absorption from 537 to 570 nm (Figure 2-3). Finally, both **SQC6OH** and **SQC7OH** tended to form H-aggregates in spin coated films before and after thermal annealing without any likely change in the slip angle (Figures 2-4 and 2-5). The presence of two types of parallel molecular arrangement in **SQC3OH**, **SQC4OH**, and **SQC5OH** and the formation of a 'zig zag' structure might account for the capability of the molecules to change the slip angle and shift the aggregation after thermal annealing. However, **SQC6OH** and **SQC7OH** possess only one type of parallel molecular arrangement, as can be seen from their crystalline structure, which may account for its inability to change the slip angle and alter aggregation after thermal annealing. These types of solid state aggregates may be advantageous in certain electro-optic applications, e.g., in enhancing both photovoltaic cell performance and efficiency.[52,53]

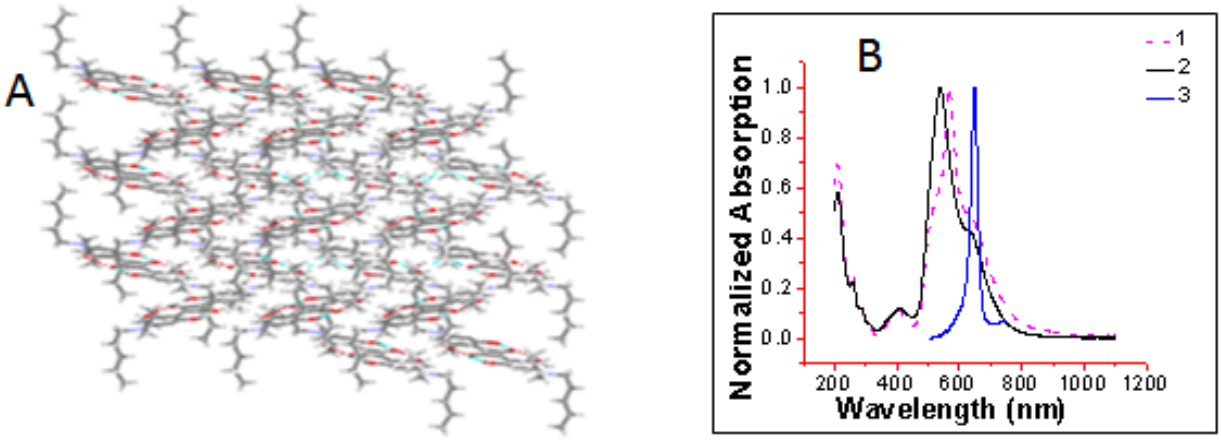

Figure 2-3. A) The crystalline packing of **SQC5OH** using single crystal X-ray diffraction data produced by Mercury 2.3. B) Comparison of the absorption spectra 1) after thermal annealing, 2) after spin coating, and 3) in $CHCl_3$ solution, λ_{max} = 648 nm.

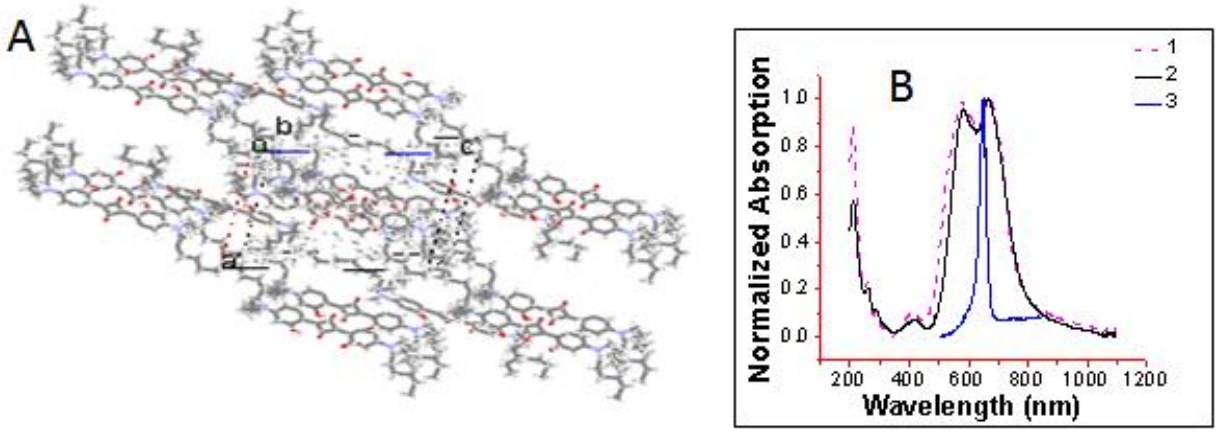

Figure 2-4. A) The crystalline packing of **SQC6OH** using single crystal X-ray diffraction data produced by Mercury 2.3. B) Comparison of the absorption spectra 1) after thermal annealing, 2) after spin coating, and 3) in $CHCl_3$ solution, λ_{max} = 650 nm.

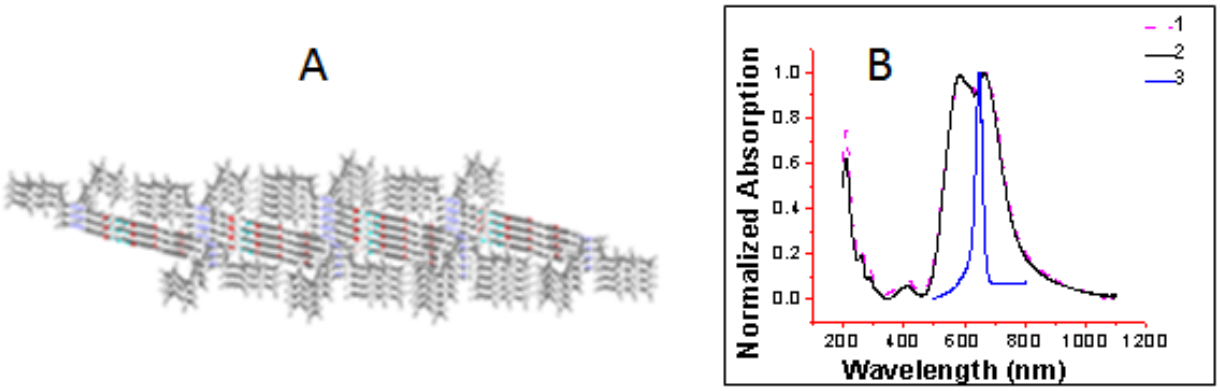

Figure 2-5. A) The crystalline packing of **SQC7OH** using single crystal X-ray diffraction data produced by Mercury 2.3. B) Comparison of the absorption spectra 1) after thermal annealing, 2) after spin coating, and 3) in $CHCl_3$ solution, λ_{max} = 653 nm.

2.3 **Photophysical Properties**

The absorption and fluorescence emission of several symmetrical and unsymmetrical squaraines with diverse molecular entities were reported.[37,54] Here, the photophysical properties for the series of squaraines based on 3-(di-n-alkylamino)phenol derivatives were investigated while exploring the possible effect of the peripheral alkyl chain on their photophysical properties. The series of the synthesized squaraine dyes were characterized by high molar absorptivity, small Stokes shifts, and relatively narrow absorption bands in solution, making this series particularly attractive for applications requiring narrow and specific excitation wavelength ranges.

Although the length of the peripheral alkyl group may slightly increase the electron-donating ability of the nitrogen atom, and, consequently, leading to an increase in the fluorescence quantum yield, this effect was negligible. Rather, we observed high fluorescence quantum yields for **SQC2OH** and **SQC3OH**, consistent with the literature and an increase in molecular rigidity for the short alkyl chain derivatives.[55] However, the rest of the series exhibited a moderate and nearly constant fluorescence quantum yield with no significant effect as a functional of alkyl chain length (Table 2-1). The reasonably high luminescence quantum yields suggest the potential of these dyes for bioimaging and lasing applications.

Table 2-1. The linear and nonlinear photophysical properties for the series of squaraine dyes.

	Molar Absorptivity, ε $LMol^{-1}Cm^{-1}X\ 10^4$	λ_{max} CH_3CN (nm)	Emission (nm)	Stock Shift (nm)	Fluorescence Quantum Yield
SQC2OH	17	640	654	14	0.73
SQC3OH	24	643	658	15	0.59
SQC4OH	20	645	660	15	0.42
SQC5OH	19	645	661	16	0.40
SQC6OH	24	645	662	17	0.38
SQC7OH	19	653	665	12	0.37

Steady state fluorescence excitation anisotropy is another important property measured for all members of the series. This technique often reveals important information regarding the electronic transitions and the molecule's rotational dynamics. A maximum excitation anisotropy value of 0.4 indicates perfectly collinear transition dipoles, i.e., the orientation of the absorption and emission transition dipole moment are parallel, which is in accord with a strong single low energy absorption band ($S_0 \rightarrow S_1$ transition).[56] The fluorescence anisotropy spectra for the series followed a consistent trend, as seen in Figure 2-6. They are characterized by a maximum excitation anisotropy value between 0.3-0.4, corresponding to $S_0 \rightarrow S_1$ transitions. Upon moving to shorter wavelengths, one encounters a change in the slope of the excitation anisotropy. At ca. 500 nm, a region where negligible absorption is observed, corresponds to a one-photon forbidden $S_0 \rightarrow S_2$ transition. At around 400 nm, a transition is observed, corresponding to higher energy $S_0 \rightarrow S_n$ transitions.

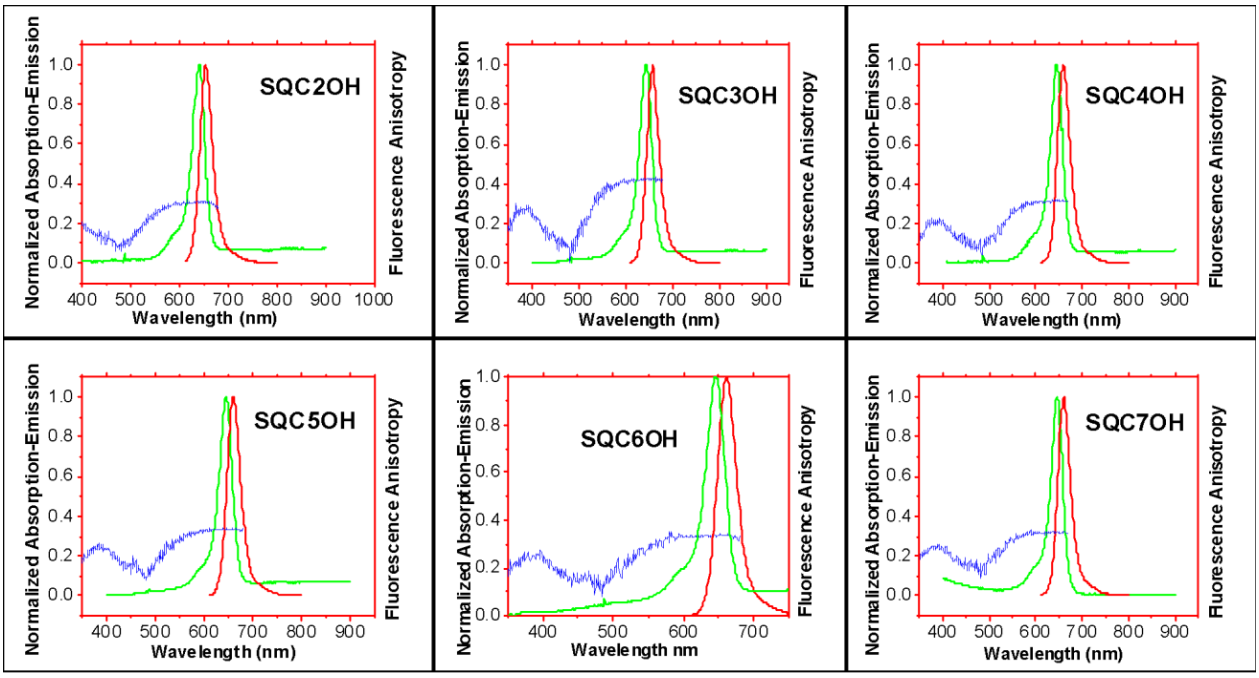

Figure 2-6. Normalized absorption-emission and steady state fluorescence excitation anisotropy for the total series. They are characterized by maximum excitation anisotropic value approximately between 3.0-4.0 corresponds to $S_0 \rightarrow S_1$ transitions. By moving further to lower wavelength and higher energies region, we start to encounter change in the slope of the excitation anisotropy; at around 500 nm, a region with negligible absorption is observed which correspond to one-photon forbidden $S_0 \rightarrow S_2$ transition. At around 400 nm, small absorption peak with high energy is observed correspond to $S_0 \rightarrow S_n$ transitions.

2.4 **Conclusion**

The difference in crystalline structures for each squaraine is evident during the aggregation in the microcrystalline state; only **SQC3OH**, **SQC4OH**, and **SQC5OH** formed H- and/or J- aggregates upon spin coating before and after thermal annealing owing to the presence of two types of parallel molecular arrangement and the formation of a 'zig zag' structure that may account for the capability of the molecules to change the slip angel and shift the aggregation after the annealing process. However, **SQC6OH** and **SQC7OH** exhibited only H-aggregation before and after annealing, possibly explained by having one type of parallel molecular arrangement as can be seen from their crystalline structure that accounts for its inability to change the slip angle and shift their aggregation after thermal annealing treatment.

Finally, the effect of the alkyl group on the photophysical properties in solution was less pervasive due to the similarity of the chromophore structure in all compounds. Derivatives **SQC2OH** and **SQC3OH** possessed higher fluorescence quantum yields relative to the other members of the series, likely due to their high rigidity. The photophysical measurements also revealed generally large molar absorptivity, luminescence quantum yields, and fluorescence anisotropy, making these squaraine derivatives particularly promising candidates for various electro-optic applications.

CHAPTER 3. **SELF-ASSEMBLY AND PHASE MORPHOLOGY OF SQUARAINE DYES IN THE LIQUID CRYSTALLINE MESOPHASE**

3.1 **Abstract**

The squaraine dye, 2, 4-bis [4-(*N,N*-di-n-hexylamino)-2-hydroxyphenyl]squaraine was synthesized and a series of squaraine dye/cholesteryl pelargonate binary mixtures with varying dye concentrations (1%, 3%, 7.5%, 10.8%, 15%, and 20% w/w) were prepared. Their phase transitions were investigated using differential scanning calorimetry, polarized light microscopy and X-ray diffraction. The squaraine dye itself exhibited no liquid crystalline behavior. The concentration of the dye in the cholesteric compound proved to have a significant effect on the dye aggregation behavior and phase transitions in cholesteryl pelargonate, resulting in the appearance of new phases and the formation of J- and H- aggregates. The texture morphology, X-ray diffraction data, and UV-vis absorbance spectra provide strong evidence of the viability of liquid crystal-directed assembly of a squaraine dye.

3.2 **Introduction**

The aggregation of the squaraine dyes in various systems has been reported in the literature, e.g., aggregation in solution,[32,37] polymers[57,58] and Langmuir-Blodgett film.[24,59] The aggregation of squaraines often leads to H- and/or J-aggregation, producing photophysical properties that are of interest in a number of fields such as second harmonic generating organic dyes, materials with large two-photon absorption cross section values, and photoconducting materials in photovoltaic cells.[1]

Liquid crystals are anisotropic materials that experience phase transitions when an external stimulus is applied. For example, when heat is applied to the crystalline phase, a change in the crystalline order occurs due to the rapid rotations of the long axis resulting in a loss of long range positional order with formation of a smectic phase characterized by short range positional order and diffuse layers. By applying more energy, the smectic phase can either lose all its order to become an isotropic liquid or lose only positional order while maintaining orientational order on the long axis to obtain the nematic phase..[60,61] By further heating, the orientational order can be disrupted, resulting in the isotropic phase. The smectic phase is basically viscous in nature while the nematic phase is more fluid. Different polymorphic smectic systems exist and can be either fluid smectic phases such as smectic A and smectic C and their chiral phases and subphases or form more ordered hexatic phases, such as smectic B, I, and F.[62,63] These phases can be identified by X-ray diffraction patterns and polarized light microscopy. Polarized light microscopy depends on the interaction of polarized light with the liquid crystalline mesophase; this interaction usually results in a characteristic texture for each phase attributed to several

factors such as defect topology,[64] surface anchoring ,deformation elasticity[65,66] and birefringence.[67,68]

In this work, a series of squaraine dye/cholesteryl pelargonate binary mixtures with varying dye concentrations were self-assembled in the liquid crystalline mesophase and their aggregation behavior was investigated using polarized light microscopy, X-ray diffraction, differential scanning calorimetry, and the absorption spectroscopy in an attempt to construct an aggregation model and grasp an insight and understanding into this type of new squaraine-mesophase system.

These squaraine-mesophase hybrid materials are advantageous since different aggregation types in the liquid crystalline mesophase can be obtained depending on the concentration of the dye in the fluid mesophases. Furthermore, by utilizing the properties of liquid crystals, switching the aggregation on and off using external stimuli, such as electric field, magnetic field, or pressure, may be feasible. Finally, the liquid crystalline mesophase most likely enhances the stability of the supramolecular aggregates owing to a host-guest recognition effect. The concept of slip angle, as demonstrated by the Frankel molecular exciton theory, is used as a model to explicate the shifts of the absorption band of the dye in the liquid crystalline mesophase towards J- or H- aggregates.[49-51]

Thus, a new aggregation system for a squaraine (SQ) dye based on liquid crystal-directed assembly is reported. Our intention was to dissolve and aggregate a squaraine dye in the liquid crystalline mesophase of cholesteryl pelargonate, a liquid crystalline (LC) materials that is characterized by both chiral nematic and smectic phases. The chiral nematic mesophase was identified by its macroscopic helical superstructure and recognized by oily streak texture when

observed by polarized light microscopy, while the smectic phase was distinguished by its focal conic texture. The LC-directed-assembly of the SQ dye was investigated using UV-vis absorption spectroscopy, X-ray diffraction, polarized light microscopy (PLM), and differential scanning calorimetry (DSC).

3.3 **Results and Discussions**

Binary mixtures of the squaraine dye 2, 4-bis [4-(*N,N*-di-n-hexylamino)-2-hydroxyphenyl]squaraine (**SQC6OH**) and cholesteryl pelargonate (a cholesteric liquid crystal), as shown in Chart 1, were prepared at various concentrations; 1, 3, 7.5, 10.8, 15, and 20%.

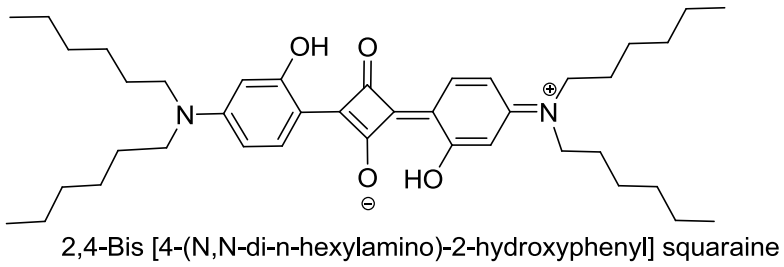

2,4-Bis [4-(N,N-di-n-hexylamino)-2-hydroxyphenyl] squaraine

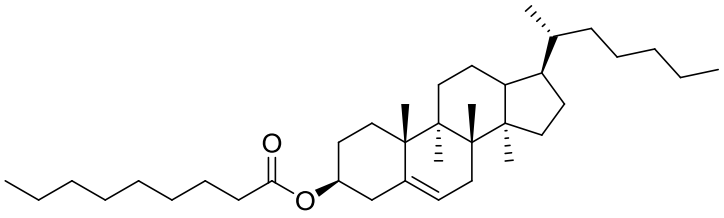

Cholesteryl Pelargonate

Figure 3-1. Structures of both 2, 4-bis [4-(*N,N*-di-n-hexylamino)-2-hydroxyphenyl]squaraine (**SQC6OH**) and the cholesteric liquid crystal, cholesteryl pelargonate.

Cholesteryl pelargonate is characterized by a smectic A phase between 55 ºC and 65 ºC and a cholesteric phase (chiral nematic) between 65 ºC and 78 ºC. Although the thermotropic behavior of cholesteryl pelargonate has been reported in the literature,[69-73] DSC measurements

(Figure 3-6), X-ray diffraction studies, and polarized light microscopy texture observations were performed for comparison and reference (Figure 3-2).

X-ray diffraction revealed the presence of the mesophases on the second cooling. The chiral nematic phase (cholesteric phase) was characterized by a relative narrow diffuse feature at about 0.24 $Å^{-1}$, which sharpens upon cooling to become a single smectic peak at 0.236 $Å^{-1}$, with a layer spacing of 26.6 Å. Although, in principle, a smectic phase can have a sequence of peaks in the ratio $q_1:q_2:q_3$ = 1:2:3, only the first order peak was apparent, an observation that is not uncommon.

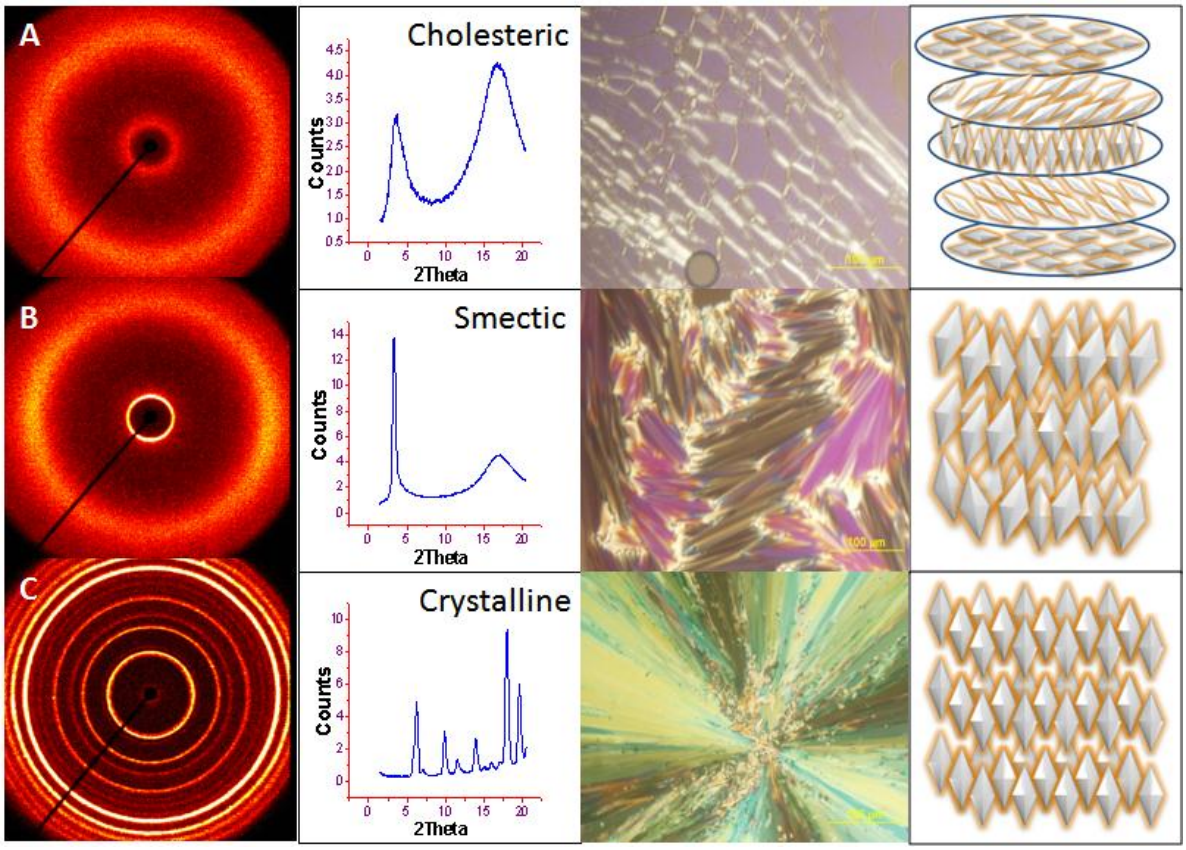

Figure 3-2. Phase transitions of cholesteryl pelargonate upon cooling the cholesteric phase. A) X-ray diffraction pattern for the cholesteric phase, the characteristic oily streaks texture as seen under PLM, and the schematic illustration of the helical superstructure of the cholesteric phase.

B) X-ray diffraction pattern for the smectic A phase, the characteristic feature of the focal conic texture as seen under PLM, and the schematic illustration of the diffuse layers of the smectic phase. C) Characteristic features of the crystalline phase.

Polarized light microscopy revealed two liquid crystalline phases, chiral nematic and smectic A. The chiral nematic phase appeared upon cooling and was identified by an oily streaks texture, a characteristic of the helical superstructure of the cholesteric phase; these oily streaks are a combination of both line defects within uniformly helical regions and elastic surface anchoring with edge dislocations. The smectic A phase is characterized by fan-shaped texture consisting of focal domains topology arranged in a pair of focal conics. Finally the crystalline phase was characterized by a spherulite morphology, as can be seen in figure 3-2.

To investigate the aggregation of the dye in the cholesteric liquid crystal six binary mixtures, varying in their dye content, were prepared and their thermotropic behavior was investigated by DSC, revealing the presence of phase transitions upon cooling as can be seen in figure 3-6, the recrystallization and melting peaks below 50ºC are attributed to the intrinsic properties of the cholesteric compound. The phase transitions were confirmed using polarized light microscopy table 3-1. In the binary mixture of one percent **SQC6OH**, the DSC data did not reveal any significant shift of the clearing point. Polarized light microscopy also did not detect the presence of any new phase. However, both the greenish oily streaks texture of the cholesteric phase and the greenish fan-shaped texture of the smectic A phase was observed. The appearance of greenish colored plates might be attributed to the birefringence and retardation effect of the dye while the blue color in figure 3-3B is a result of the selective reflection phenomena.

Figure 3-3. The phase transition of the mixture of 1% **SQC6OH** in cholesteryl pelargonate. A) The oily streaks texture of the cholesteric phase. B) The cholesteric phase during transition to the smectic A phase at 78 ºC, the color change is the result of selective reflection phenomena. C) The focal conic texture of the smectic A phase.

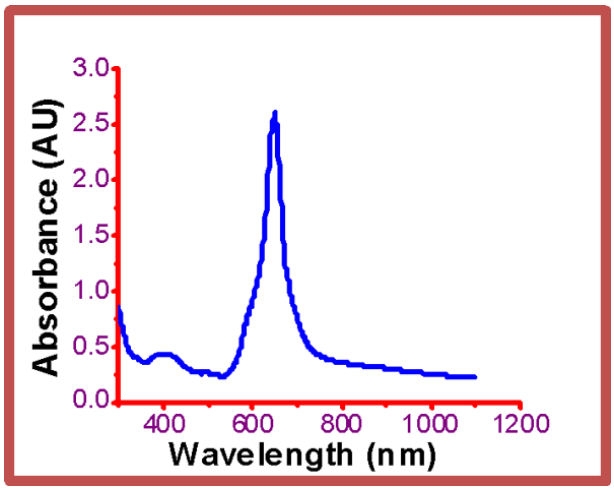

Figure 3-4. Both 1% and 3% dye in cholesteryl pelargonate mesophase revealed identical absorption bands with a 649 nm maximum, no aggregation behavior was observed for either of these binary mixtures.

A binary mixture of 3% of **SQC6OH** in cholesteryl pelargonate also did not reveal any aggregation behavior; both oily streak and smectic phase texture was observed. However, due to the deformations of the smectic phase during the sample preparation process, a polygonal texture of the smectic A phase was seen with half focal-conic domains (Figure 3-5B). When shear stress

was applied on the sample, what appeared to be a new smectic A texture was fashioned 3-5C most likely as a result of both splay, twist and bend distortions and bulk elasticity.

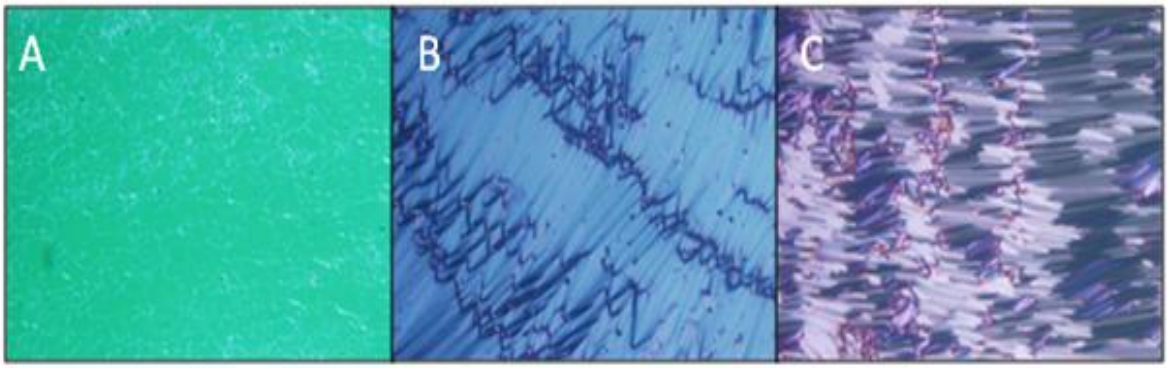

Figure 3-5. Texture morphology of the mixture of 3% dye in the cholesteric liquid crystal. A) The oily streak texture. B) A polygonal texture of the smectic A phase forming half focal conic domains. C) Deformed texture of the smectic A.

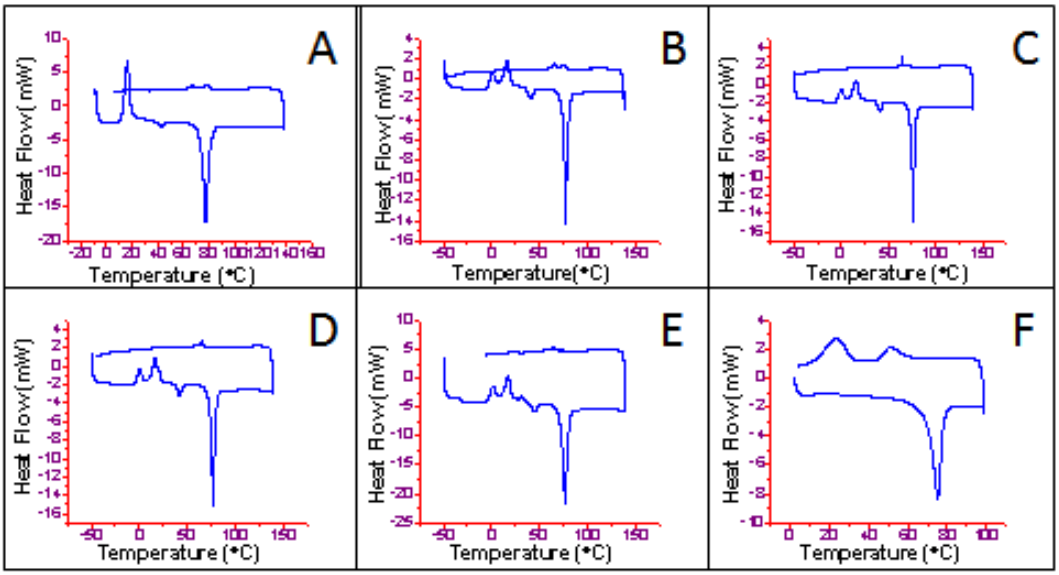

Figure 3-6. Differential scanning calorimetry for the mixtures of squaraine dye with cholesteryl pelargonate. A) Both pure cholesteryl pelargonate and the binary mixture of 1% dye in cholesteryl pelargonate revealed identical DSC thermogram. B) 3% dye in cholesteryl pelargonate. C) 7.5% dye in cholesteryl pelargonate. D) 10.8% dye in cholesteryl pelargonate. E) 15% dye in cholesteryl pelargonate. F) 20% dye in cholesteryl pelargonate. The phase transitions can be clearly seen upon cooling. The disappearance of the melting point at 135ºC of squaraine dye indicates complete miscibility of the dye in the mesophase.

Table 3-1. The thermotropic behavior for the series of **SQC6OH**-cholestryl pelargonate binary systems upon cooling. I: isotropic; N*: chiral nematic; SmA: smectic A; Sm B: smectic B; Cr: Crystalline.

Percentage SQC6OH in Cholesteryl Pelargonate	Phase Transitions for the Series of SQC6OH-Cholestryl Pelargonate mixtures upon cooling using PLM			
0% Dye	I-N* 78°C	N-SmA 65°C	SmA-Cr 55°C	
3% dye	I-N* 77.5°C	N-SmA 65°C	SmA-Cr 55°C	
7.5% dye	I-SmA 68°C	SmA-Cr 64°C		
10.8% dye	I-SmA 68°C	SmA-Cr 63°C		
15% dye	I-SmA 67°C	SmA-Cr 63°C		
20% dye	I-SmA 67°C	SmA-PhaseX 66°C	PhaseX-Cr_2 55°C	Cr_2-Cr 33°C

When 7.5% of the squaraine dye was dissolved in the cholesteric liquid crystal, DSC revealed a shift in the transition temperature due to an increase of the concentration of the dye in the liquid crystal (Figure 3-6C). X-ray investigation upon cooling (Figure 3-7) revealed the presence of a mesophase with a single peak at 0.2355 $Å^{-1}$ that may be ascribed to either a smectic phases with a layer spacing of $d=2\pi/q=26.7Å$ or a hexagonal columnar phase with an intercolumnar spacing of $d=2\pi/(q \cos 30)=30.8$ Å. The strong similarity in both the transition temperature and the peak position of the smectic phase seen in cholesteryl pelargonate suggests that it is most likely the same smectic phase, only slightly modified by the addition of the SQ dye. Miscibility of the SQ dye was likely due to both the host-guest recognition effect and intermolecular interactions.

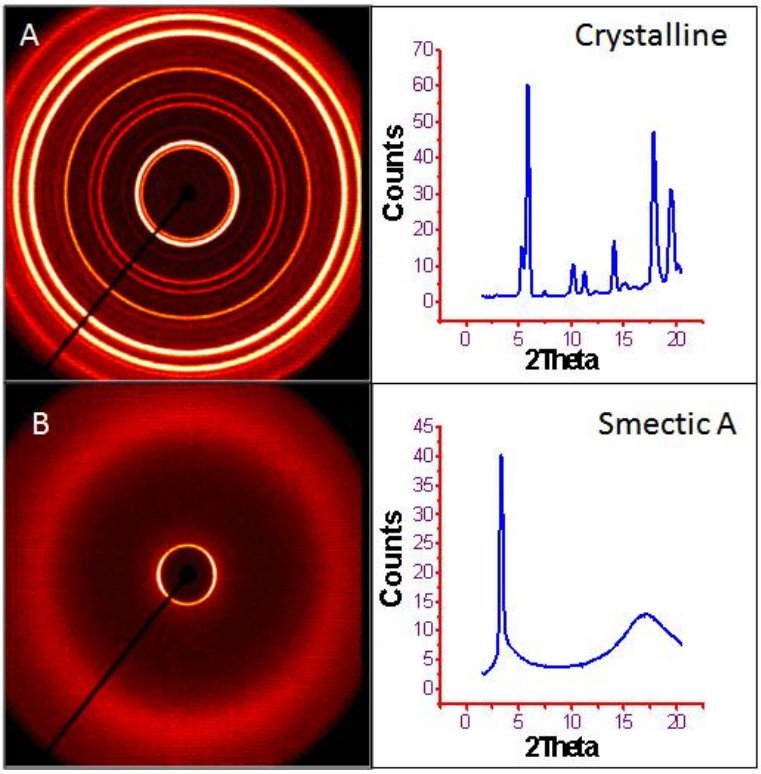

Figure 3-7. X-ray pattern for the crystalline phase (A) and the mesophase (B) for the binary system of 7.5% SQC6OH in cholesteryl pelargonate mesophase at 68 ºC.

The aggregation of the SQ dye in the smectic A mesophase manifests itself in both the texture morphology and the UV-vis absorption spectrum. The texture growth from the isotropic phase can be seen in figure 3-8A, 3-8B and 3-8C as a focal conic texture, the characteristic texture of smectic A. However, the cholesteric phase disappeared and no oily streaks morphology was observed. By cooling the mixture, the crystalline phase began to appear (Figures 3-8D and 3-8E). When the sample was annealed by sequential heating and cooling at the phase transition temperature, unusual texture morphology appeared as metastable "rotating petals", followed by recrystallization (Figure 3-8F). The UV-vis spectrum revealed a J-aggregate

band at 678 nm, indicating that the dye arranged itself within the smectic phase in a head-to-tail manner (characteristic of J-aggregation).

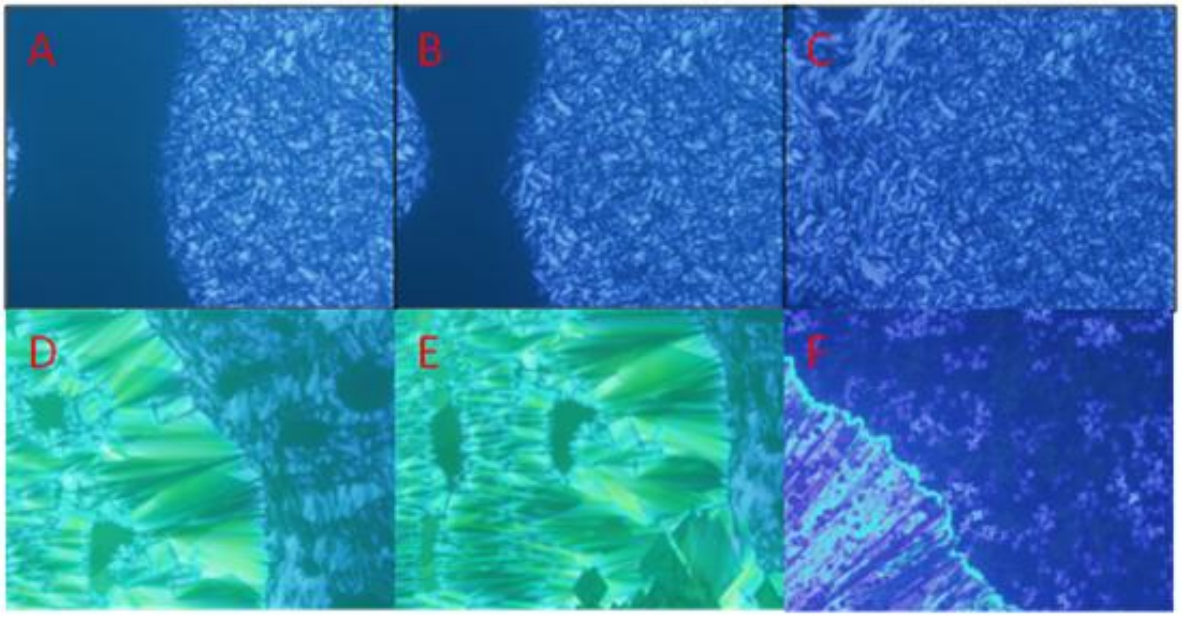

Figure 3-8. In A, B, and C the texture grows from the isotropic phase to form the focal conic texture, the characteristic texture of the smectic A mesophase. D and E represens smectic A to crystalline phase transitions. F) Metastable "rotating petals" followed by recrystallization.

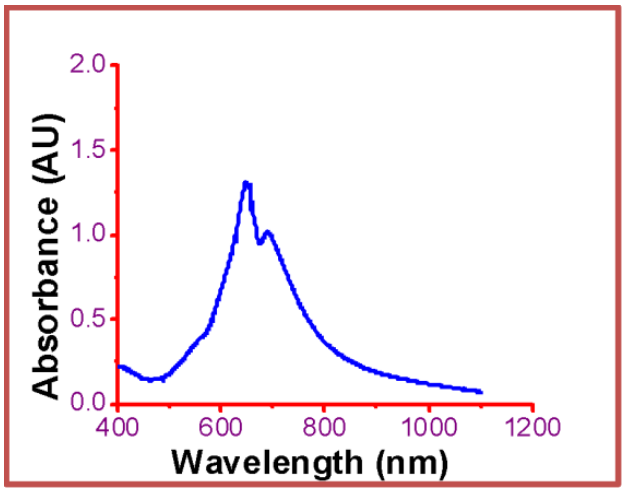

Figure 3-9. The appearance of J-aggregate band at 686 nm for the binary system of 7.5% of squaraine dye is in cholesteryl pelargonate mesophase.

Both the smectic A texture and the absorption band allowed us to build a model showing the arrangement of the dye within the smectic phase, as illustrated in Figure 3-10. In this model, the molecules in the smectic A phase are randomly arranged within the layer, their molecular axis is perpendicular to the plain of the layers, and the molecules rotate freely around their long axis.[74]

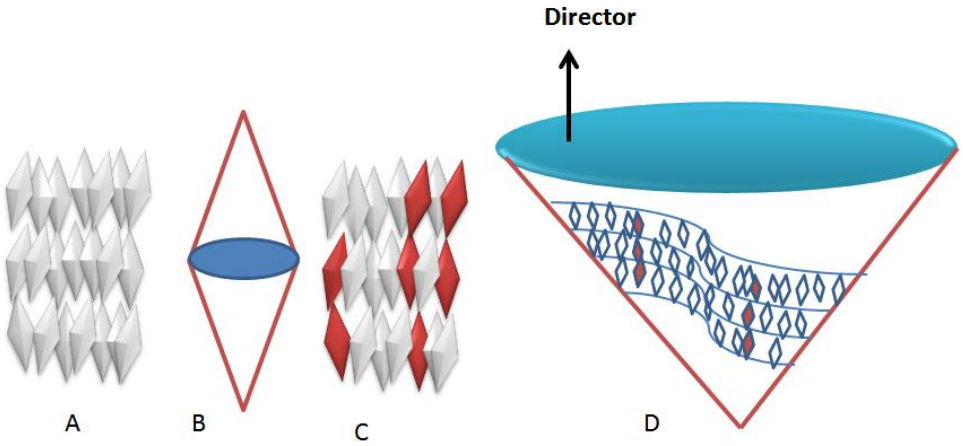

Figure 3-10. A) The molecules in the smectic A phase are randomly arranged within the layer, their molecular axis is perpendicular to the plain of the layers, and the molecules rotate freely around their long axis. B) The focal conic structure of the smectic A phase. C) The SQ dye is arranged head-to-tail in the mesophase. D) The arrangement of the SQ dye and the smectic layers within the focal conic model (for simplicity, half-focal conic picture is shown).

When 10.8% of **SQC6OH** is dissolved in cholesteryl pelargonate, we observe a new feature upon heating, with a sharp peak at 0.3756 $Å^{-1}$ superimposed upon a broad nematic-like maximum (Figure 3-11B). This structure is most likely described the low-temperature crystal phase of SQC6OH coexisting with a nematic liquid crystal phase. Upon heating, we again observe a mesophase with a peak at 0.228 $Å^{-1}$, almost certainly indicating the same smectic phase with a layer spacing of $d=2\pi/q=19.7Å$ that is observed in cholesteryl pelargonate.

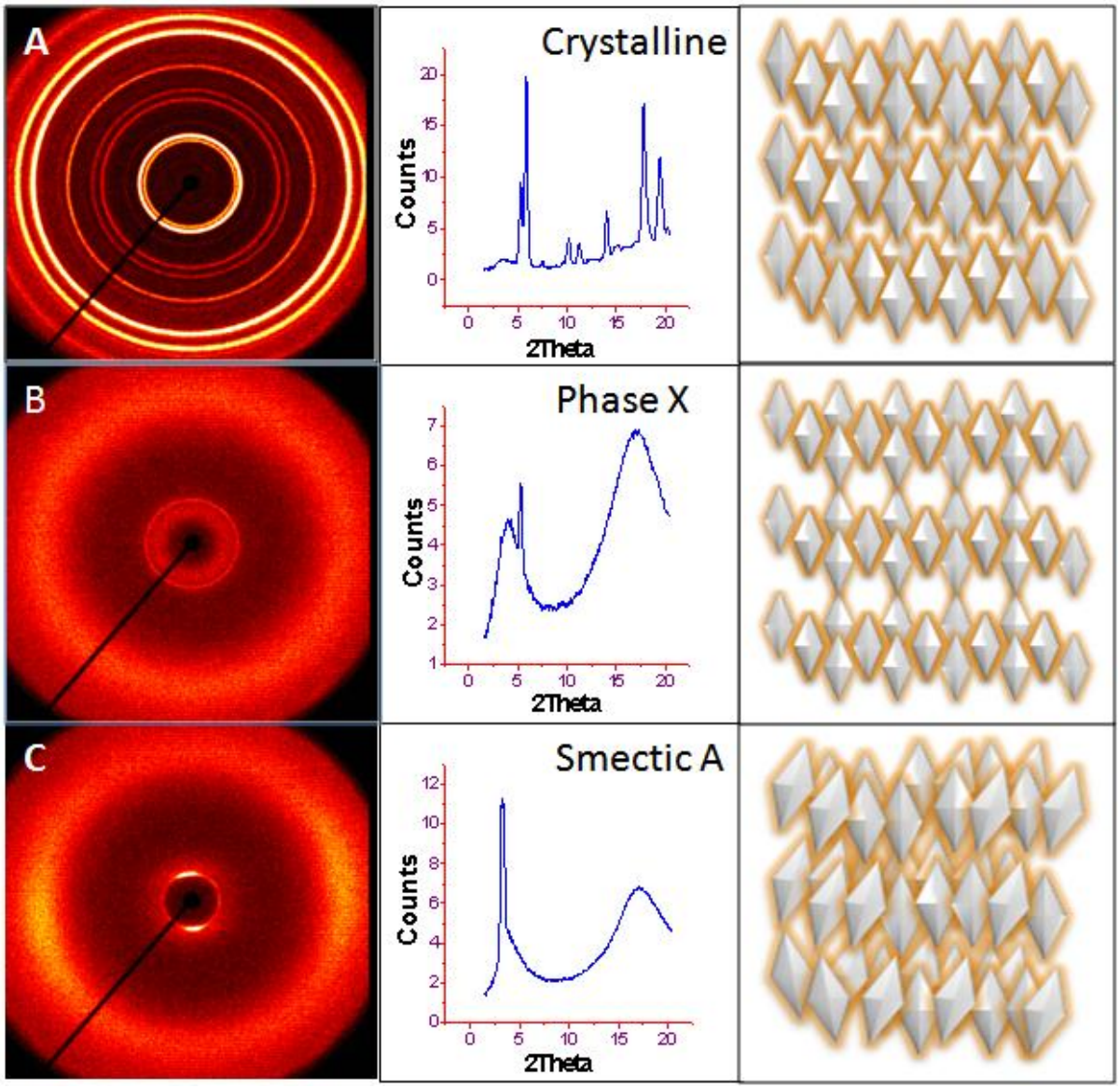

Figure 3-11. X-ray diffraction pattern of combination of 10.8% **SQC6OH** in cholesteryl pelarogate. A) The crystalline phase and its schematic arrangement. B) Phase X upon heating (coexist with nematic) and its schematic arrangement. C) Smectic phase A upon cooling and its schematic arrangement.

Polarized light microscopy also confirmed the presence of the mesophase as shown in figure 3-12. In figure 3-12A, the mesophase is characterized by a focal conic texture, where the bright texture regions may be attributed to dislocations emanating from an impurity. However,

Figure 3-12B exhibits the transition of the smectic A phase to the crystalline phase. In figure 3-12C, a stable texture of "rotating petals" appears as a result of the interaction of the polarized light with the optical axis of the phase morphology. This phenomenon can be explained as follows: when an incident beam of polarized light enters the mesophase of thickness placed between polarized and analyzer, the polarized light splits into two waves; extraordinary n_e and ordinary n_0 waves. Their polarization and amplitude are perpendicular to each other and propagate within the mesophase at different velocities, exiting the sample with different electric vibrations that result in a phase difference. The resultant intensity of the light transmitted out of the sample is given by:

$$I = I_0 \sin^2 2\beta \sin^2 \left[\frac{2\pi}{\lambda}(n_e - n_0)d\right]$$

Where I is the transmitted light, I_0 is the incident light, and β is the angle formed between the molecular optical axis, during the planar alignment, and either the polarizer or the analyzer. When the angle β is either zero or 90º, parallel to either the polarizer or the analyzer, the result is minimum transmitted intensity as observed by the dark fans in figure 3-13, while the bright fans present maximum transmitted intensity when the angle β equals 45º. These observations leads to the construction of a topological map representing the alignment of these molecules toward each other (Figure 3-13).

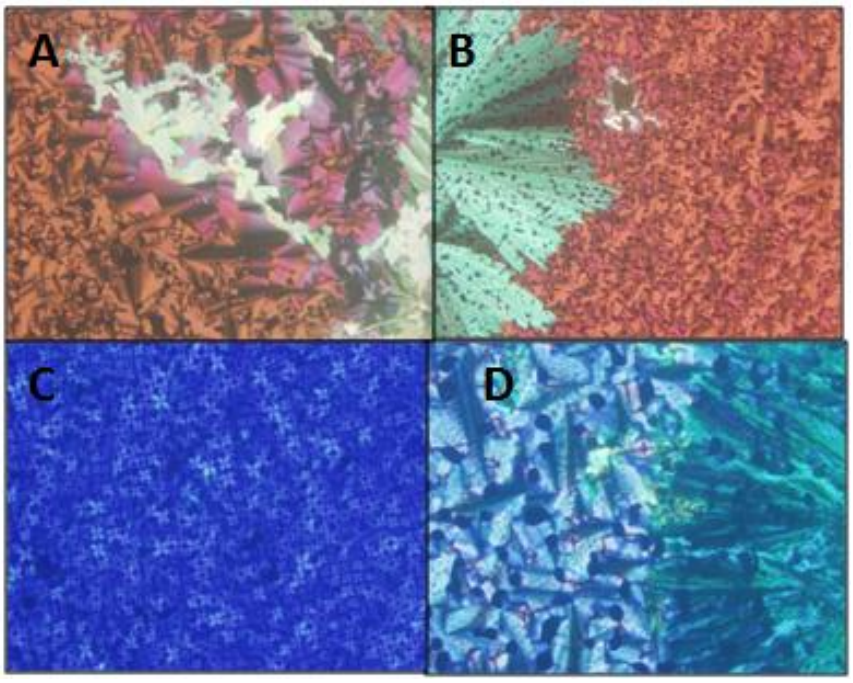

Figure 3-12. A) The mesophase is characterized by a focal conic texture; the bright texture regions may be attributed to dislocations emanating from an impurity. B) Transition of the smectic A phase towards the crystalline phase. C) Stable texture of "rotating petals". D) Tubular-like texture upon rubbing the sample (shear stress).

The absorption spectra of the smectic A texture revealed aggregation; the bathochromic shift from 649 nm to 703 nm of the absorption band indicates the presence of J-aggregate with SQ dye molecules arranged head-to-tail within the smectic layers based on the concept of the slip angle according to Frankel molecular exciton theory (Figure 3-14).

By applying shear stress on the sample by rubbing the slides, a new tubular-like texture appeared (Figure 3-12D). The absorption band of this texture revealed a small absorption at 847 nm, likely attributable to a J-aggregate band; the same texture also suggested the beginning of the transition to the crystalline phase.

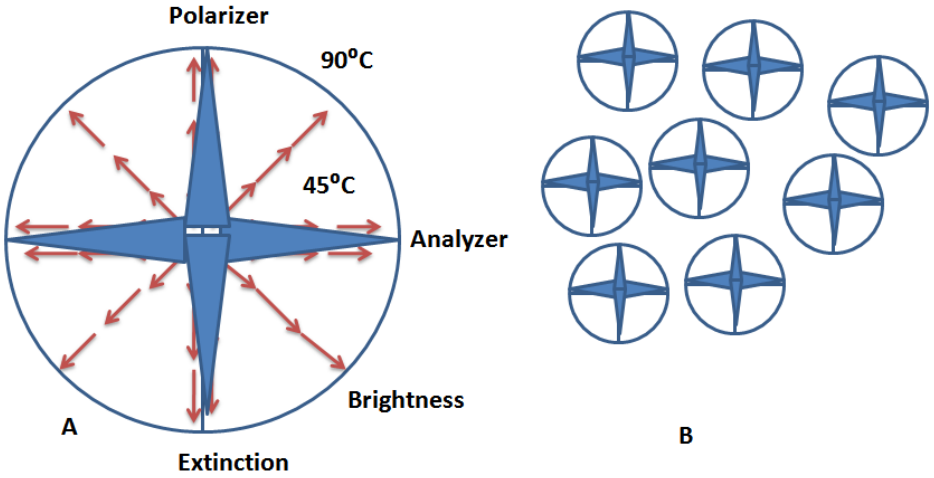

Figure 3-13. A) When the angle formed between the molecular optical axis (indicated as a small arrow) and the polarizer is either zero or 90°, the result will be a minimum transmitted intensity as you can see from the dark fans, while the bright fans present maximum transmitted intensity when the angle equals to 45°.B) A schematic presentation of the "rotating petals" under PLM.

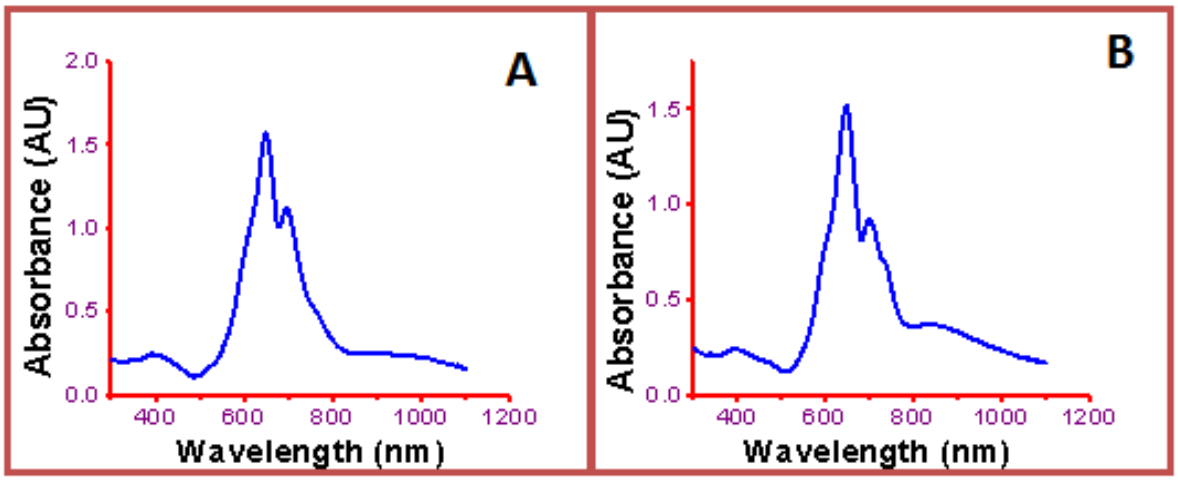

Figure 3-14. A) The absorption band of **SQC6OH** J-aggregate appears at 698 nm for the mixture of 10.8% **SQC6OH** in cholesteryl pelargonate mesophase. B) Upon applying shear stress by rubbing the slides, a new tubular-like texture appeared (Figure 12D); the absorption band of this texture revealed a small absorption at 847 nm, likely attributable to a J-aggregate band.

In the 15% **SQC6OH**/cholesteryl pelargonate mixture (Figure 3-15), we again observed the x-ray signature of phase X or crystal-nematic coexistence, with a sharp peak at $q=4\pi/\lambda=0.377$ $Å^{-1}$ superimposed on a diffuse maximum.. A mesophase was not observed upon cooling, but the signal levels were quite low due to sample flow, and this should not be considered proof of the lack of such a phase. Indeed, PLM confirmed the presence of a mesophase upon cooling, consistent with the previous smectic A characteristics (Figure 3-16).

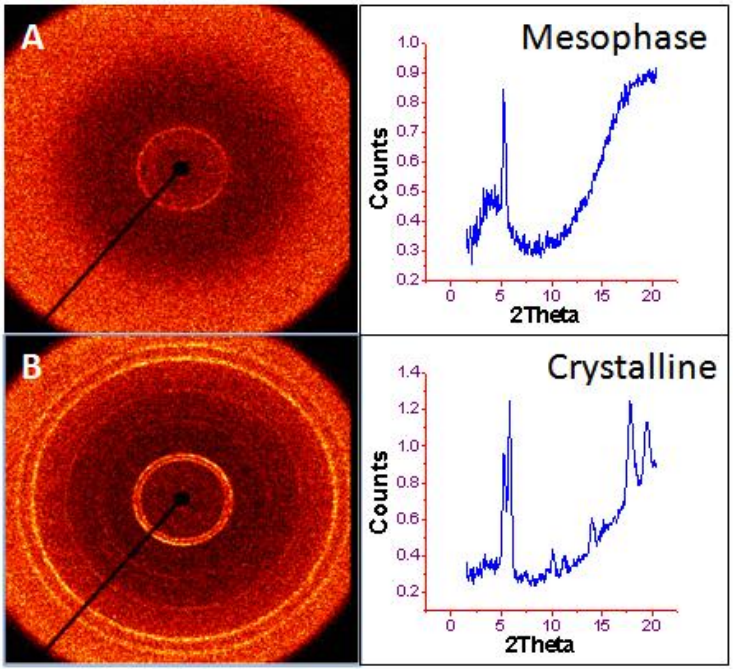

Figure 3-15. X-ray diffraction pattern for the binary system of 15% SQC6OH in the mesophase of cholesteryl pelarogate. A) Coexistence phases upon heating. B) The crystalline phase.

Polarized light microscopy clearly showed the "rotating petals" texture in Figures 3-16A and 3-16B, while figures 3-16C reveals the transition to the crystalline phase. Figures 3-16D, 3-16E and 3-16F represent different types of deformations of the focal conic texture of the smectic A phase when shear stress is applied.

The absorption spectra of the smectic A texture (Figure 3-17).revealed an aggregation with an absorption at 850 nm, the bathochromic shift is consistent with formation of a J-aggregate with dye molecules arranged head-to-tail within the smectic layers.

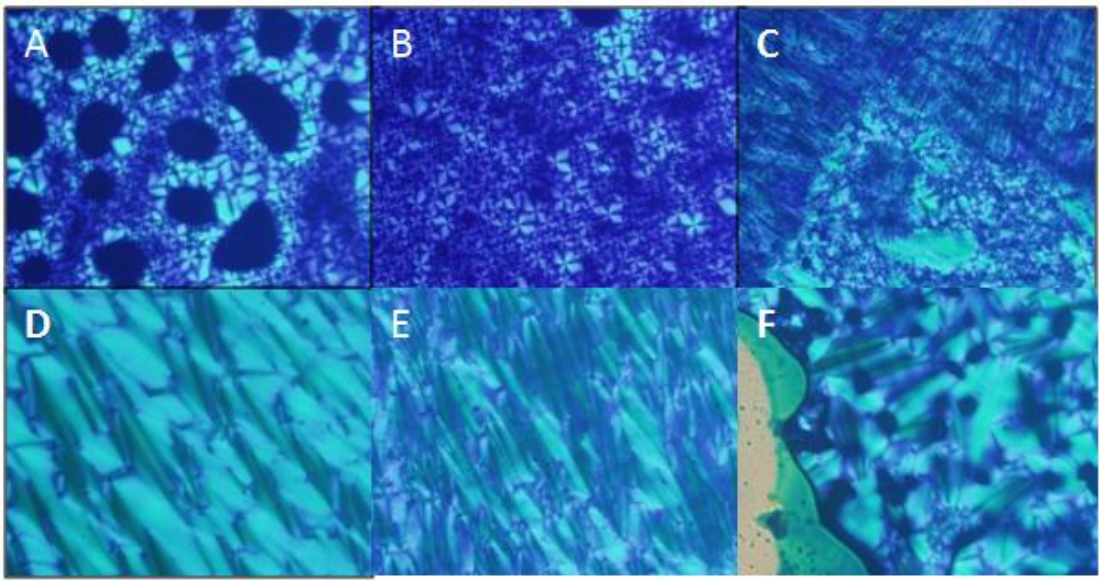

Figure 3-16. Polarized light microscopy images for 15% **SQC6OH** in cholesteryl pelarogate mesophase clearly showing the "rotating petals" texture in A and B, while the transition to the crystalline phase can be seen in C, D, E, and F represent different types of deformations of the focal conic texture of the smectic A phase when shear stress was applied.

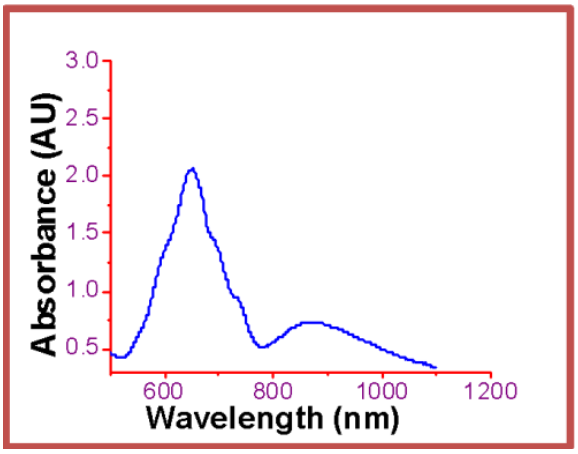

Figure 3-17. The absorption spectra for 15% **SQC6OH**/cholesteryl pelarogate mesophase. The spectrum exhibited small aggregate absorption bands at 698 nm and 741 nm and a major band at 850 nm.

In the 20% dye sample, X-ray measurements revealed a phase X (possibly crystalline-3) coexisting with a nematic or smectic phase on heating. On cooling, phase X was observed coexisting with a nematic phase, and then phase X coexisting with the mesophase or a crystal phase (Figure 3-18A) with peaks at 0.236 $Å^{-1}$ and 0.376 $Å^{-1}$. The observation in the 20% sample of higher-order peaks that are not either in the 1:2:3 ratio characteristic of a smectic phase or the $1:\sqrt{3}:2:\sqrt{7}$ ratio characteristic of a columnar phase, together with the observation of sharp spots at wide angle (Figure 3-17B), indicates that this is, in fact, a crystalline phase of some sort (Crystal-2), most likely coexisting with the cholesteric phase.

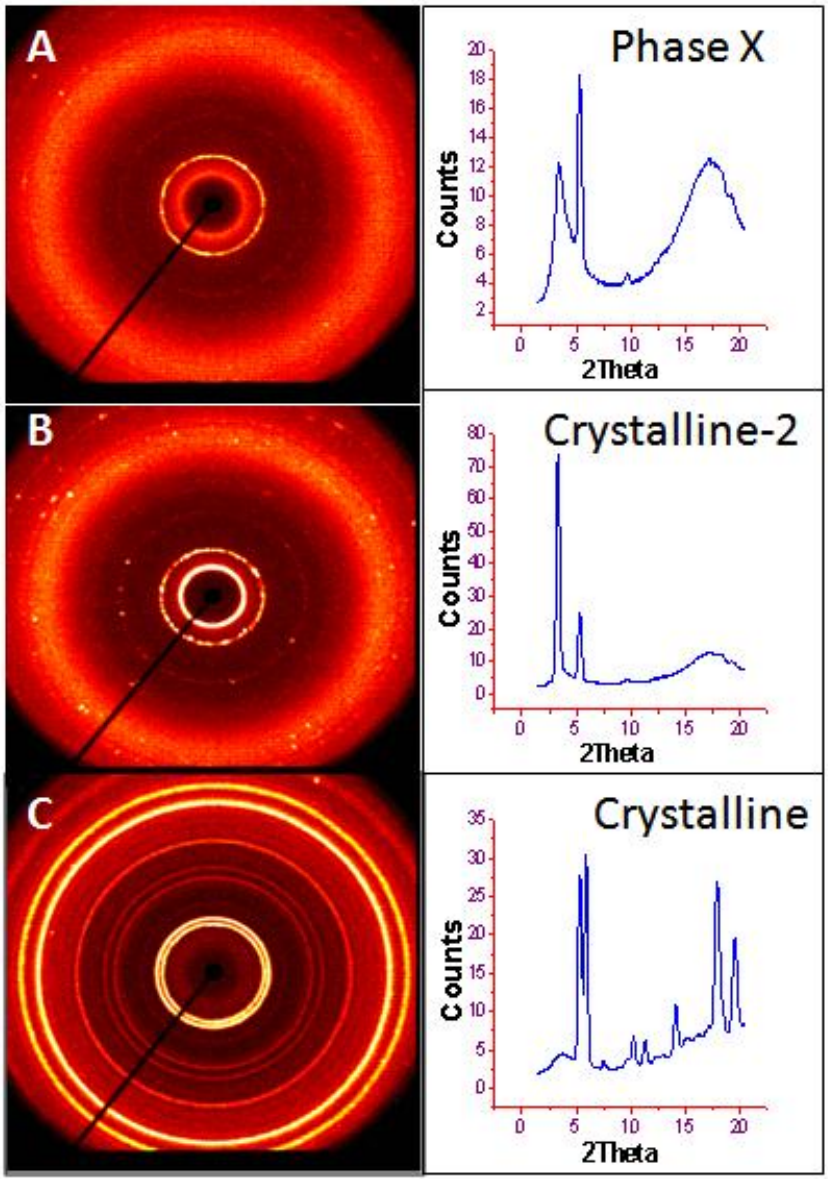

Figure 3-18. X-ray diffraction patterns of 20% **SQC6OH** in cholesteryl pelarogate. A) Phase X upon cooling. B) The appearance of Crystal-2 phase. C) The crystallinity of the phase was clearly demonstrated by the existence of sharp diffraction rings at wide angles as well as the replacement of powder rings by sharp spots after annealing, indicating the formation of relatively large individual crystallites.

Phase X is considered intermediate between the smectic A phase and the crystalline phase, it is highly likely to be considered as highly ordered smectic phase or crystalline-3 phase; In the

hexagonal closed-packed array model for such phases, the molecules are normally placed in layers and the molecular long axis is orthogonal to the layer planes.[74] The molecules also might rotate rapidly about the molecular axis (Figure 3-21).

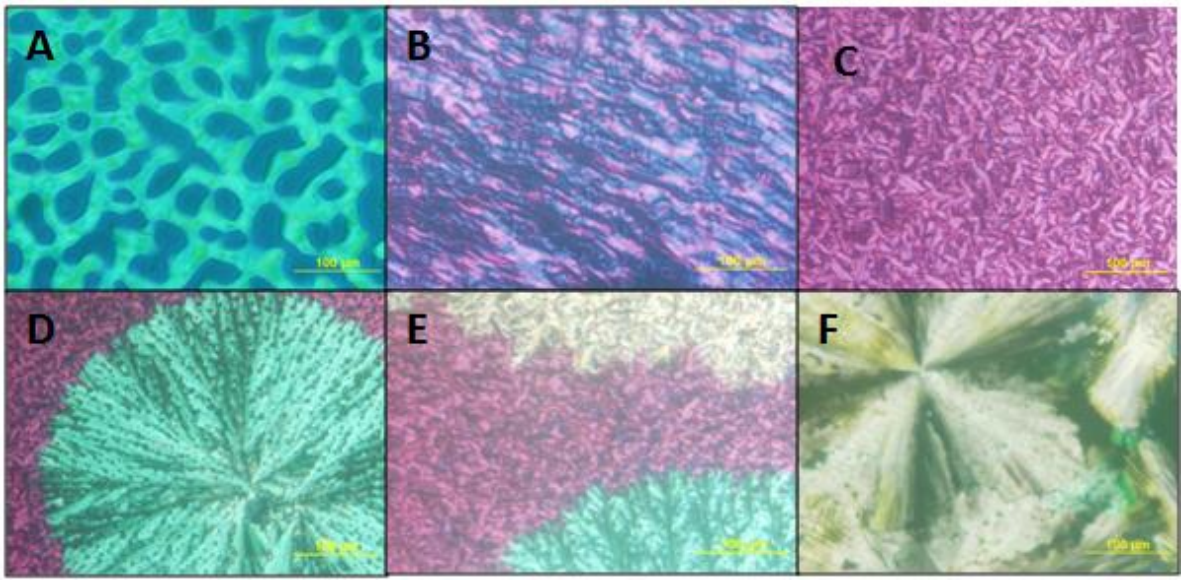

Figure 3-19. The phase transitions upon cooling a mixture of 20% SQC6OH in cholesteryl pelargonate mesophase. A) The transition of the isotropic liquid to the mesophase. B) The mesophase starts to fashion, forming the mosaic texture. C) Phase X at different thickness and birefringence. D) Phase X to crystal-2 phase transition. E) The presence of the three phases; Phase X, crystal-2 ,and the crystalline phase. F) Spherulite of the crystalline phase.

Polarized light microscopy observations were consistent with X-ray diffraction studies. The transition from the isotropic state to the mesophase can be seen in Figure 3-19A. The mesophase begins to form in figures 3-19B and 3-19C producing the texture of phase X. Figure 3-19D reveals the crystal-2 phase transition while figure 3-19E illustrates the presence of the three mesophases; phase X, crystal-2, and the crystalline phase. Finally, figure 3-19F shows the spherulite of the crystalline phase.

The absorption spectra (Figure 3-20) also revealed the presence of the aggregation in the Phase X. Both H- and J- aggregates start to appear when 20% w/w of of **SQC6OH** is incorporated in the smectic phase.

H-aggregates exhibit an absorption at 495 nm as a result of parallel plane-to-plane stacking and formation of a sandwich-type arrangement, which is a result of forming a large slip angle between the long axis of the SQ dye molecule and the straight line passing through the center of the molecular aggregates. This behavior can only be attained when the SQ dye molecules are situated within the crystalline or smectic short positional order layers of the the Phase X (Figure 3-21). However, J-aggregates were also detected with absorption bands at both 694 nm and 816 nm due to formation smaller slip angles between the long axis of the SQ dye molecule and the straight line passing through the center of the molecular aggregates, resulting in an end-to-end stacking and formation of head-to-tail arrangement, an occurrence only feasible when the SQ dyes are arranged in both the long orientational and positional order of the Phase X or the crystalline phases (Figure 3-21).

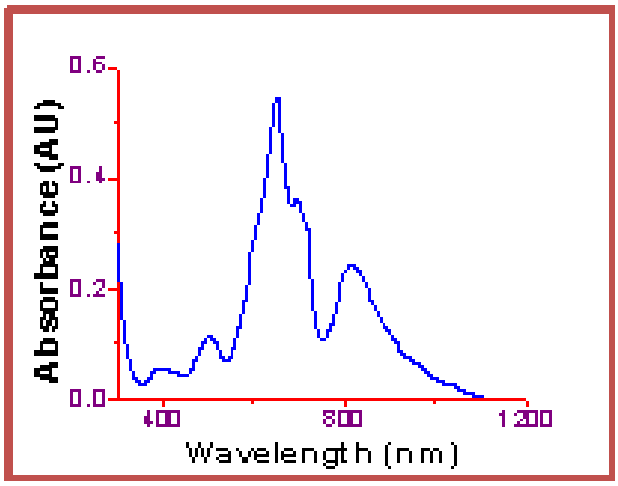

Figure 3-20. UV-vis absorption spectrum for 20% **SQC6OH** in cholesteryl pelargonate mesophase; H-aggregate absorption band appears at 495 nm while J-aggregate absorption can be seen at both 694 and 816 nm.

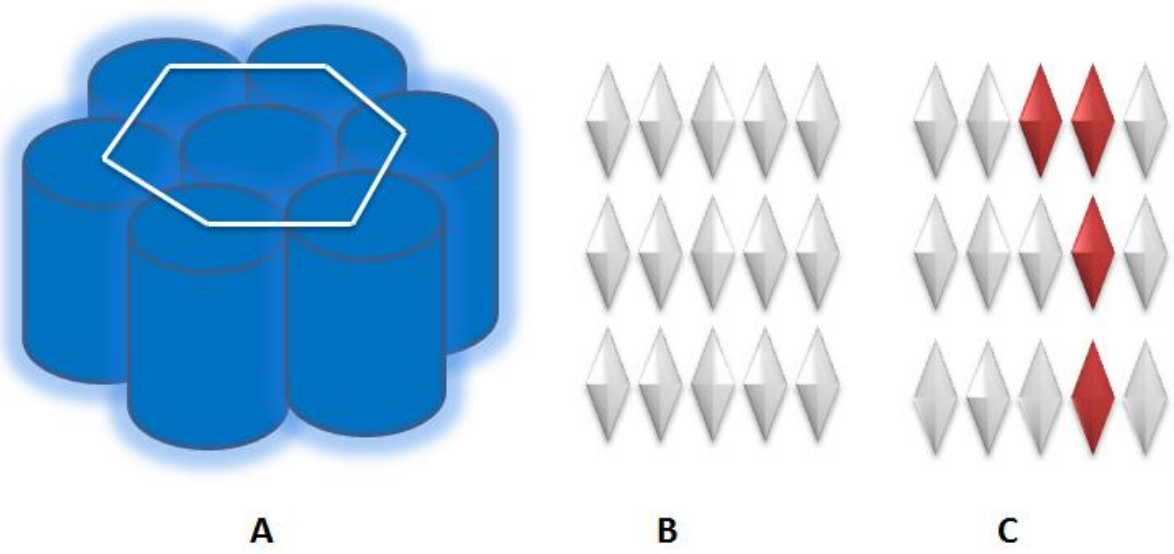

Figure 3-21. Schematic illustration of the aggregation model for 20% **SQC6OH** in the phase X. A) The proposed hexagonal arrangement of the phase X. B) Molecular arrangement in the phase X. C) Head-to-tail (J-aggregate) and plane-to-plane (H-aggregate) arrangement of the SQ dye in phase X.

3.4 **Experimental Section**

3.4.1 *Materials and Methods*

1-Bromohexane, aminophenol(99%), 3, 4-dihydroxy-3-cyclobutane-1,2-dione (99%), and cholesteryl pelargonate (cholesteryl nonanoate) were purchased from Acros Organics and Aldrich and used as received. 3-(N,N-di-n-hexylamino)phenol was prepared as previously reported. Thermogravimetric analysis (TGA) was performed using a TGA Q5000 thermogravimetric analyzer (TA Instruments) at a heating rate of 10 °C/min. The thermotropic behavior of all compounds was determined by a combination of differential scanning calorimetry (DSC) and the polarized light microscopy (PLM). A TA Instruments Q1000 differential scanning calorimeter was used to determine the thermal transitions during the heating and cooling cycles. All heating and cooling rates were 10 °C/min. while thermal transitions were read from reproducible second scans. An Olympus BX51 polarized optical microscope (magnification ×40) equipped with both a DP70 digital camera and an Instec HCS302 heating/cooling stage was used to detect and image the phase transitions by observing thin samples between a clean glass slide and a cover slip. Absorption measurements were performed using an Agilent 8453 UV-visible spectrophotometer. X-ray diffraction measurements employed a Bruker-Nonius FR591 fine-focus generator with a Cu target (λ=1.542 Å), Osmic confocal optics, and a Bruker HiStar wire detector. Measurements were carried out at a fixed sample-detector distance of 11 cm. The scattered intensity was recorded for scattering vectors in the range 0.2 $Å^{-1} \leq q (=4\pi \sin(\theta)/\lambda) \leq$ 1.7 $Å^{-1}$. Measurements were made between room temperature and the clearing point upon both heating and cooling. The heating and cooling rates were both 10 °C/min, and data were collected for 5 min at each temperature. Primary data analysis was performed using Datasqueeze

[reference: http://www.datasqueezesoftware.com]. ^{1}H and ^{13}C NMR analyses were performed in $CDCl_3$ (referenced to TMS at δ 0.0 ppm) on a Varian Gemini spectrometer (300 MHz for ^{1}H and 75 MHz for ^{13}C). High resolution LC-MS data were recorded in the Chemistry Department at the University of Florida.

3.5 **Conclusion**

Liquid crystal-directed aggregation of a squaraine dye was found to be an effective method of supramolecular assembly, as demonstrated by the appearance of H- and J- aggregate absorption bands. The concentration of the dye in the cholesteric compound proved to have a significant effect on the dye aggregation behavior and phase transitions in cholesteryl pelargonate, resulting in the appearance of new mesophases and the formation of J- and H-aggregates. DSC, PLM, and X-ray diffraction studies provide compelling support for the existence of mesophases, even at high **SQC6OH** levels. Models were proposed to explain the SQ dye aggregation in the LC mesophase. To the best of our knowledge, this study represents the first supramolecular assembly of squaraine-mesophase systems as a paradigm for H- and J-aggregate self-assembly. Considering the accessibility to the large number of liquid crystalline structures along with those that can be designed, a myriad of squaraine-mesophase entities can be generated, giving rise to new hybrid systems capable of combining the unique photophysical properties of both the liquid crystals and the squaraine dyes.

CHAPTER 4. **FUTURE PLANS**

Although the obtained results proved that aggregation of squaraines is viable method, further efforts can be done in order to enhance J-aggregation, and ultimately, to take maximum advantage of this system. In this chapter we discuss how this system can be improved, as well as further modifications that can be completed to improve the system.

4.1 **Improvements to the Aggregation by Spin Coating Method**

To enhance the J-aggregation behavior of the dye via spin coating method, the structures of our squaraine dyes can be modified to trigger the formation of a small tilt angle, e.g., SQC4OH can be modified by adding alkoxybenzoic acid to the phenolic group by an esterfication process (see Scheme 4-1). This modification will result in changing the planarity of the system. In addition, the length and branching of the alkyl group can be tailored, most likely will playing important role in changing the tilt angle and eventually enhancing the aggregation process.

Scheme 4-1. The modification of the synthesized squaraine dyes

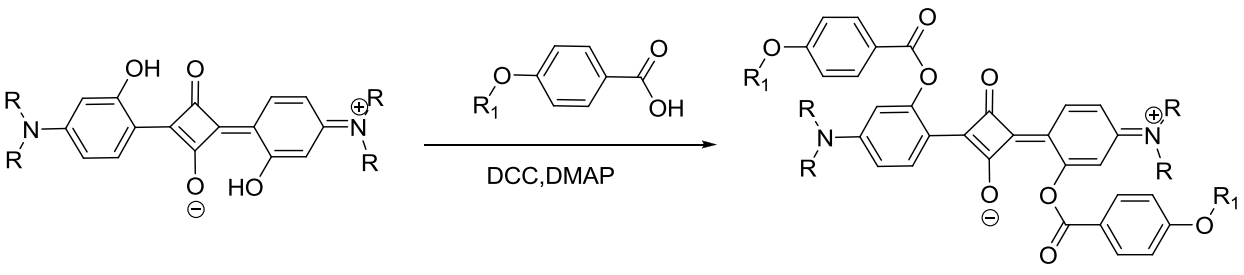

4.2 **Improvements to the Aggregation in the Liquid Crystalline Mesophase**

To enhance the aggregation process in the liquid crystalline mesophase, larger quantities of squaraine dye needs to be dissolved in the mesophase. This behavior can only be feasible by enhancing the compatibility and the solubility parameters between the squaraine dye and liquid crystalline mesophase. This can be accessible by either modifying the dye to enhance the intermolecular interactions or design liquid crystals capable of dissolving large quantities of the squaraine dye.

In our future studies, aggregation in both the nematic and discotic mesophases also need to be addressed. These efforts may include addressing the challenge of finding and designing nematic and discotic mesophases in liquid form at room temperature. These properties will be advantageous for any further photophysical properties investigation, e.g., measuring the two-photon absorption cross section. Once room temperature liquid crystal-directed supramolecular H- and/or J-aggregates are developed, two-photon absorption can be measured to determine if there is an enhancement in the two-photon absorption cross section of the supramolecular aggregate relatively to molecules in an isotropic solution.

APPENDIX A: ^{1}H AND ^{13}C NMR SPECTRA OF THE SERIES OF SQUARAINES

^{1}H NMR for

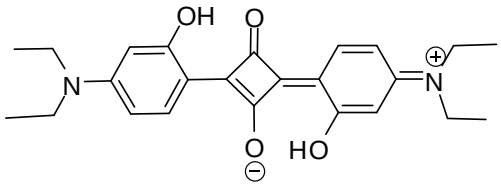

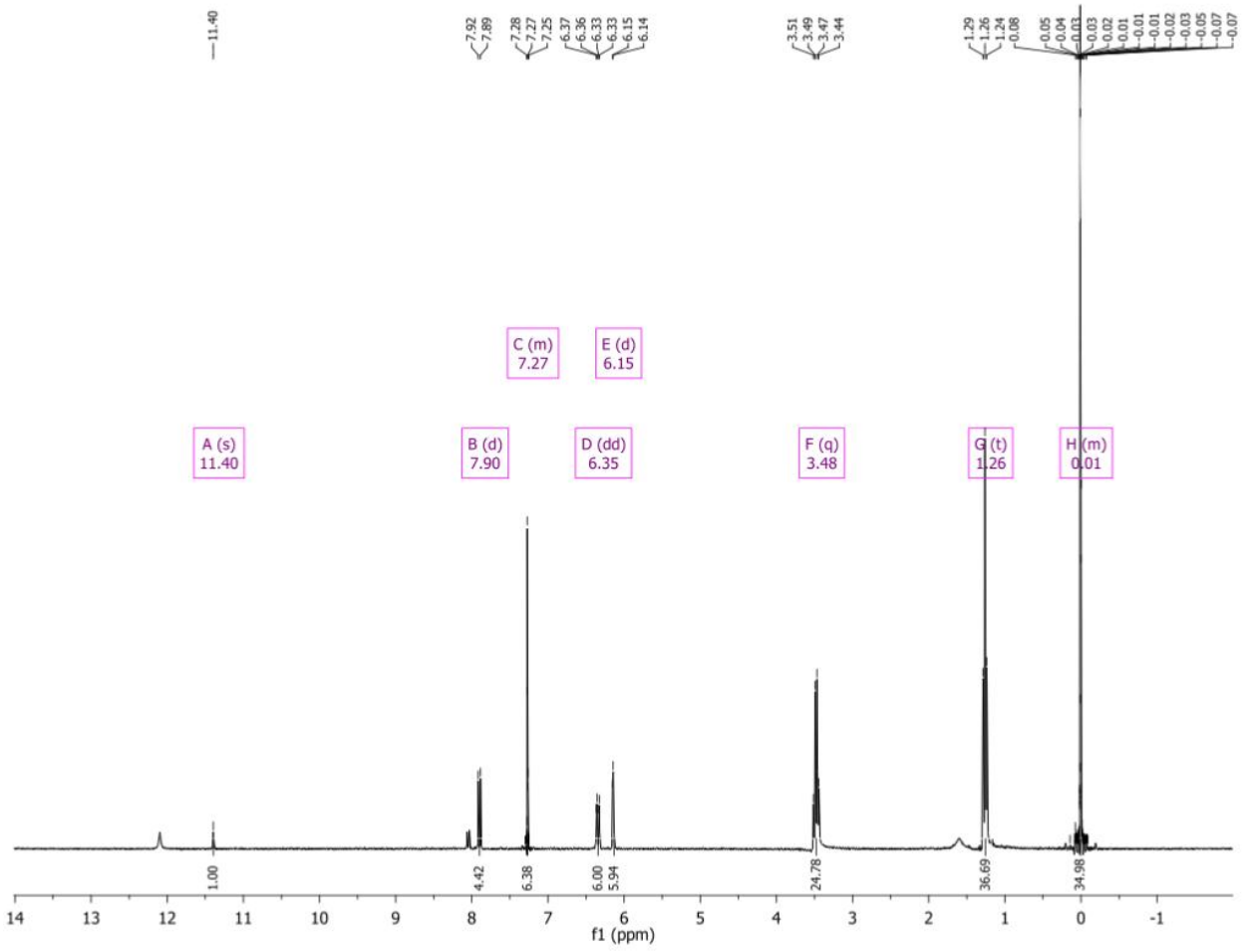

^{1}H NMR: 2, 4-Bis [4-(*N, N*-diethylamino)-2-hydroxyphenyl]squaraine (SQC2OH).

^{13}C NMR for

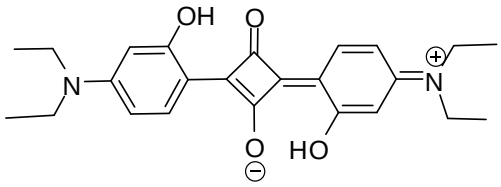

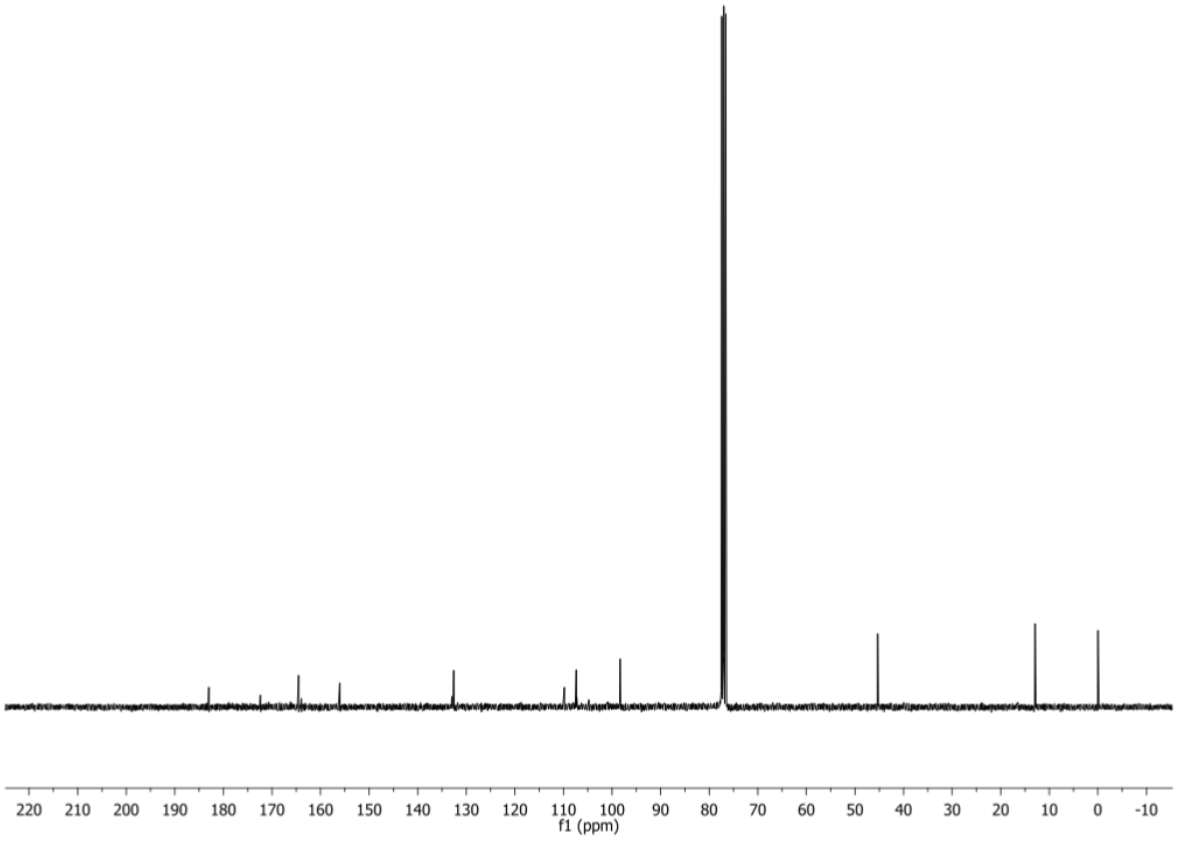

^{13}C NMR: 2, 4-Bis [4-(*N, N*-diethylamino)-2-hydroxyphenyl] squaraine (SQC2OH).

^{1}H NMR for

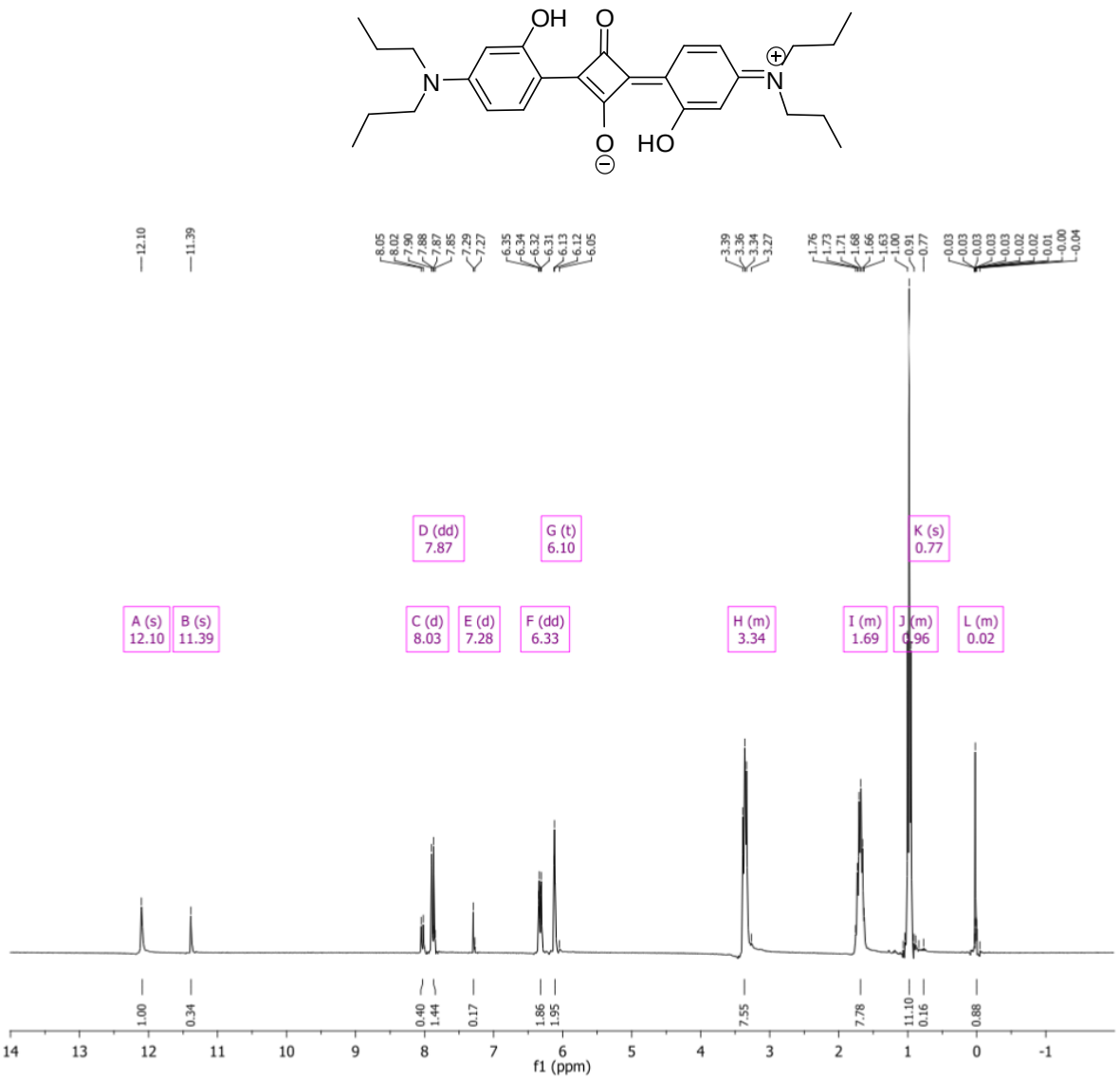

^{1}H NMR: 2, 4-Bis [4-(*N, N*-di-n-propylamino)-2-hydroxyphenyl] squaraine (SQC3OH).

^{13}C NMR for

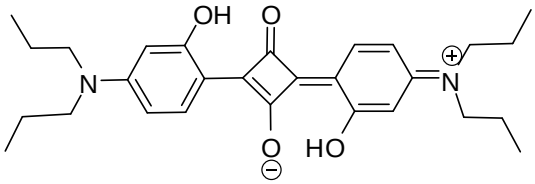

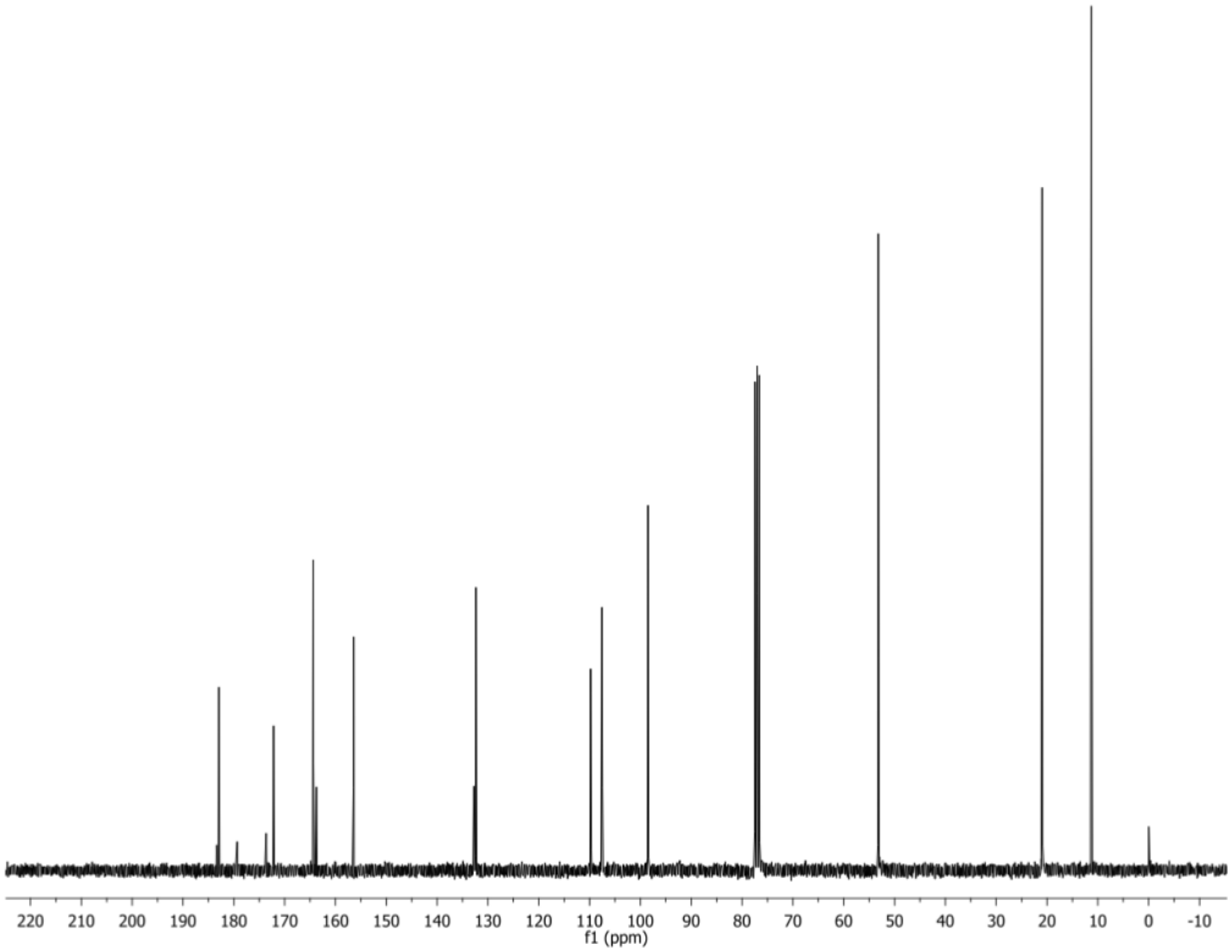

^{13}C NMR: 2, 4-Bis [4-(*N, N*-di-n-propylamino)-2-hydroxyphenyl] squaraine (SQC3OH).

^{1}H NMR for

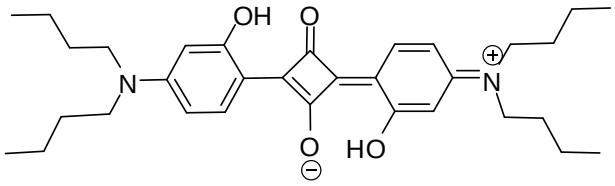

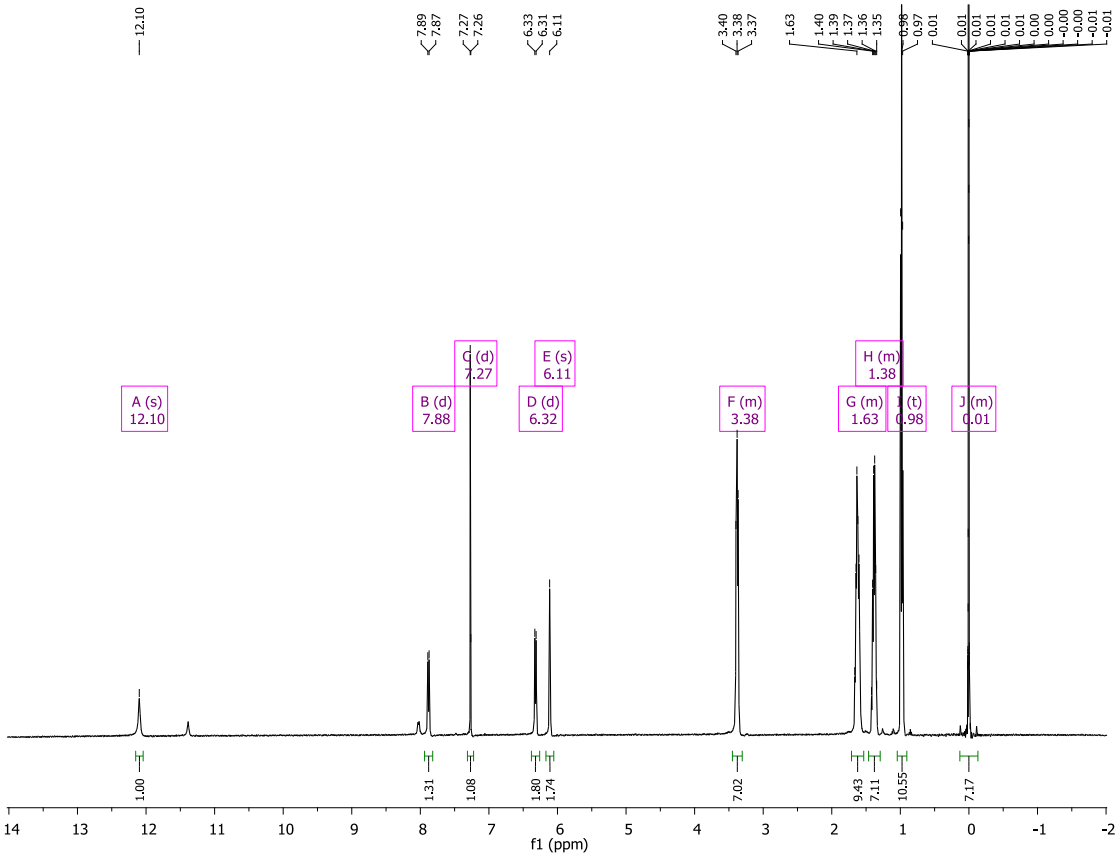

^{1}H NMR: 2, 4-Bis [4-(*N, N*-di-n-butylamino)-2-hydroxyphenyl] squaraine (SQC4OH).

^{1}H NMR for

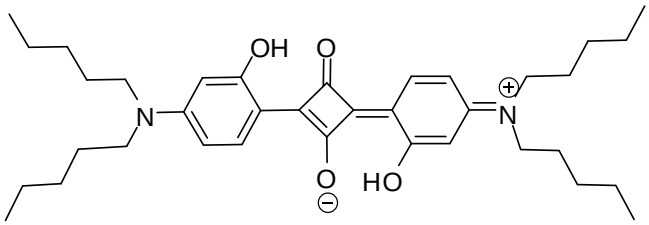

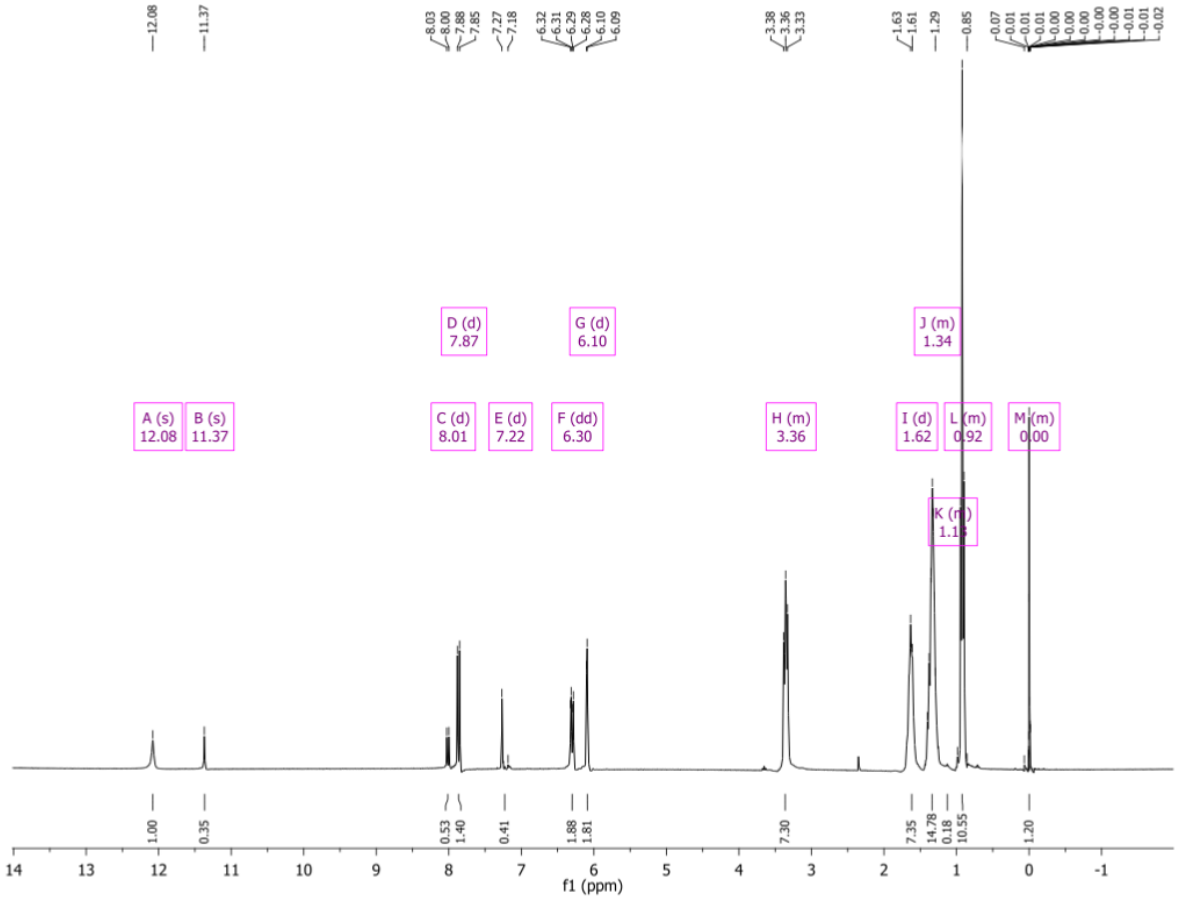

^{1}H NMR: 2, 4-Bis [4-(*N, N*-(di-n-pentylamino)-2-hydroxyphenyl] squaraine (SQC5OH).

^{13}C NMR for

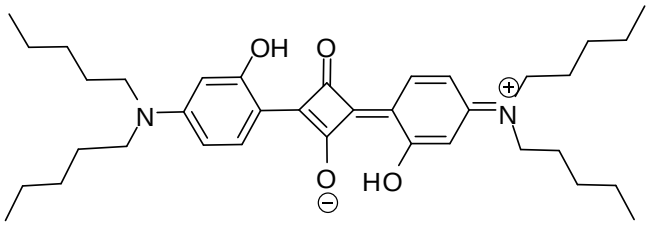

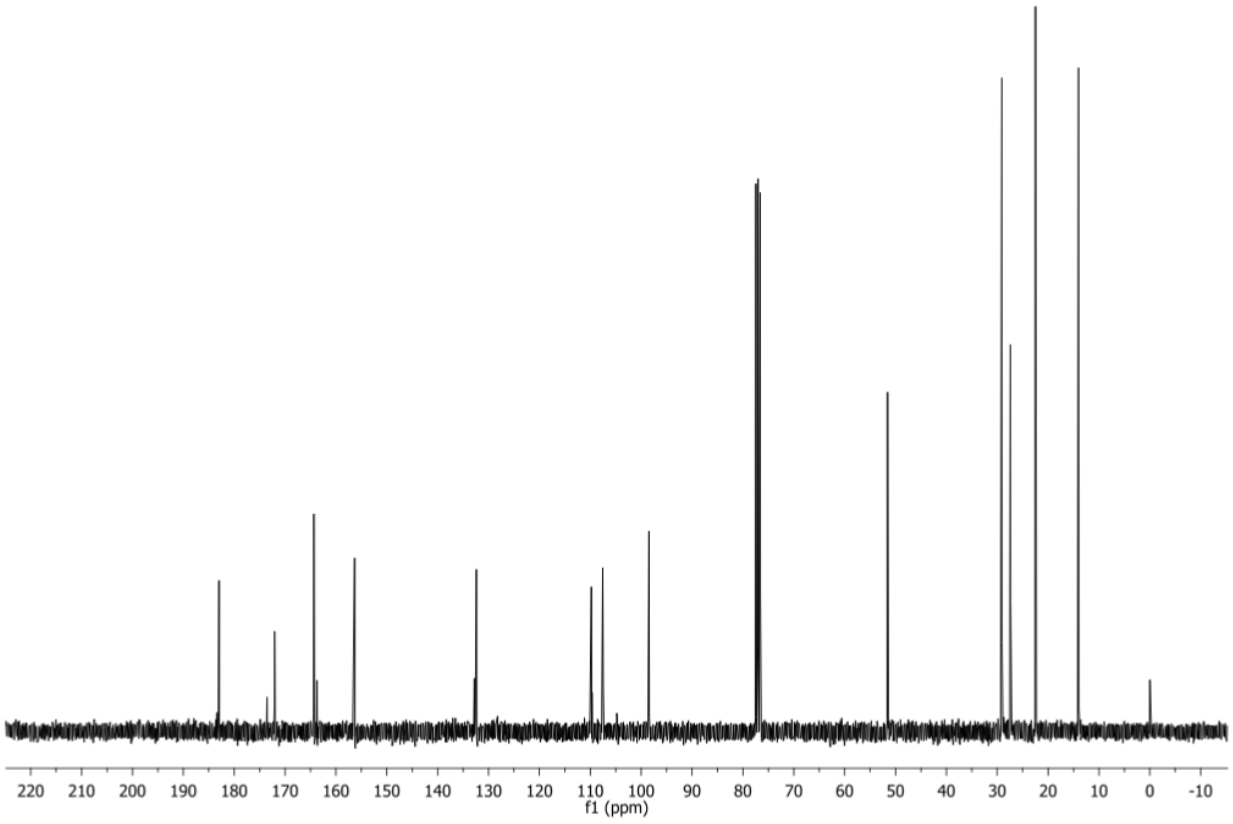

^{13}C NMR: 2, 4-Bis[4-(*N,N*-(di-n-pentylamino)-2-hydroxyphenyl] squaraine(SQC5OH).

^{1}H NMR for

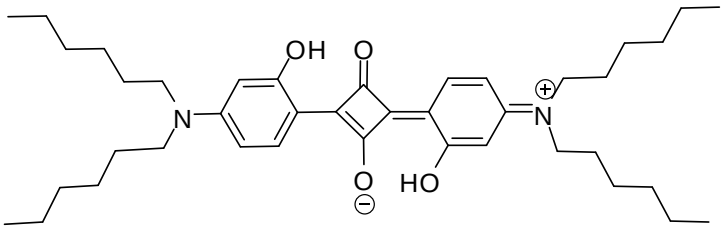

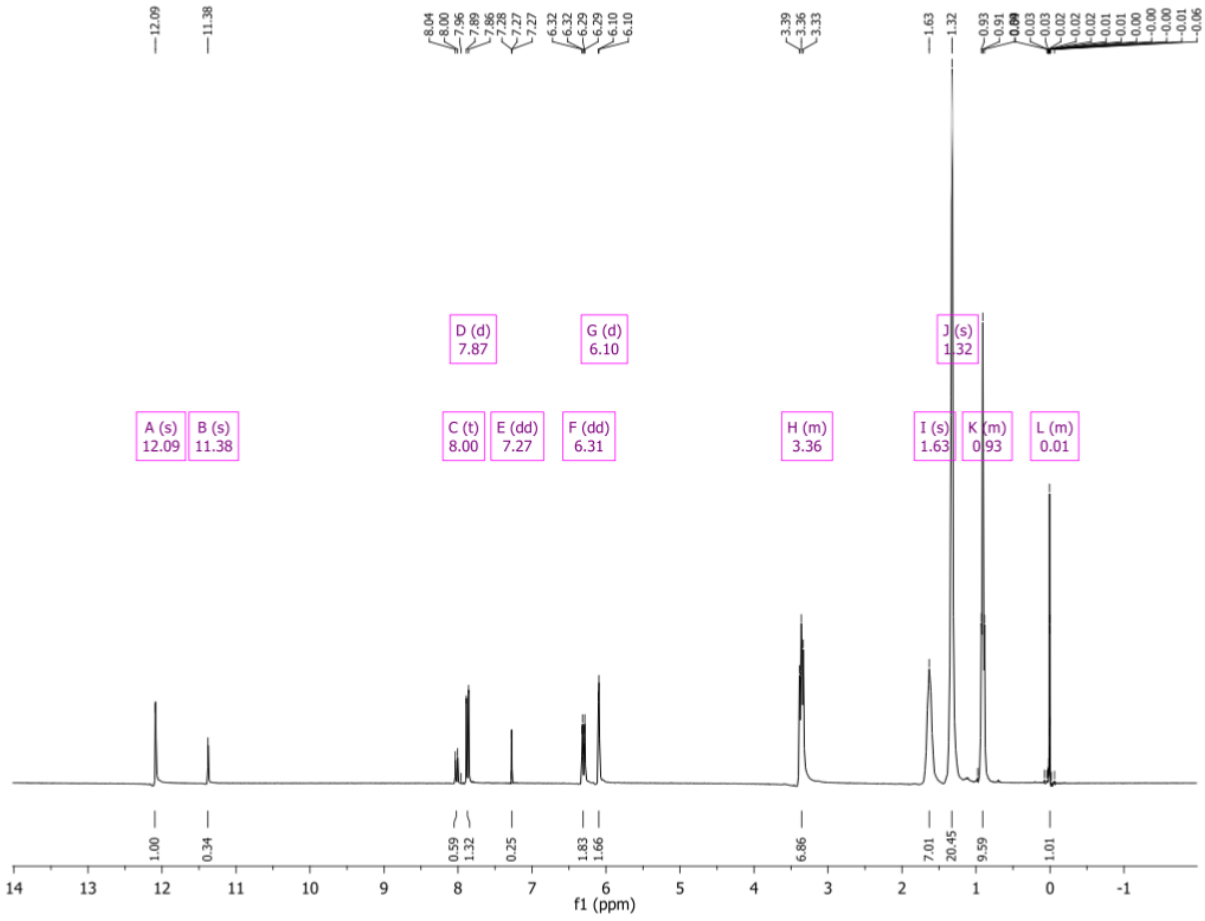

^{1}H NMR: 2, 4-Bis [4-(*N, N*-di-n-hexylamino)-2-hydroxyphenyl] squaraine (SQC6OH).

^{13}C NMR for

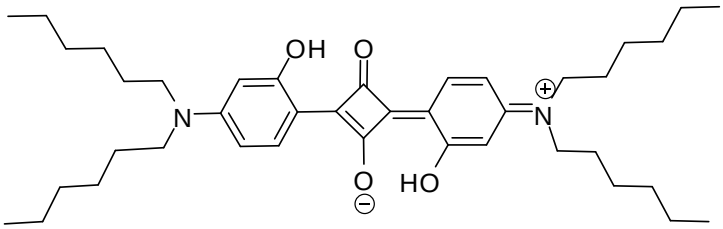

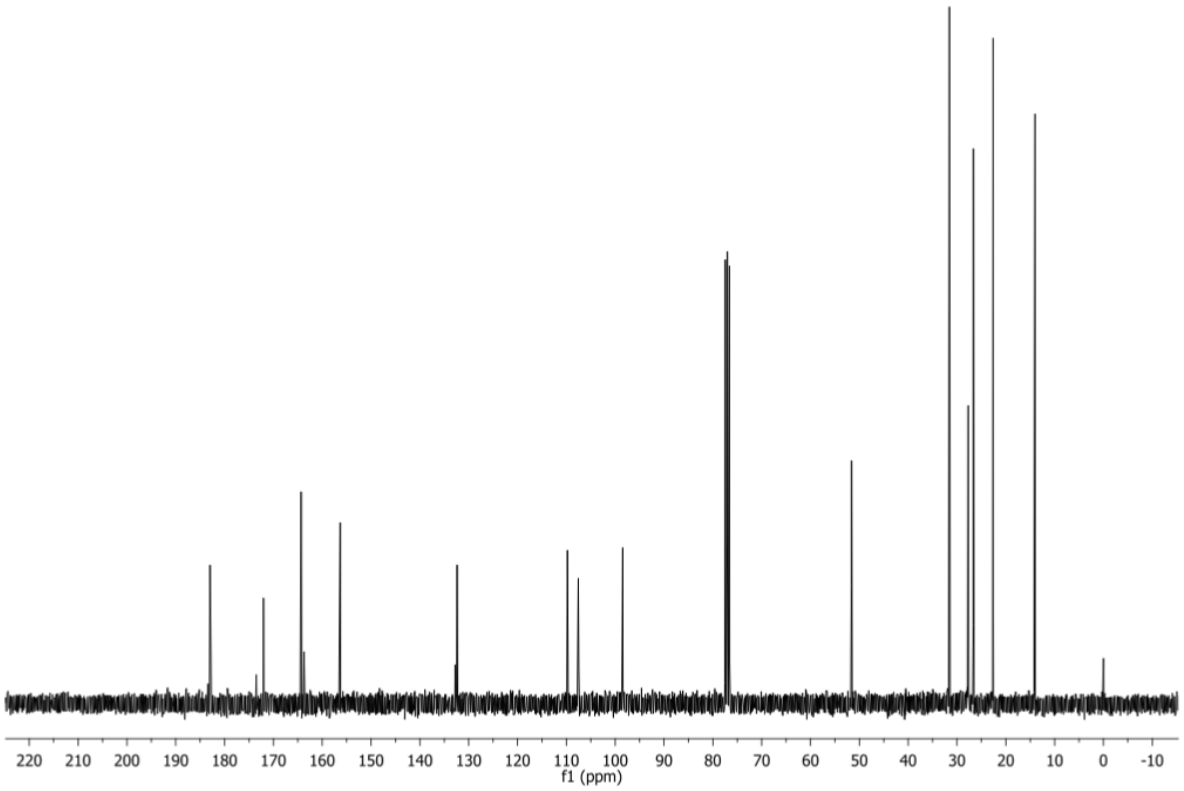

^{13}C NMR: 2, 4-Bis [4-(*N, N*-di-n-hexylamino)-2-hydroxyphenyl] squaraine (SQC6OH).

^{1}H NMR for

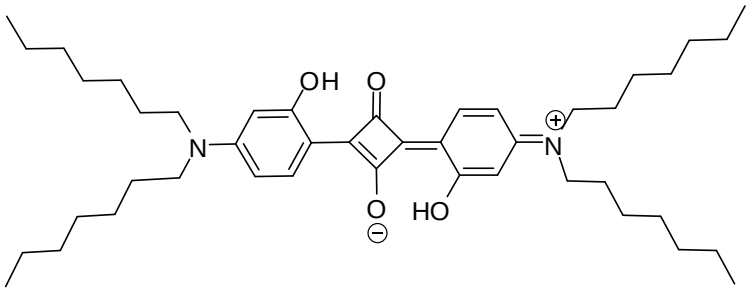

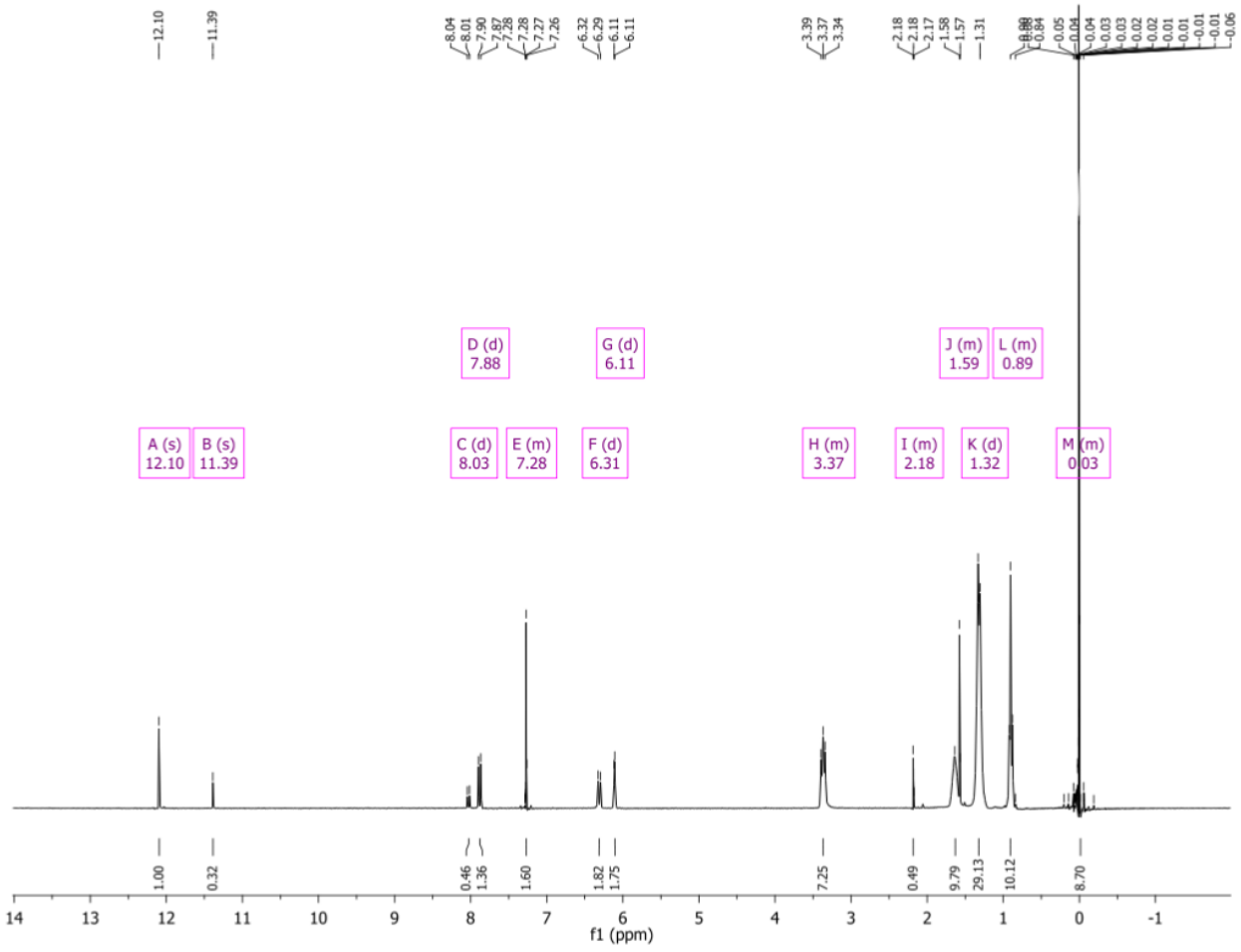

^{1}H NMR: 2, 4-Bis [4-(*N, N*-di-n-heptylamino)-2-hydroxyphenyl] squaraine (SQC7OH)

^{13}C NMR for

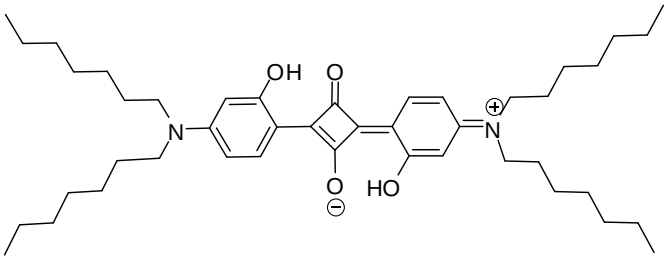

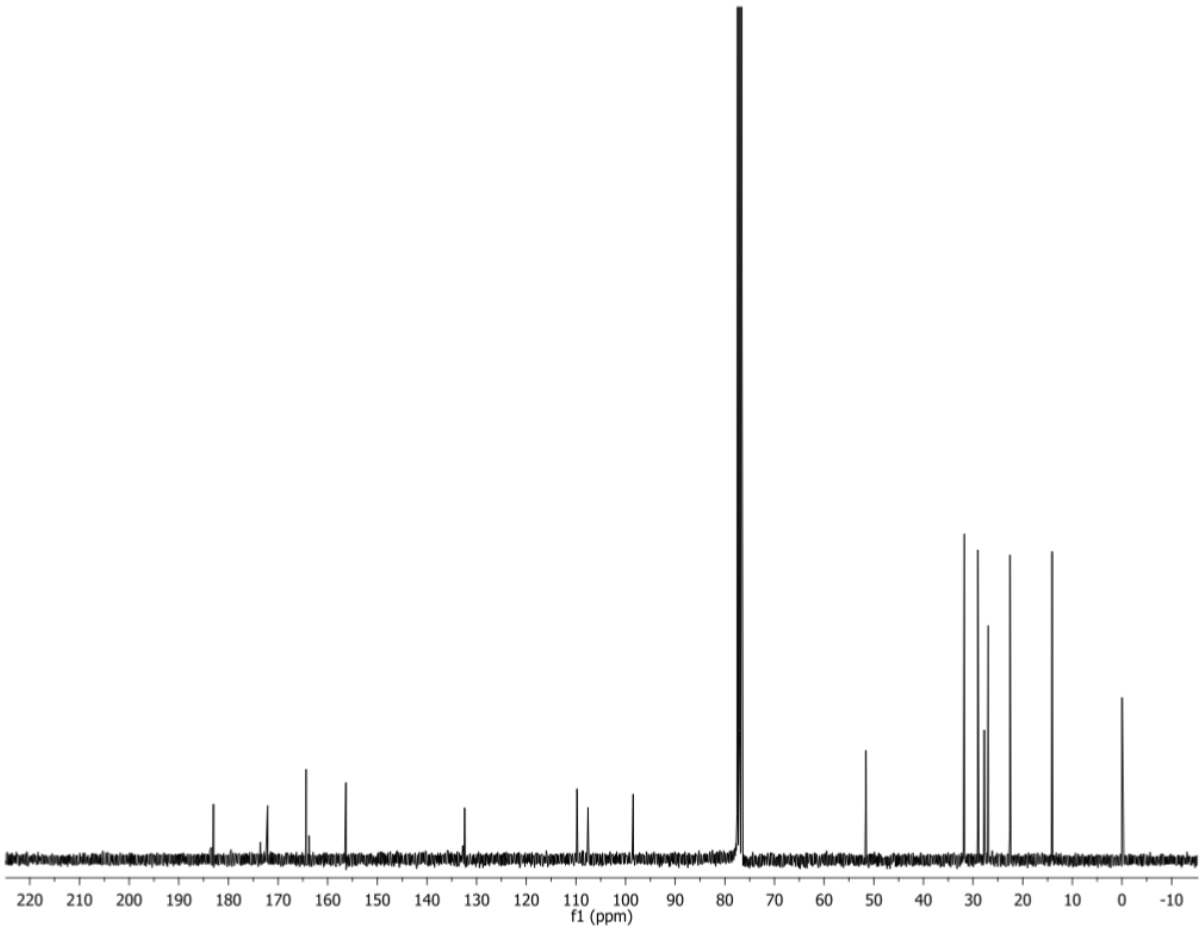

^{13}C NMR: 2, 4-Bis [4-(*N, N*-di-n-heptylamino)-2-hydroxyphenyl] squaraine (SQC7OH)

APPENDIX B: POLARIZED LIGHT MICROSCOPY IMAGES

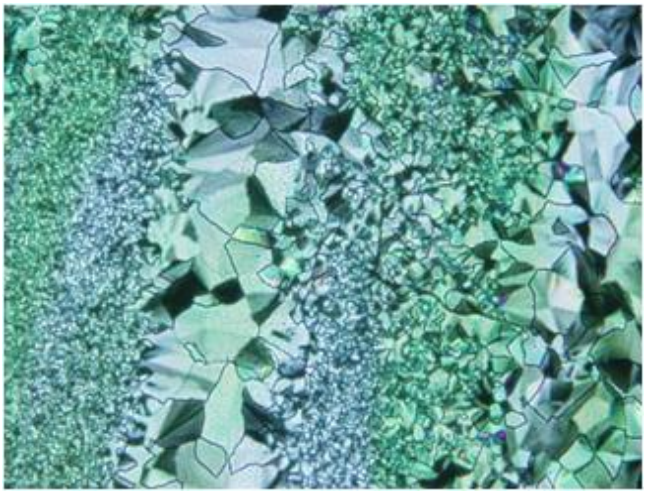

Crystalline-Mesophase Transition of **SQC4OH**

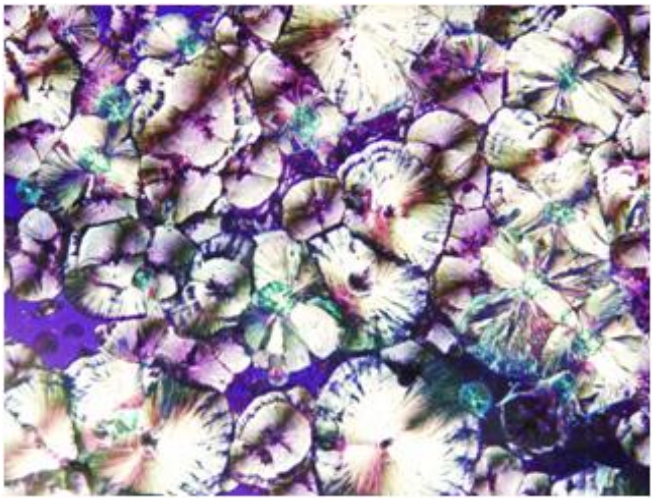

Mesophase- Crystalline Transition of **SQC4OH**

Crystalline Phase for Thin Texture of **SQC4OH**

Crystalline Morphology of **SQC4OH**

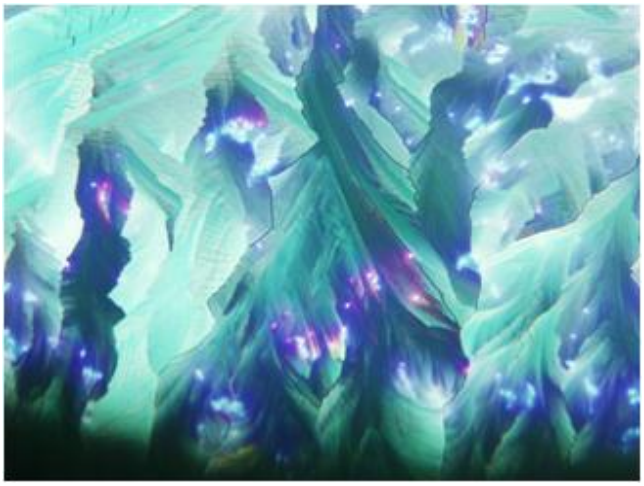

Crystalline Morphology for Thin Film of **SQC4OH**

Crystalline Morphology for Thin Film of **SQC4OH**

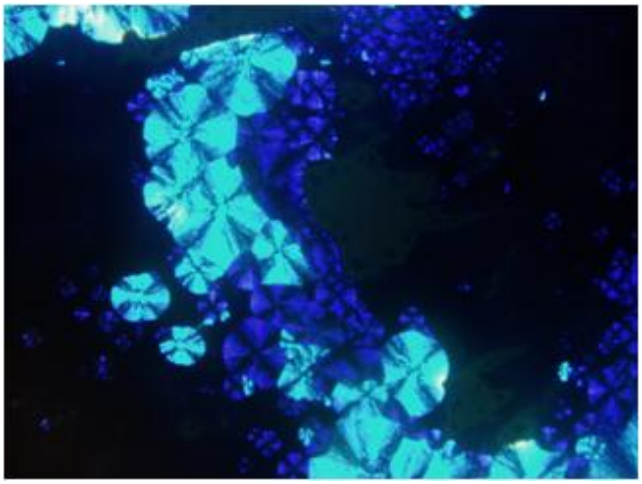

Mesophase Morphology upon Cooling of **SQC4OH**

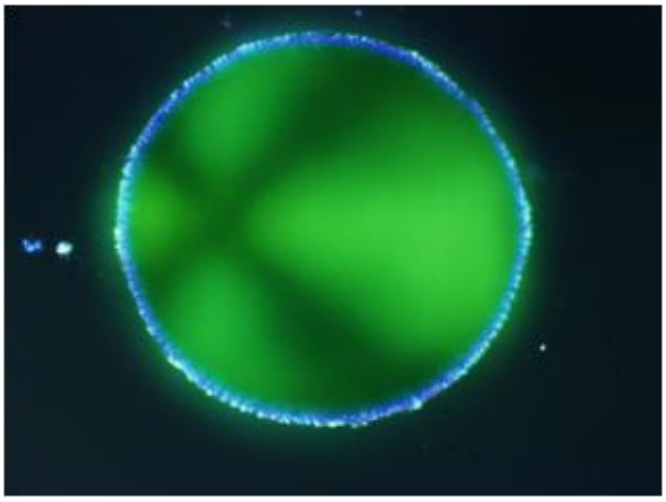

Mesophase-Isotropic Transition upon Heating of **SQC4OH**

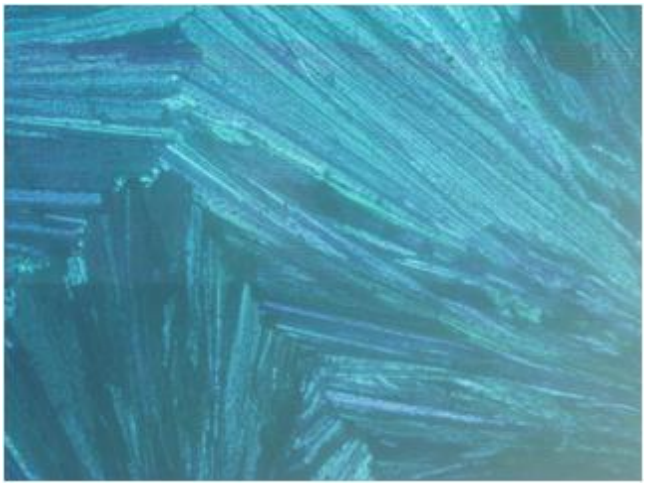

Crystalline Texture of **SQC7OH**

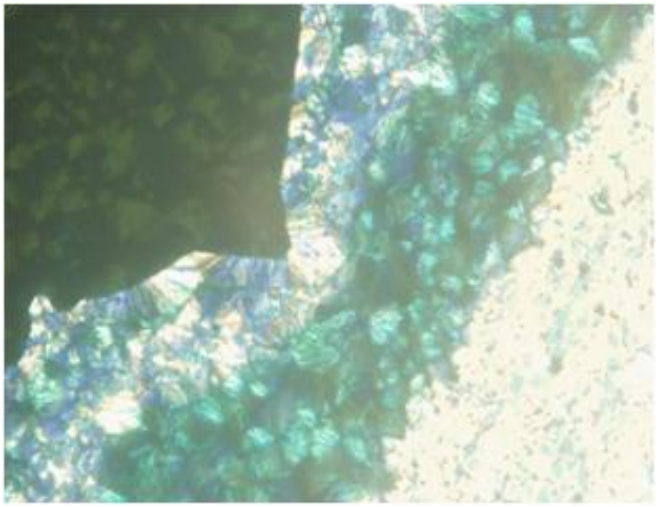

Crystalline-Nematic at Equilibrium of SQC7OH

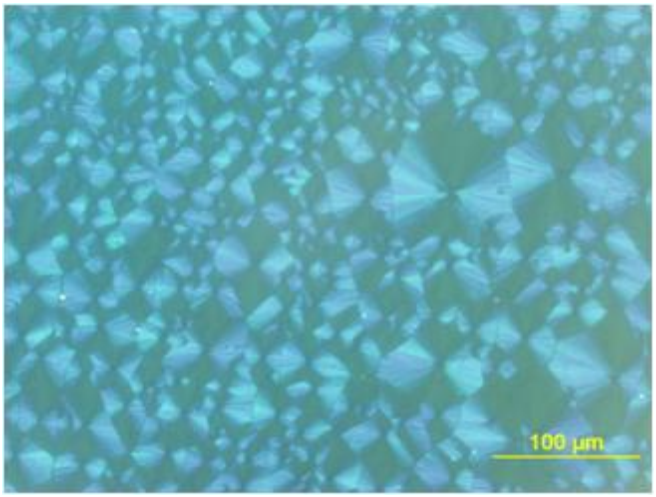

Nematic Phase under Shear Stress of **SQC7OH**

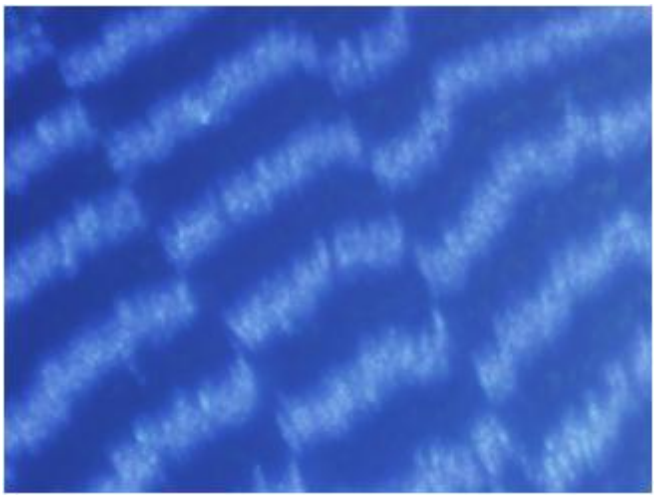

Nematic Texture of **SQC7OH**

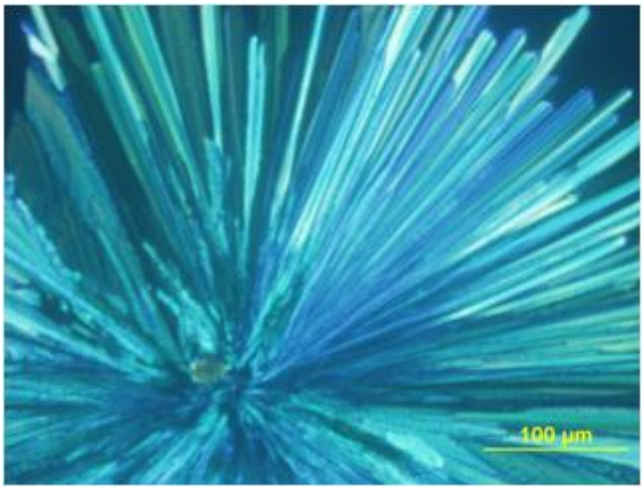

Crystalline Spherulite of SQC7OH

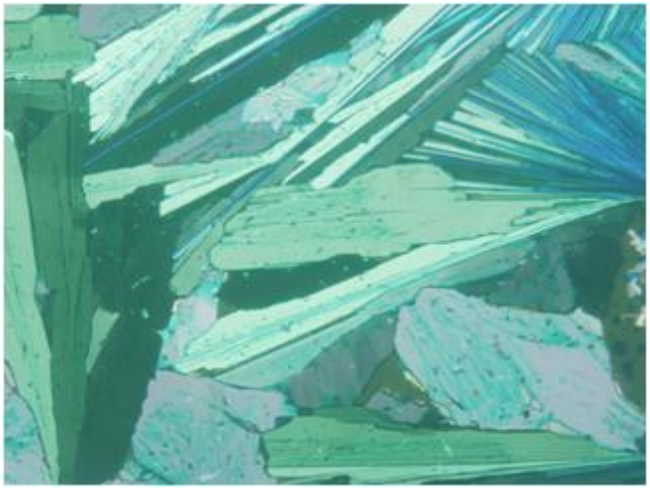

Crystalline Texture of SQC7OH

LIST OF REFERENCES

(1) Beverina, L.; Salice, P. *Eur. J. Org. Chem.* **2010**, 1207-1225.

(2) McEwen, J. J.; Wallace K. J. *Chem. Commun.* **2009**, 6339-51.

(3) Umezawa, K.; Citterio, D.; Suzuki, K. *Anal. Sci.* **2008**, *24*, 213-7.

(4) Sreejith, S.; Carol, P.; Chithra, P.; Ajayaghosh, A. *J. Mater. Chem.* **2008**, *18*, 264-274.

(5) Ros,-L. J.; V.; Garcia, B.; Jimenez, D.; Martinez,-M. R.; Sancenon, F.; Soto, J.; Gonzalvo, F.; Valldecabres, M. C. *J. Am. Chem. Soc.* **2004**, *126*, 4064-5.

(6) Ramaiah, D.; Eckert, I.; Arun, K. T.; Weidenfeller, L.; Epe, B. *Photochem. Photobiol.* **2004**, *79*, 99-104.

(7) Kruhlak, R. J.; Kuzyk, M. G. *J. Opt. Soc. Am. B* **1999**, *16*, 1756-1767.

(8) Terpetschnig, E.; Szmacinski, H.; Ozinskas, A.; Lakowicz, J. R. *Ana.l Biochem.* **1994**, *217*, 197-204.

(9) Terpetschnig, E.; Szmacinski, H.; Ozinskas, A.; Lakowicz, J. R. *Anal. Biochem.* **1994**, *217*, 197-204.

(10) Law, K. Y. *J. Imaging Sci. Technol.* **1990**, *34*, 38-44.

(11) Toro, C.; De Boni, L.; Yao, S.; Ritchie, J. P.; Masunov, A. E.; Belfield, K. D.; Hernandez, F. E. *J. Chem. Phys.* **2009**, *130*, 214504/1-214504/6.

(12) Sreejith, S.; Carol, P.; Chithra, P.; Ajayaghosh, A. *J. Mater. Chem.* **2008**, *18*, 264-274.

(13) Law, K. Y.; Bailey, F. C. *J. Org. Chem.* **1992**, *57*, 3278-86.

(14) Law, K. Y.; Bailey, F. C. *Dyes Pigments* **1988**, *9*, 85-107.

(15) Law, K. Y.; Bailey, F. C. *Can. J. Chem.* **1986**, *64*, 2267-73.

(16) Saito, K. *J. Phys. Chem. B* **2001**, *105*, 4235-4238.

(17) Dimitriev, O. P. *J. Mol. Liq*. **2005**, *120*, 131-133.

(18) Tian, M.; Furuki, M.; Iwasa, I.; Sato, Y.; Pu, L. S.; Tatsuura, S. *J. Phys. Chem. B* **2002**, *106*, 4370-4376.

(19) McKerrow, A. J.; Buncel, E.; Kazmaier, P. M. *Can. J. Chem.* **1995**, *73*, 1605-15.

(20) Kazmaier, P. M.; Hamer, G. K.; Burt, R. A. *Can. J. Chem.* **1990**, *68*, 530-6.

(21) Schmidt, A. H. *Oxocarbons* **1980**, 185-231.

(22) Sprenger, H. E.; Ziegenbein, W. *Angew. Chem., Int. Ed. Engl.* **1967**, *6*, 553-4.

(23) Lynch, D. E.; Byriel, K. A. *Cryst. Eng.* **2000**, *2*, 225-239.

(24) Ashwell, G. J.; Bahra, G. S.; Brown, C. R.; Hamilton, D. G.; Kennard, C. H. L.; Lynch, D. E. *J. Mater. Chem.* **1996**, *6*, 23-6.

(25) Qaddoura M. A.; Belfield K. D. *Int J Mol Sci* **2009**, *10*, 4772-88.

(26) Demus, D.; J. G.; Gray, G. W.; Spiess, H. -W.; Vill, V. In *Handbook of Liquid Crystals Low Molecular Weight Liquid Crystal*, Ed.; Wiley-VCH: Weinheim, 1998, p 3-20..

(27) Mortensen, K. *Texture of liquid crystal,* Ed.; Wiley-VCH: Weinheim, 2004; Vol.1

(28) Geurst, J. A. *Phys. Lett. A* **1971**, *34*, 283-4.

(29) Chandrasekhar, S.; Ranganath, G. S. *Adv. Phys.* **1986**, *35*, 507-96.

(30) Delaney, J.; Morrow, M.; Eckhardt, C. J. *Chem. Phys. Lett.* **1985**, *122*, 347-51.

(31) Tristani-Kendra, M.; Eckhardt, C. J.; Bernstein, J.; Goldstein, E. *Chem. Phys. Lett.* **1983**, *98*, 57-61.

(32) Law, K. Y.; Chen, C. C. *J. Phys. Chem.* **1989**, *93*, 2533-8.

(33) Liang, K.; Law, K.-Y.; Whitten, D. G. *J. Phys. Chem.* **1994**, *98*, 13379-84.

(34) Chen, H.; Herkstroeter, W. G.; Perlstein, J.; Law, K.-Y.; Whitten, D. G. *J. Phys. Chem.* **1994**, *98*, 5138-46.

(35) Crossley, M. L.; Dreisbach, P. F.; Hofmann, C. M.; Parker, R. P. *J. Am. Chem. Soc.* **1952**, *74*, 573-8.

(36) Sprenger, H. E.; Ziegenbein, W. *Angewandte Chemie* **1966**, *78*, 937-8.

(37) McKerrow, A. J.; Buncel, E.; Kazmaier, P. M. *Can. J. Chem.* **1995**, *73*, 1605-15.

(38) Law, K. Y.; Bailey, F. C. *Dyes Pigments* **1993**, *21*, 1-12.

(39) Law, K. Y. *J. Imaging Sci. Technol.* **1992**, *36*, 567-73

(40) Wei, G.; Lunt, R. R.; Sun, K.; Wang, S.; Thompson, M. E.; Forrest, S. R. **2010** *Nano Lett. 10*, 3555-3559.

(41) Saito, K. *J. Phys. Chem. B* **2001**, *105*, 4235-4238.

(42) Li, J.-r.; Li, B.-f.; Li, X.-c.; Tang, J. a.; Jiang, L. *Thin Solid Films* **1996**, *287*, 247-251.

(43) Chudinova, G. K.; Barachevskii, V. A. *Zh. Fiz. Khim.* **1995**, *69*, 1311-14.

(44) Tanaka, M.; Sekiguchi, T.; Matsumoto, M.; Nakamura, T.; Manda, E.; Kawabata, Y. *Thin Solid Films* **1988**, *160*, 299-302.

(45) Kim, S.; Furuki, M.; Pu, L. S.; Nakahara, H.; Fukuda, K. *J. Chem. Soc., Chem. Commun.* **1987**, 1201-3.

(46) Ashwell, G. J.; Williamson, P. C.; Green, A.; Bahra, G. S.; Brown, C. R. *Aust. J. Chem.* **1998**, *51*, 599-604.

(47) Ashwell, G. J.; Jefferies, G.; Rees, N. D.; Williamson, P. C.; Bahra, G. S.; Brown, C. R. *Langmuir* **1998**, *14*, 2850-2856.

(48) Ashwell, G. J. *J. Mater. Chem.* **1998**, *8*, 373-376.

(49) Tani, T. *J-Aggregates;* Kabayashi, T., Ed.; World Scientific Publishing: Singapore, **1996**; P 209-228.

(50) Scherer, P. O. J. *J-Aggregates;* Kabayashi, T., Ed.; World Scientific Publishing: Singapore, **1996**; P 95-110.

(51) Knoester, J.; Spano, F. C. *J-Aggregates;* Kabayashi, T., Ed.; World Scientific Publishing: Singapore, **1996**; P 111-160.

(52) Servaites, J. D.; Yeganeh, S.; Marks, T. J.; Ratner, M. A. *Adv. Funct. Mater.*, *20*, 97-104.

(53) Afolabi, O. M.; Ajayi, I. R.; Siyanbola, W. O. *Global J. Pure Appl. Sci.* **2004**, *10*, 435-439.

(54) Wojtyk, J.; McKerrow, A.; Kazmaier, P.; Buncel, E. *Can. J. Chem.* **1999**, *77*, 903-912.

(55) Law, K. Y. *J. Phys. Chem.* **1987**, *91*, 5184-93.

(56) Lepkowicz, R. S.; Cirloganu, C. M.; Przhonska, O. V.; Hagan, D. J.; Van Stryland, E. W.; Bondar, M. V.; Slominsky, Y. L.; Kachkovski, A. D.; Mayboroda, E. I. *Chemical Physics* **2004**, *306*, 171-183.

(57) Fukuda, K.; Nakahara, H. *Colloid Surface A.* **1995**, *102*, 57-68.

(58) Tatsuura, S.; Tian, M.; Furuki, M.; Sato, Y.; Pu, L. S.; Wada, O. *Jpn J Oppl Phys 1.* **2000**, *39*, 4782-4785.

(59) Kuramoto, N.; Enomoto, S.; Ozaki, Y. *Langmuir* **1995**, *11*, 2195-200.

(60) Qaddoura, M. A.; Belfield, K. D. *Materials*. **2010** *3*, 827-840.

(61) Qaddoura, M. A.; Belfield, K. D. *Int. J. Mol. Sci.* **2009**, *10*, 4772-4788.

(62) Demus, D. *Liq. Cryst.* **1989**, *5*, 75-110

(63) Demus, D.; J. G.; Gray, G. W.; Spiess, H.-W.; Vill, V. *Handbook of Liquid Crystals Low Molecular Weight Liquid Crystal*, Ed.; Wiley-VCH: Weinheim, 1998; Vol. 3; p 540.

(64) Bouligand, Y. *Dislocations Solids* **1980**, *5*, 299-347.

(65) Kurik, M. V.; Lavrentovich, O. D. *Mol. Cryst. Liq. Cryst.* **1982**, *72*, 239-46.

(66) Lavrentovich, O. D.; Kleman, M. *Chirality Liq. Cryst.* **2001**, 115-158.

(67) Demus, D.; Richter, L. *Textures of Liquid Crystals*, ed.; Wiley-VCH: Weinheim, 1978.

(68) Demus, D.; Richter, L. *Textures of Liquid Crystals. 2nd ed*.; Wiley-VCH: Weinheim, 1980.

(69) Coates, D.; Gray, G. W. *J. Chem. Soc., Chem. Commun.* **1974**, 101 (70) Gibson, H. W. *J. Phys. Chem.* **1976**, *80*, 1310-14.

(71) McMillan, W. L. *Phys. Rev. A* **1972**, *6*, 936-47.

(72) Price, F. P.; Fritzsche, A. K. *J. Phys. Chem.* **1973**, *77*, 396-9.

(73) Terauchi, H.; Takeuchi, T.; Nakatsu, K.; Maruyama, N. *Jpn. J. Appl. Phys.* **1974**, *13*, 1203-10.

(74) Gray, G. W.; Goodby, J. W. *Smectic Liquid Crystals: Textures and Structures*, ed.; Leonard Hill: Glasgow, 1984..